SIMULATING THERMODYNAMICS AND KINETICS OF LIVING POLYMERIZATION

A Thesis
Presented to
The Academic Faculty

by

Yanping Qin

In Partial Fulfillment
of the Requirements for the Degree
Doctor of Philosophy in the
School of Chemistry and Biochemistry

Georgia Institute of Technology
August 2007

SIMULATING THERMODYNAMICS AND KINETICS OF LIVING POLYMERIZATION

Approved by:

Dr. Rigoberto Hernandez, Adviser
School of Chemistry and Biochemistry
Georgia Institute of Technology

Dr. Jean-Luc Brédas
School of Chemistry and Biochemistry
Georgia Institute of Technology

Dr. Robert M. Dickson
School of Chemistry and Biochemistry
Georgia Institute of Technology

Dr. C. David Sherrill
School of Chemistry and Biochemistry
Georgia Institute of Technology

Dr. Peter J. Ludovice
School of Chemical and Biomolecular Engineering
Georgia Institute of Technology

Date Approved: July 3, 2007

ACKNOWLEDGEMENTS

I would like to begin by expressing my sincerest thanks to my advisor, Professor Rigoberto Hernandez for his consistent support and guidance throughout my graduate studies. His guidance has been invaluable over the years. I would also like to thank Professor Jean-Luc Brédas, Professor Robert M. Dickson, Professor C. David Sherill and Professor Pete Ludovice for having served on my thesis committee and for their comments and suggestions. Thanks also goes to Dr.Alexander Popov for many insightful discussions from which I learned a lot, and my group members for their friendship.

I would like to thank my parents and brother, who have been giving me love and encouragement during my hard working time. I would like to thank my husband, Jie Zheng, who supported my research and gave me strength to move forward and finish my graduate work at Georgia Tech.

This work was partially funded by the National Science Foundation, the Research Corporation, and the Goizueta Foundation.

TABLE OF CONTENTS

LIST OF TABLES

LIST OF FIGURES

SUMMARY

The generalized Langevin equation (GLE) has been used to describe the dynamics of particles in a stationary environment. To better understand the dynamics of polymerization, the GLE has been generalized to the irreversible generalized Langevin equation (iGLE) so as to incorporate the non-stationary response of the solvent. This non-stationary response is manifested in the friction kernel and the behavior of the projected (stochastic) force. A particular polymerizing system, such as living polymerization, is specified both through the parameters of the friction kernel and the potential of mean force (PMF). Equilibrium properties such as extent of polymerization have been obtained and are consistent with Flory-Huggin's theory. In addition, time-dependent non-equilibrium observables such as polymer length, the polymer length distribution, and polydispersity index (PDI) of living polymerization have been obtained. These have been compared to several experiments so as to validate the models, and to provide additional insight into the thermodynamic and kinetic properties of these systems.

In addition to the iGLE, a stochastic model has been used to study the effect of non-equilibrium reactivity on living polymerization. This model can be used to determine whether the reaction is controlled by kinetics or diffusion. A combination of the iGLE and stochastic models may help us obtain more information about living polymerization.

CHAPTER I

INTRODUCTION

The term "living polymers" was first suggested by M. Szwarc in 1956 in the anionic polymerization of styrene with an alkali metal/naphthalene system in tetrohydrofuran [5, 6]. He found that viscosity increases as the reaction proceeds, reaching a maximal value for a fixed amount of monomers. The addition of monomers will continue the reaction and the viscosity will increase again. After his remarkable discovery, a lot of techniques such as cationic polymerization, free radical polymerization and ring-opening polymerization [7] have been developed in the last fifty years to study this "livingness" —a special feature of living polymers [8, 9].

Living polymerization [10, 11] is a powerful technique for synthesizing homopolymers and copolymers/block polymers. Block copolymers have found great applications in drug delivery, photonics and fuel cells. One example is polystyrene-b-poly(methyl methacrylate)(PS-b-PMMA), which can be made by first polymerizing styrene, and then subsequently polymerizing MMA from the reactive end of the polystyrene chains. The active sites on the living polymers allow the propagation and depropagation steps to occur simultaneously and ideally there are no termination/transfer reactions happening. If the rate of chain initiation is much faster than the rate of chain propagation, the polymer chains grow at a more constant rate and the chain length be kept at a constant length, that is, they have a very low polydispersity index (PDI). The PDI indicates the distribution of the individual molecular weight in a batch of polymers and has a value always greater than 1. As the polymer chain length approaches a uniform chain length, the PDI approaches 1. By terminating the reaction before depolymerization becomes important, one can obtain polymers with narrow molecular weight distributions. The physical properties of equilibrium polymerization strongly depend on the molecular weight and molecular weight distribution.

The factors that affect polymerization include the initiator concentration, monomer

concentration and temperature. Polymerization proceeds only if the standard Gibbs energy ($\Delta G = \Delta H - T\Delta S$) is zero or negative. For polymerization with positive enthalpy and entropy, the polymerization will begin when the temperature of the system increases above a critical "floor temperature." For polymerization with negative enthalpy and entropy, the polymerization will begin when the temperature of the system is below a critical "ceiling temperature." The latter case has been observed most often. One example is polymerization of α-methylstyrene. As the temperature increases, the entropy term becomes more positive, and free energy will increase and become less negative. This results in an increase in the number of monomers in solution and the monomers are in a dynamic equilibrium with the polymers. Most models of polymerization systems have focused on equilibrium polymerization and don't have sufficient detail. The goal of this work is to develop models to investigate the time-dependent molecular structure and the macroscopic structure. The molecular structure includes the average polymer length and its distribution. The macroscopic structure includes the viscosity.

1.1 Living Polymerization and Experimental Systems

1.1.1 Mechanism and Molecular Weight Distribution

Living polymerization is a special case of chain polymerization where it occurs in three stages. In the initiation step an activated species, such as a free radical from an initiator, attacks and opens the double bond of a monomer molecule, producing a new activated species. In the propagating step, this activated species adds a monomer unit and in doing so activates the newly added monomer. The growth usually happens in seconds to microseconds. Although in theory this process may continue forever, it always terminates due to a variety of specific chain-terminating reactions. To prevent chain termination, free radical polymerization such as atom transfer radical polymerization (ATRP) and reversible addition-fragmentation chain transfer (RAFT) polymerization have been developed in the twentieth century. Various reagents, solvents and conditions have been used to keep the activated end "alive". In this work, however, we will focus on the conventional anionic polymerization.

For polymerization processes, the degree of polymerization (DP) is an important theoretical quantity. Although the polymer length is important to know, it is not as important as the polymer length distribution or molecular weight distribution. If one could count the number of " mers" on each molecule and the number of this length of molecule occurs in the sample, then one could draw a histogram to describe the distribution of polymers. Besides this number distribution, another useful distribution is the molecular weight distribution including the number-average molecular weight distribution (M_n) and the weight-average weight distribution (M_w). These distributions help to characterize the size of the polymer and to understand the properties of the polymer such as the viscosity. The number-average weight is the mass of a given quantity of material divided by the number of chains found in the sample:

$$M_n = \frac{\sum_{i=1}^{\infty} N_i M_i}{\sum_{i=1}^{\infty} N_i} \ , \tag{1}$$

The weight-average MW can be described as:

$$M_w = \frac{\sum_{i=1}^{\infty} N_i M_i^2}{\sum_{i=1}^{\infty} N_i M_i} \ , \tag{2}$$

where N_i is the number of polymers with the molecular weight of M_i. The ratio of the weight-average and number-average molecular weights can be used to describe the polydispersity of the polymers (PDI).

In 1958, Brown and Szwarc [12] derived the equilibrium molecular weight distribution of living polymers and the rate of change of the distribution when the initial distribution is not the equilibrium distribution. They assumed that the rate constants are independent of chain length. Based on their results, in 1965, Miyake and Stockmayer [13] obtained a complete analytic solution for a living polymer system without transfer and termination reactions provided the monomer concentration was constant. In 1997, Milchev studied the molecular weight distribution MWD using Monte Carlo methods on a two-dimensional lattice and confirmed the cross over from Schulz-Zimm to exponential distributions as the system moved from the dilute to semi-dilute case [14].

For reversible, equilibrium polymerization, there are three stages for which the MWD has been predicted by theory and experiment [12, 15]. In the initial stage, the initial MWD

is a Poisson distribution since the polymerization is much faster than the depolymerization. In the intermediate stage, M_n will remain constant, but M_w will continue to increase until equilibrium. In this stage, equilibrium between monomer and polymer is established, and finally reaches Flory-Schulz distribution after a long time. The Flory-Schulz distribution becomes the exponential distribution predicted by the Flory-Huggins lattice model [16] and kinetic study [17] when the number average degree of polymerization is large. The ideal, living, irreversible polymerization usually gives a narrow, sharp Poisson distribution. This is shown in appendix A. The non-uniformity with respect to degree of polymerization (PDI) can be estimated by $1 + 1/n$, where n is the polymer length; Although the experimental values are usually higher. Different techniques have been developed to get more accurate results. The most popular experimental techniques to determine the molecular weight distribution for living polymerization include gel permeation chromatography (GPC)/size exclusion chromatography (SEC), gas chromatography (GC) and the photocopy method. The SEC is a special kind of liquid chromatography that separates molecules according to size instead of according to affinities toward the porous substrate.

The polymerization rate constants are average constants that average all of the propagating species such as ion pairs, free ions etc. Ion pairs have much lower propagation rate than free ions and the contribution of ion pairs to the rate constant is larger than free ions. A plot of $K_p = f(T)$ does not follow an Arrhenius-type relationship since dissociation of ion pairs are strongly temperature dependent and overall propagation constants are averages over the contribution of different proportions of ion pairs at different temperatures. But in most cases, since usually only one ion structure dominates in the polymerization process, use of an Arrhenius-type relationship to determine the activation energy is still widely accepted.

1.1.2 Some Interesting Systems

Living polymers are easily terminated by exposure to air and water. This makes it difficult to perform living polymerization process in the lab. Some experimental systems studied in the lab with the operating conditions and results are shown below. A few of them will be

used to validate our model.

1.1.2.1 α-methylstyrene

Living polymerization of α-methylstyrene in the solvent tetrahydrofuran initiated by sodium naphthalide or cesium naphthalide has been studied by Greer and coworkers [1, 15]. The ceiling temperature of this system in solvent is $250-320K$. This reaction is very convenient to operate in the lab. In this experiment, to initiate the polymerization reaction, one mixes the reaction mixture above the polymerization temperature, and then quenches to a lower temperature to make sure the initiation process has finished before the propagation begins. The repeat unit of α-methylstyrene is shown in Figure 1. This experimental data has been widely used by recent theorists for comparison.

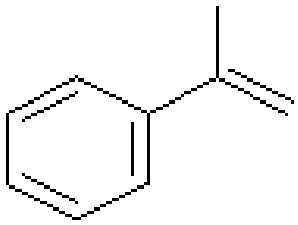

Figure 1: Repeat unit of α-methylstyrene

1.1.2.2 4-cyano-α-methylstyrene

The living anionic polymerization of 4-cyano-α-methylstyrene was carried out in tetrohydrofuran at -78 degrees Celsius with various initiators [18] and shows similar behavior to the reversible polymerization of α-methylstyrene. The heat of polymerization is -7.64 ± 0.5 $kcal/mol$ and the corresponding entropy is -25.5 ± 1 $kcal/molK$. The ceiling temperature for a $1M$ solution is 27 ± 3 degrees Celsius. The kinetic study shows that the apparent rate constant is:

$$\log k_p = -1.83 * 10^3/T + 5.741/mols \ , \tag{3}$$

and the activation energy is 3.6 ± 0.2 $kcal/mol$ [19] which is a little bit smaller than the activation of α-methylstyrene because of the electron-withdrawing group. The rate of polymerization is much slower than that of α-methylstyrene due to the use of lithium naphthalenide. Under the same conditions of polymerization as α-methylstyrene, 4-cyano-α-methylstyrene

has only 12% conversion at -78 degrees Celsius after 2 hours, and 61% conversion after 48 hours. The SEC result shows that this polymer has a sharp and narrow molecular weight distribution, indicating that there are no termination reactions happening.

Different initiators would also affect the reaction rate. For 4-cyano-α-methylstyrene, potassium naphthalenide and cesium initiators accelerate reaction rates much faster than when lithium naphthalenide is used, which is contrary to α-methylstyrene [18].

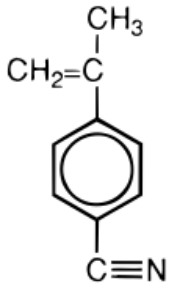

Figure 2: Repeat unit of 4-cyano-α-methylstyrene

1.1.2.3 Tetrahydrofuran

Polymerization of tetrahydrofuran using the catalyst p-chlorophenyldiazoinum hexafluorohosphate ($p - C_lC_6H_4N_2PF_6$) has proved to be a cationic polymerization without termination and transfer [20]. Dreyfuss has studied the conversion as a function of time and temperature. Compared to α-methylstyrene, this polymerization only requires one initiator molecule to form the propagating species. By using this initiator, it has been found that the distribution could be broadened from the Poisson distribution to a Flory distribution with a larger polydispersity. The possible factors that affect the distribution are: equilibrium effects, chain transfer reactions, slow initiation reactions and ion pair structure [21]. The activation energy for this reaction is $51kJ/mol$.

1.1.2.4 4-vinylbenzocyclobutene

Polymerization of 4-vinylbenzocyclobutene with the initiator sec-butyllithium at room temperature was studied by Mays [3]. A linear first-order semi-logarithmic time-conversion plot was obtained and indicated that there is no termination reaction. The molecular weight as

a function of conversion is linear, indicating there is no transfer reaction (the number of the polymers remains constant all the time). The UV-vis spectrum of the living polymerization shows two absorbance bands for a long time. This indicates that the concentration of the propagating species remains constant during polymerization. By plotting Mw/Mn as a function of conversion, the MWD is narrow. As the polymerization time increased, the monomer conversion and number-average molecular weight increased. The concentration of the initiator is $7.7e-4mol/l$ and the initial monomer concentration is $0.24mol/l$ at room temperature. This reaction is an irreversible polymerization.

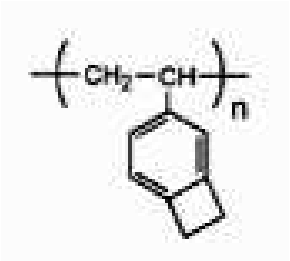

Figure 3: Repeat unit of 4-vinylbenzocyclobutene

1.1.2.5 styrene

Polymerization of styrene with initiator sec-butyllithium in cyclohexane in a temperature range of 10-60 degree Celsius was studied by Schubert [22]. The activation energy for this reaction is $63KJ/mol$. Chang [4] also studied this experimental system using SEC and temperature gradient interaction chromatography (TGIC) and found the TGIC method is more accurate. The initiator concentration is $0.00048M$ and the monomer concentration is $0.29M$. This is an anionic polymerization process.

1.2 Stochastic models and reaction dynamics

"An actual polymer molecule is an extremely complex mechanical system with an enormous number of degrees of freedom. To study the detailed motions of this complicated system and their relations to the non-equilibrium properties would be prohibitively difficult. As a result, it has been customary for polymer scientists to resort to mechanical models to simulate the mechanical behavior of the macromolecules."

The above statement made in 1987 by Hassager [23] told us that it is not necessary to include all degrees of freedom and chemical interactions of a realistic chain to simulate polymer systems. To make the simulation possible, one has to reduce the complexity and make the computation time feasible. The reduction of the complexity of the model is called coarse-graining. The most accurate way to describe the time evolution of a system of chemically reacting molecules is to do a molecular dynamics (MD)simulation. The level of detail information obtained from MD is determined by the complexity of the force field. If there is a large separation of time scales governing the motion of different component of the system, Brownian dynamics (BD) becomes a very useful method. For a polymer in a solution, if the detailed motion of solvent molecules is not of interest, the motion of solvent molecules can be removed from the simulation and their effect can be represented by a dissipative and random (stochastic) force term. This elimination allows one to investigate the polymer dynamics on longer time scales, thus Newton's equations of motion will become the Langevin equation.

The chemical reaction can be described as an effective particle moving on a potential characterized by two (or more) adjacent wells separated by a barrier [24, 25, 26, 27, 28, 29]. In Kramer's model [24], a particle is trapped in a one-dimensional well which is separated from another well by a barrier height. He assumed that the particle is immersed in a medium such that the medium exerts a friction force on the particle, but at the same time activates the particle so that the particle can gain enough energy to escape from the well. Kramer found the rate of escape of the particle from the well over the barrier. Also, the barrier crossing dynamics at low and high friction are different. At very low friction, the rate is limited by the energy diffusion process. The escape rate is increased with friction. On the contrary, at high friction, the over-damped regime, the rate is limited by the spatial diffusion process, the escape rate is decreased with the the increase of static friction. Kramer didn't obtain a single theory valid for the entire friction regime. This is the Kramer turnover problem. He did realize that there is a maximal rate for a intermediate friction. Many attempts have been made to provide a single expression to link these two friction limits [30, 31]. In 1986, Pollak found that the Kramer's expression can be derived from transition

state theory (TST) which leads to the solution of the Kramer's turnover problem [32, 30, 33].

Transition state theory (TST) uses the flux over population method to derive the rate of passage over the barrier. TST theory relates the reactant with product through the barrier height. This works for reactions in the gas phase. For reactions with solvent, it overestimates the rate of systems at the low-friction regime and high-friction regime because it does not consider the particle recrossing the barrier. To correctly describe a chemical reaction, one could use the Fokker-Planck equation. By solving the Fokker-Planck equation one obtains distribution functions from which any average of macroscopic variables are obtained by integration. An alternative way is to use the Langevin equation proposed by Kramer in 1940. It can be used to describe the time evolution of the motion of Brownian particles in a potential. The potential relates the reactant, product and transition state complex.

By using the Langevin equation to describe a chemical reaction such as a polymerization process, one has to assume the tag molecule is larger than the solvent molecules, so there is no memory left after the tagged particle and solvent particles collide. If the molecules are all the same size in the system, then one has to consider the memory effect. The Langevin equation can be generalized by taking into account this variation by introduction of space-dependent friction [34, 35, 36, 37]. Besides modifying the friction kernel, another way to include more complex interactions with the environment is to modify the potential of mean force (PMF).

1.3 Polymerization Dynamics

1.3.1 Equilibrium Polymerization

Equilibrium polymerization has been used to describe not only linear polymers, but also nonlinear aggregation such as micelles, networks, and other kinds of clustering processes and collective assembles. The term "equilibrium polymerization" includes reversible polymerization and processes approaching equilibrium [38]. According to Tobolsky [39], polymerization equilibrium processes can classified as equilibrium polymerization reaction whether the reaction requires initiators or not. The polymerization of e-caprolactam initiated by water, amine or organic aids and some cases of cationic and anionic polymerization of vinyl

monomers are examples of polymerization with initiators. Thermal polymerization of sulfur, certain types of equilibrium vinyl polymerization, and the polymerization of rings to larger rings are examples of reactions that proceed without initiators. To specify equilibrium from the experimental view, equilibrium concentrations of monomers, the equilibrium number average degree of polymerization and the equilibrium concentration of initiator are the important measurable quantities.

Equilibrium polymerization can be considered to be a phase transition. This was proved by Oosawa [40, 41, 42], Ivin [43], Semenchenko [44] and Wheeler [45]. Monomers in the solvent are in one phase, and polymers in equilibrium with monomers in solvent are in another phase. As the system moves back and forth between these two phases, polymer length increases or decreases. The thermodynamic properties of amorphous polymer phases were calculated by Flory [46], Meyer [47], and Huggins [48] using statistical mechanical methods. These calculations count the number of conformations of each polymer and the number of configurations of a specified polymer. Flory studied semi-flexible linear chains whose stiffness arises exclusively from intramolecular nearest neighbors [49, 50] and Gibbs got a more general formula to describe the properties of polymers which incorporates the chain stiffness and the variation of volume with temperature [51, 52]. Except these quasi-lattice models for fixed-length polymers, there are also some approaches to study the growth of polymers and polymers with variable bond lengths [39]. N$\rightarrow$ 0 vector model[45] and Freed's lattice model[16] are two popular models to study the properties of equilibrium polymerization.

1.3.1.1 n$\rightarrow$ 0 Vector Model

In the n vector magnet model, n refers to the dimension of the order parameter of the magnetic phase transition. For a polymer system where n$\rightarrow$ 0, the n vector magnet model can be mapped to a lattice model of equilibrium polymerization. In 1972, de Gennes proved that the partition function for a very long polymer chain in a good solvent is equivalent to the partition function for a magnet that has a magnetic moment with 0 dimension [53]. In 1975, des Cloizeaus also showed that the two partition functions are equivalent in an

external magnetic field when n$\rightarrow$ 0 [54]. The relation between the "magnetic" problem and the polymer problem was also addressed by Sarma [55].

For a system of N vector spins located on the sites of a three-dimensional lattice, the Hamiltonian is:

$$H = -J \sum_{<i,j>} \mathbf{S}_i \mathbf{S}_j - m_0 H \sum_i S_i^{(1)} \ , \tag{4}$$

where S_i, S_j are the nearest neighbor spins, and $S^{(1)}$ is the component parallel to the field. $\mathbf{S}$ is the classical n-component vector spin with length $n^{1/2}$.

$$|\mathbf{S}|^2 = \sum_{\alpha=1}^{n} (S^{(\alpha)})^2 = n \ . \tag{5}$$

In the limit of n$\rightarrow$ 0, the partition function Z and free energy f of this model can be written as:

$$Z = e^{Vf} \quad = \quad \sum_{N_b, N_p} (\beta)^{N_b} (h^2)^N \Gamma(N_b, N_p, V) \ ,$$

where V is the volume of total lattice sites, $\beta = J/k\mathbf{T}$ and $h = \mu_0 H/k\mathbf{T}$, $\mathbf{T}$ is the temperature of the reference n-vector model, N_b is the total number of bonds on the lattice, N_p is the number of linear polymers with excluded volume, and $\Gamma(N_p, N_b, V)$ is the number of ways to place polymers on the lattice sites. It has been proved by Wheeler [45] that this n$\rightarrow$ 0 vector model is the same as the earlier Tobolsky-Eisenberg theory of equilibrium theory in the mean field limit. The non-mean field theory requires the value of the entropy and enthalpy. The assumptions made in this model are used to explain the behavior of the different experimental systems described previously. Since pure organic monomer α-methylstyrene is very viscous, the polymerization process usually reacts in solution. If there is solvent, the model would become the dilute n$\rightarrow$ 0 vector model with an additional parameter, polymerization temperature (T_p). The dilute n$\rightarrow$ 0 model gives a little bit better results than the mean field approximation which is evident by comparing the chi-square values. Wheeler and coworkers have studied the polymerization properties such as the heat capacity, mass density, extent of polymerization etc.

1.3.1.2 Freed and Douglas's Lattice Model

Flory-Huggins theory is a simple theory to calculate the free energy of polymer solutions which can be described by a lattice model, where each lattice site is occupied by either solvent or monomers. The thermodynamic properties of the polymer system can be calculated from the free energy. In Freed and Douglas's lattice model, they include the interaction between polymer and solvent, the chain stiffness and variable initiator concentration. The average polymer length L, the fraction of monomers converted to polymers, entropy, specific heat and chain length distribution are calculated. It turns out the stiffness and equilibrium constant won't affect thermodynamic properties. The physical parameters required for this model are the entropy and enthalpy. The chemical reaction for the polymer system with monomer M and initiator I is:

$$2M + 2I \rightarrow M_2I_2 \tag{6}$$

$$M_iI_2 + M \rightleftharpoons M_{i+1}I_2 \ , \tag{7}$$

where M_2I_2 is bi-functional dimer. Conservation of mass requires:

$$n_m^0 = n_m + \sum_{i=2}^{\infty} i n_i \ , \tag{8}$$

where n_m^0 is the number of the initial monomers, n_m is the number of the monomers after polymerization, and n_i is the number of the initiators.

The free energy for this system can be written [16]:

$$\frac{F}{N_l K_B T} = \phi_s \ln \phi_s + \phi_m \ln \phi_m + \sum_{i=2}^{\infty} \frac{\phi_s}{i+2} \ln \phi_i + \phi_s \phi_m \chi + \phi_s \chi \sum_{i=2}^{\infty} \phi_i + \sum_{i=2}^{\infty} \phi_i f_i \ , \tag{9}$$

where the number of lattice sites $N_l = n_s + n_m^0 + n_I$, the mole fraction of monomer $\phi_m = n_m/N_l$, the mole fraction of the solvent $\phi_s = n_s/N_l$, the mole fraction of the initiator $\phi_i = n_i(i+2)/N_l)$, χ is the interaction parameter of the monomer and solvent, f_i is the dimensionless free energy of an i-mer, and k_B is the Boltzmann constant.

Compared to the $n \rightarrow 0$ vector model, this lattice model shows that the relation among the average chain length L, the extent of polymerization, and initial monomer concentration is linear for fixed initiator concentration. It also predicts three different polymerization

lines: the temperature at which the polymer first starts to grow (T_p^x); the true polymerization temperature at which the specific heat has the maximum value and the extent of polymerization shows an inflection point (T_p); and the equilibrium temperature at which the polymer length won't change anymore for fixed initiator concentration.

1.3.2 Non-equilibrium Polymerization

Non-equilibrium polymerization concerns situations where the system under study is not in thermodynamic equilibrium. There are two possible reasons that the system is in a non-equilibrium state: (1)The system is in a steady state and there are external forces acting on the system. (2)The system is in a non-equilibrium state because of the initial conditions. Under both situations, the systems will approach thermodynamic equilibrium after some time.

The usual approach to obtain time-dependent information is performing a molecular dynamics (MD) simulation. Due to the complexity of polymer systems, a stochastic method has been used to study the properties of the polymerization process.

1.3.2.1 Langevin Equation

The Langevin equation is a stochastic differential equation describing Brownian motion in a potential. The difference between the Langevin equation and Newton's equations of motion is that there are two additional forces as shown in the equation,

$$\dot{v} = -\gamma_0 v(t) + \xi(t) - F(t) \, , \tag{10}$$

where $F(t)$ is the mean force, γ_0 is the damping constant or friction coefficient, and $\xi(t)$ is the random force. In this equation, the dissipative force and the random force have been added to approximate the effect of neglected degrees of freedom. The friction force is proportional to the velocity of the particle $v(t)$, and the random force is independent of the motion of the particles. The friction coefficient is related to the fluctuations of the random force by the fluctuation-dissipation theorem:

$$\langle \xi(t)\xi(t') \rangle = 2k_{\mathrm{B}} T \gamma_0 \delta(t - t') \, . \tag{11}$$

Although the Langevin equation is a simple model, it has been used to study polymer translocation through nanopores[56], dynamics of semi-flexible polymers in a flow field, [57] etc.

The Langevin equation was generalized by modifying the friction kernel to account for more complex interactions with the environment. It can be used to model the dynamics of a reactive coordinate in dissipated bath particles. In the generalized Langevin equation (GLE), the friction kernel is extended to include non-local memory so as to model delayed environmental responses to the system. The GLE with position-dependent friction was developed by Carmeli and Nitzan [35].

$$\dot{v} = -\int^{t} dt' \gamma(t,t') v(t') + \xi(t) - F(t) \ , \tag{12}$$

where $v(t)$ is the velocity of the effective particle, $\xi(t)$ is the random force, and $F(t)$ is the external force due to the potential of mean force. The GLE reduces to the Langevin equation if the friction kernel is a delta function.

The GLE, as written above, can not describe the reaction dynamics of a system in a non-equilibrium/time dependent environment because $\gamma(t,t')$ depends on the time difference $(t-t')$ instead of the absolute time. For example, in thermosetting polymerization, the polymerization process causes a dramatic viscosity change with time. Since this viscosity change is time-dependent, it is necessary to include absolute time in the friction kernel. Using a similar construction as that used for the projection of a stationary open Hamiltonian system onto the GLE, a generalized model called the iGLE was developed to describe non-stationary process [58]. The details of this model will be introduced in chapter II.

1.3.2.2 Dissipated Particle Dynamics

Dissipated Particle Dynamics (DPD) [59, 60] is a relatively new method initially developed by Hoogerbrugge and Koelman to simulate the hydrodynamic behavior of colloidal suspensions [61, 62]. The DPD is a coarse-graining procedure that leads to a structure similar to the LE containing random and dissipative force terms. The difference between DPD and the LE is that the random force and the dissipation force are treated pairwise in the DPD method. The most important feature of the DPD forces is that momentum is conserved.

The conservation of momentum by the DPD model allows for the use of this method to describe the hydrodynamic behavior of a fluid at large scales. Large scale systems relax very slowly. They are underdamped for a long time even with a large friction coefficient. Since the coupling of the system with the bath in Langevin dynamics is much stronger than in the DPD method, and we are interested in the PMF in the overdamped regime, we will focus on Langevin dynamics.

1.4 Overview

In chapter II, an irreversible generalized Langevin equation (iGLE) has been introduced to model living polymerization. In this model, the mechanism of living polymerization was included and manipulated by the friction term and potential of mean force (PMF). The friction is a function of the absolute time, and a phenomenological potential of mean force has been used to describe the interaction between an attaching monomer and its partnering polymer. An approximate method for the direct analytic calculation of the PMF is included in Appendix B. A critical assumption involves the treatment of the polymer distribution as obeying an equilibrium distribution—viz., the Boltzmann distribution,—although the process is evidently far from equilibrium. Nevertheless, this short time scale adiabatic-like approximation provides a view of the structure of the PMF. Phenomenological attempts to characterize this behavior as well as the non-equilibrium effects have been fairly successful as described in Chapter II. In particular, non-equilibrium properties such as polymer length, the polymer length distribution, and polydispersity index (PDI) have been captured by these models.

The thermodynamics and kinetics of the living polymerization system α-methylstyrene has been extensively studied by Greer and coworkers [63, 2, 1]. They measured phase equilibrium, the extent of polymerization, the chemical kinetics and molecular weight distribution. It is the best example for the study of reversible equilibrium polymerization. Other anionic living polymerization systems include polymerization of 4-vinylbenzocyclobutene with initiator sec-butyllithium at room temperature and the polymerization of styrene with the same initiator in cyclohexane. The common feature for these three systems is that there

are no transfer and termination reaction under the experimental conditions described. The latter two systems show simple kinetics. The target questions to be addressed in this work include: Can the kinetics be predicted using the iGLE? How should the time scale be identified and used to describe the polymerization process? By predicting the kinetics, can one gain more understanding about these polymerization process?

In chapter III of this work, we use available experimental data to validate the iGLE model. The results that we have obtained are consistent with kinetic theory and provide a easy way to calculate the dynamics under different temperatures with the identical experimental conditions such as the concentration of monomers and initiators (for α-methylstyrene).

In chapter IV, a stochastic model will be introduced based on the diffusion rate theory. This model was used to study the diffusion effect of anionic polymerization. We applied this model to α-methylstyrene and found that the polymerization is a kinetically controlled process indicating that diffusion effects play a small role in this polymerization.

In chapter V, we study the effect of friction on equilibrium properties using an analytical method. We start from the iGLE Hamiltonian, and then obtain Hamilton's equation of motion. We use a double well potential as a example and found that the friction stretches the double well and the minima change under certain conditions.

In the last chapter, the results of this study will be summarized. We studied the properties of living polymerization in a non-equilibrium environment by using two different models. Also, we use an analytical method to investigate whether the equilibrium properties were affected by the friction. We also show how to get an analytical form of the PMF. The future work includes developing models to describe living polymerization with a high activation energy, and to develop the irreversible chemical Langevin equation by including memory effects to describe the diffusion effects of living polymerization.

CHAPTER II

IGLE AND LIVING POLYMERIZATION

2.1 Introduction

Using Langevin and generalized Langevin equations to describe the stochastic motion along a projected coordinate assumes that the environment is stationary during the dynamic process and obeys the fluctuation-dissipation theorem [64, 65, 66, 67, 68, 69]. But in most cases, the response of the environment is not the same and changes during the reaction. To include this non-stationary environment response, one can use the irreversible generalized Langevin equation (iGLE):

$$\dot{v} = -\int^{t} dt g(t)g(t')\gamma_0(t-t')v(t') + g(t)\xi_0(t) - F(x,t) \ , \tag{13}$$

where the first term is the friction force resulting from the memory of the particle's velocity at earlier time by the environment, the second term is the random force resulting from the projection of the fluctuating force due to the bath modes, and the last term is the uniform force due to the potential of mean force (PMF) that results from the projection of all the bath particles. The random force $\xi(t)$ is balanced by the friction according to the fluctuation-dissipation theorem

$$\langle \xi(t)\xi(t') \rangle = k_{\mathrm{B}} T g(t)g(t')\gamma_0(t-t') \ . \tag{14}$$

Since since iGLE has been developed, it has been explored in many ways. It has shown that the iGLE is the projection of an explicit time-dependent open Hamiltonian system [58], and numerical simulations of this mechanical system indicate that the time-dependent observed total energy and the solvent force correlation are equivalent to the projected iGLE [70]. This model has been used to study the dynamics of thermosetting polymerization where polymerization ends due to the diffusion-limited mechanism [71]. In this model, the nonstationary environment response was included by a R dependent dissipation term through $g(t)$. Without an extension of the iGLE, it is impossible to describe living polymerization because

of the different mechanism. The polymerization will be quenched due to the depletion of the monomers and the number of polymers are limited by the number of the initiators. Because of this living polymerization has some unique properties. Although ideally, the growth of living polymers will stop when there are no monomers in solution, in most cases, the extent of polymerization is less than 100% due to steric hindrance or chemical equilibrium. This new mechanism should be included either through the friction kernel, or more accurately, through $g(t)$, or/and through modifying the potential of mean force.

The Potential of Mean Force (PMF) was first introduced by Kirkwood in 1935 [72]. For a system with N molecules, the average force acting on a particle j is dependent on the density and configurations of all the other molecules. The definition of the PMF is:

$$-\nabla_j w^n(q_1, q_2 \cdots q_n) = \frac{\int \exp^{-\beta V}(-\nabla_j V) dq_{n+1} \cdots dq_N}{\int \exp^{-\beta V} dq_{n+1} \cdots dq_N} \, , j = 1, 2, \cdots, n \tag{15}$$

where $\nabla_j w^{-n}$ is the average force acting on molecule j, w^n is the potential of mean force (PMF) in a projected subsystem consisting of n molecules, $\beta = q/k_B T$, k_B is Boltzmann's constant and T is the absolute temperature.

The PMF can be used to determine how the free energy changes as a function of the coordinates of the system. The double well potential has been used to describe simple chemical reactions. The biased potential is one of the simple potentials used in the study of polymers:

$$V(R) = -f_b R \, , \tag{16}$$

where R is the reaction coordinate and f_b is a constant external force. Another phenomenological potential called the polymer growth potential is constructed based on a series of merged double well potentials with barrier heights and an external force. Suppose the well frequency is the same as the barrier frequency, then the PMF is written as:

$$V'_{PMF}(R) \equiv \begin{cases} \frac{1}{2}\omega_0^2 (R - nl)^2 - f_b(n-1)l \\ \text{for } R < R'_m + 1/2l \text{ with } n = 1 \text{ or } R'_m + (n - 1/2)l < R < R'_m + nl; \\ \frac{1}{2}\omega_0^2 (R - nl - 2R'_m)^2 - f_b(n-1)l + E_+^\dagger \\ \text{if } R'_m + nl < R < R'_m + (n + 1/2)l \end{cases} ,$$

where R'_m is the relative position of the potential

$$R'_m = \frac{l}{4} - \frac{f_b}{\omega_0^2} \,, \tag{17}$$

and ω_0 is the frequency.

$$\omega_0 = 2f_b(2E_+^\dagger + f_b E_+^\dagger - 2E_+^\dagger\sqrt{1+f_b l})^{-1/2} \,, \tag{18}$$

where l is the monomer length and $E^\dagger$ is the barrier height in the forward reaction. This PMF is an extension of the double well model of Straub et.al [73]. Also included in the PMF is the self-similarity of the polymer. Without the barrier height, the polymer PMF becomes a biased potential.

To connect the iGLE with living polymerization, we have to modify the iGLE, obtain the properties of living polymerization and compare it to the experiments. To the best of our knowledge, no one has used the generalized Langevin equation (GLE) or irreversible generalized Langevin equation (iGLE) to study the dynamics of living polymerization.

2.2 iGLE and Modified Friction Kernel

Living polymers are known to quench when the monomers are used up. If one considers the self-similarity when monomers add to the activate end of the chain during the polymerization process independent of polymer length, the potential of mean force (PMF) can be approximated by a series of harmonic oscillators. First, we will consider a modification of the friction kernel. The difference between the GLE and iGLE is the form of the friction kernel and random force. The iGLE has the function $g(t)$ included in the friction kernel and random force. This $g(t)$ characterizes the irreversibility in the non-equilibrium environment. Before polymerization, $g(t)$ has to be 1 since the system is in equilibrium. At this time, the GLE is recovered. Once polymerization starts, the chain grows fast at the beginning and then slows down. Based on these conditions, a new form of $g(t)$ has been constructed:

$$g(t) = (1 - \frac{A}{N}\int dR(R/l)P(R;t))^{-\zeta} \,, \tag{19}$$

where A is the number of activated monomers, N is the number of total monomers, $P(t)$ is the normalized probability distribution of polymers of a given R at time t, R/l is the

effective number of monomers for a polymer with contour length R, and ζ is a scaling factor used to characterize the effect of diffusion rate during the polymerization process and it is a function of temperature. This $g(t)$ specifies the dynamics of the iGLE. Now we will use the polymer growth PMF shown in Eq.(17) and the above $g(t)$ to do numerical simulations. The bottom figure in Figure 4 is a plot of $g(R)$ as a function of the average polymer length R. As polymer grows longer, the friction, vis-a.vis $g(t)$ increases to a very large value because there are increasingly fewer monomers available in the solution. The top of Figure 4 shows the polymer length as a function of time with the parameters: $A = 128, N = 102340, \zeta = 3.5, \gamma_0 = 0.15, f_b = 10, E^{\dagger} = 5k_BT$(top). The number of the activated monomers and the total number of monomers are obtained based on the concentration of the initiators and monomers. Here we choose the mole fraction of monomer to be 0.14680, the ratio of mole fraction of initiator to the mole fraction of monomer to be 0.0025, and the concentration of monomer to be $1.7M$. These data are from Greer's experiment, but assume the initiator only has one active site. It shows the polymers grow fast at the beginning and then slow down after a longer time. It is hard to tell when the polymerization process stops, that is, when the friction quenches the solvent response. To accelerate this process, we decrease the value of ζ. In Figure 5, the bottom figure is a plot $g(t)$ vs.$\langle R\rangle$. The top figure shows the polymer length as a function of time with the parameters: $A = 128, N = 102340, f_b = 10, E^{\dagger} = 5k_BT, \zeta = 0.7, \gamma_0 = 10$. In this simulation, it shows that polymerization quenched around 799 with a very high friction. So what we want to do next is to find out the shape of the potential of mean force in the high friction limit. From the shape of the PMF, we can estimate when polymerization is quenched.

In the above numerical simulations, the mass of the monomers has been set to unity and the size of the monomers is taken to be 1 for simplicity. The use of dimensionless units gives a dimensionless time scale. Using dimensionless units of parameters in the simulation is a useful way to obtain a general physical understanding of the system behavior, but if one wants to relate the simulation results with experimental data, the dimension of the units has to be determined. In the next chapter, we will talk about how to identify the time scale if we want to use a Langevin type equation with dimensionless units to describe the

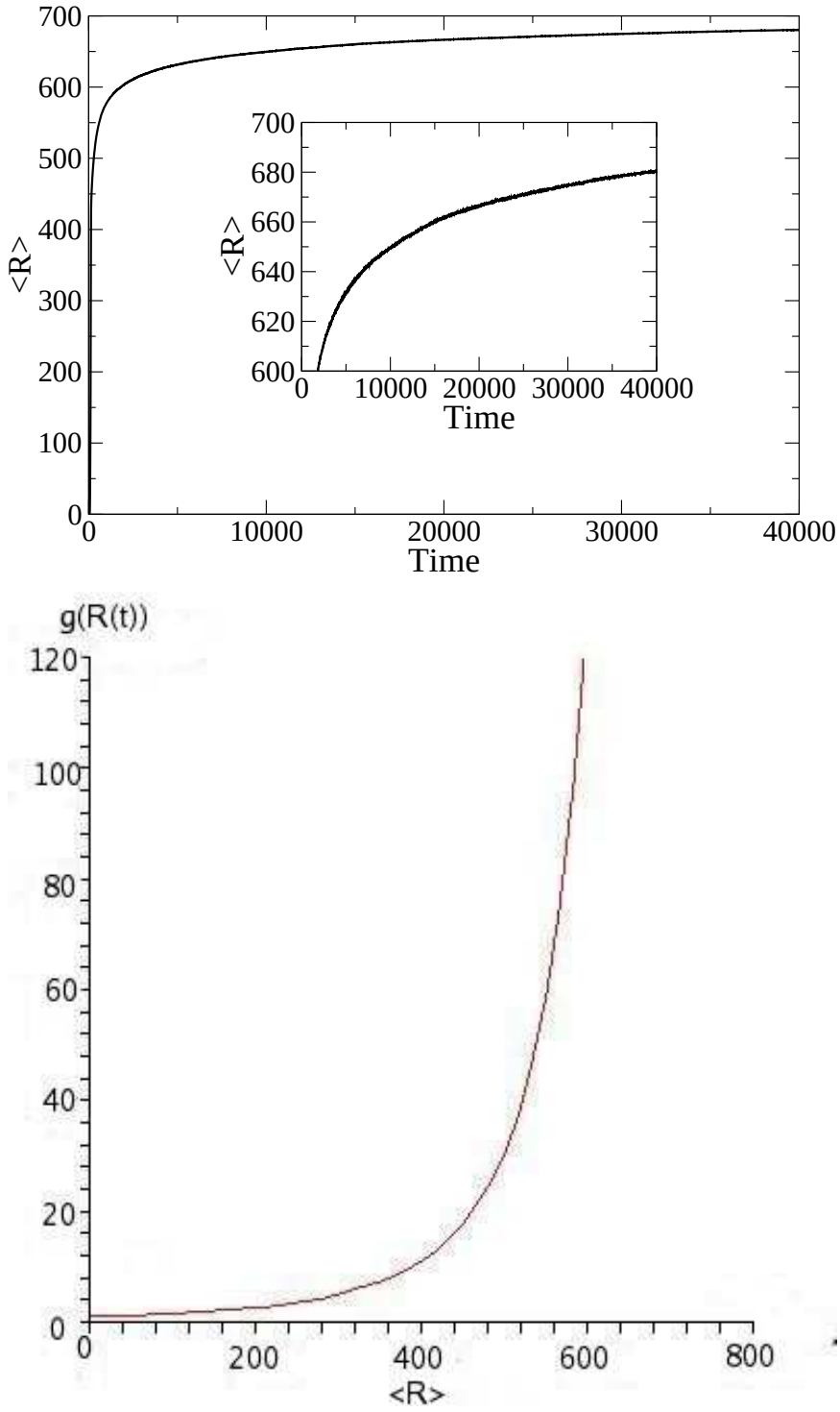

Figure 4: Polymer length as a function of time with $A = 128, N = 102340, \zeta = 3.5, \gamma_0 = 0.15, E^{\dagger} = 5k_BT$, all in arbitrary units. In this simulation, the merged harmonic PMF was used and the shape of $g(R(t))$ shown in the bottom figure. This $g(R(t))$ appears in the friction kernel and random force of the model and specify the dynamics. The inset of the top figure clearly shows that the polymers continue grow after a long time.

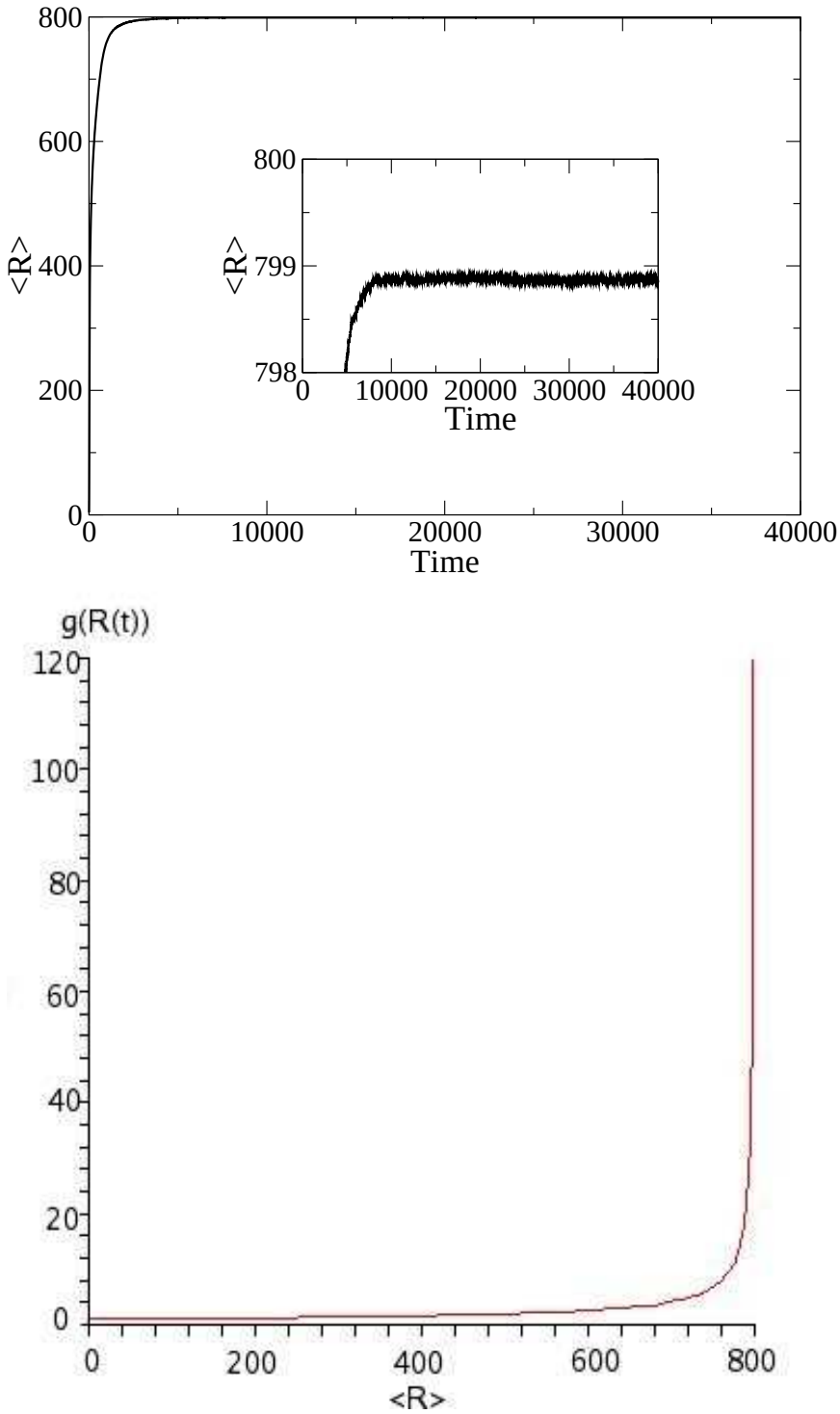

Figure 5: Polymer length as a function of time with $A = 128, N = 102340, \zeta = 0.7, \gamma_0 = 10.0, E^{\dagger} = 5k_BT$, all in arbitrary units. In this simulation, the merged harmonic PMF was used and the shape of $g(t)$ shown in the bottom figure. This $g(R(t))$ appears in the friction kernel and random force of the model and specify the dynamics. The inset of top figure clearly shows that the polymers stop growing when there is no monomers left in the solutions.

polymerization process.

2.3 Potential of Mean Force by Elimination of the Fast Variables

As we mentioned before, the potential of mean force is important to know since it can help to explain the results and provides a deep understanding from the simulations. Usually it is very hard to get the exact PMF using an analytical method. The most common way to do this is to make assumptions to simplify the problem. One way to simplify the iGLE is to ignore the memory. The other way is to eliminate the irrelevant variables. One simple elimination procedure consists of setting the time derivative of the fast variables equal to zero. If the random force is position dependent, then it is necessary to consider an alternative elimination procedure [74]. The iGLE shown in Eq. 13 is a general form. To describe polymerization reaction, $g(t)$ has to be a function of the polymer length R and is written as $g(R(t))$. The iGLE becomes the irreversible Langevin equation (iLE) if the memory is ignored. The iLE can be described by the equations of motion for the momentum p and position q of the Brownian particles:

$$\frac{dq(t)}{dt} = p(t) \ , \tag{20a}$$

$$\frac{dp(t)}{dt} = -\lambda(q(t))p(t) - \phi'(q(t)) + g(q(t))\xi(t) \ , \tag{20b}$$

where $\phi(q(t))$ is the potential energy surface of the particle, λ is the friction coefficient, $\phi'(q(t))$ is the derivative of ϕ with respect to q and the random force is assumed to be Gaussian white noise with zero mean and correlation

$$\langle \xi(t)\xi(t') \rangle = 2\delta(t - t') \ . \tag{21}$$

The fluctuation dissipation theorem relates $g(q)$ and $\lambda(q)$ by

$$g(q)^2 = k_B T \lambda(q) \ . \tag{22}$$

To eliminate p, one has to integrate Eq 20b:

$$p(t) = -\int_0^t e^{-\int_s^t \lambda(q(t'))dt'} \phi(q(s))' ds + \int_0^t e^{-\int_s^t \lambda(q(t'))dt'} g(q(s))\xi(s) ds \ , \tag{23}$$

The two terms in the above equation are of order λ^{-1} and $\lambda^{-1/2}$. To simplify the memory kernel, $\lambda(q(t'))$can be expanded as follows:

$$\lambda(q(t')) = \lambda(q(t)) - \frac{d\lambda(q(t))}{dq(t)}(q(t) - q(t')) + \dots \ , \tag{24}$$

where $q(t) - q(t')$ can be expressed as:

$$\begin{aligned} q(t) - q(t') &= -\int_{t'}^{t} ds' \int_{0}^{s'} e^{-\int_{s}^{s'} \lambda(q(t''))dt''} \phi'(q(s))ds \\ &+ \int_{t'}^{t} ds' \int_{0}^{s'} e^{-\int_{s}^{s'} \lambda(q(t''))dt''} g(q(s))\xi(s)ds \ . \end{aligned} \tag{25}$$

Substituting Eq. 25 into Eq. 24,we obtain

$$\begin{aligned} \lambda(q(t')) &= \lambda(q(t)) - \frac{d\lambda(q(t))}{dq(t)} \int_{t'}^{t} ds' \\ &\times \int_{0}^{s'} e^{-\int_{s}^{s'} \lambda(q(t''))dt''} g(q(s))\xi(s)ds + O(\lambda^{-1}) \\ &= \lambda(q(t)) + O(\lambda^{-1/2}) \ . \end{aligned} \tag{26}$$

With the large friction coefficients λ, the following result is obtained :

$$\begin{aligned} e^{-\int_{s}^{t} \lambda(q(t'))dt'} &= e^{-\int_{s}^{t} \lambda(q(t))dt'} \times e^{-\int_{s}^{t} O(\lambda^{-1/2})dt'} \\ &= e^{-\lambda(q(t))(t-s)}[1 + O(\lambda^{-1/2})] \ . \end{aligned} \tag{27}$$

Similarly $g(q)$ and $\phi(q)$ can be expanded as $\lambda(q)$:

$$\begin{aligned} g(q(s)) &= g(q(t)) - \frac{dg(q(t))}{dq(t)} g(q(t)) \int_{s}^{t} dt' \\ &\times \int_{0}^{t'} e^{-\lambda(q(t))(t-t')} \xi(s')ds' + O(\lambda^{-3/2}) \ , \end{aligned} \tag{28}$$

$$\phi'(q(s)) = \phi'(q(t)) + O(\lambda^{-2/3}) \ . \tag{29}$$

Substituting the above three equations into Eq. 20b, the basic stochastic equation can be obtained:

$$\begin{aligned} \dot{q}(t) &= -\frac{\phi'(q(t))}{\lambda(q(t))} + g(q(t)) \int_{0}^{t} e^{-\lambda(q(t))(t-s)} \xi(s)ds \\ &- \frac{dg(q(t))}{dq(t)} g(q(t)) \int_{0}^{t} e^{-\lambda(q(t))(t-t')} \xi(t')dt' \\ &\times \int_{t'}^{t} ds \int_{0}^{s} e^{-\lambda(q(t))(s-s')} \xi(s')ds' + O(\lambda^{-3/2}) \ . \end{aligned} \tag{30}$$

The second term of the above equation can be approximated as:

$$\begin{aligned}\bar{\xi}(t) &= \int_0^t e^{-\lambda(q(t))(t-s)}\xi(s)ds \\ &\simeq \frac{\xi(t)}{\lambda(q(t))} + O(\lambda^{-2}) \ . \end{aligned} \tag{31}$$

For particles with density $\rho(q,t)$, the conservation law requires:

$$\frac{\partial \rho}{\partial t} + \dot{q}\frac{\partial \rho}{\partial q} = 0 \ . \tag{32}$$

Substituting Eq. 30 into the above equation,

$$\begin{aligned}\frac{\partial \rho(q,t)}{\partial t} &= -\dot{q}(t)\frac{\partial \rho}{\partial q} \\ &= \frac{\partial}{\partial q}\frac{\phi'(q)}{\lambda(q)}P(q,t) - \frac{\partial}{\partial q}\frac{g(q)}{\lambda(q)}\xi(t)\rho(q,t) \\ &+ \frac{\partial}{\partial q}\frac{\partial g(q)}{\partial q}g(q)\int_0^t e^{-\lambda(q)(t-t')}dt' \\ &\times \int_{t'}^t ds\int_0^s e^{-\lambda(q)(s-s')}ds'\xi(t')\xi(s')\rho(q,t) \ , \end{aligned} \tag{33}$$

Now taking the average of Eq. 30 over the stochastic force with $P(q,t) = \langle \rho(q,t)\rangle_\xi$,we obtain:

$$\begin{aligned}\frac{\partial P(q,t)}{\partial t} &= \frac{\partial}{\partial q}\frac{\phi'(q)}{\lambda(q)}P(q,t) - \frac{\partial}{\partial q}\frac{g(q)}{\lambda(q)}\langle \xi(t)\rho(q,t)\rangle \\ &+ \frac{\partial}{\partial q}\frac{dg(q)}{dq}g(q)\int_0^t e^{-\lambda(q)(t-t')}dt' \\ &\times \int_{t'}^t ds\int_0^s e^{-\lambda(q)(s-s')}ds'\langle \xi(t')\xi(s')\rho(q,t)\rangle \ , \end{aligned} \tag{34}$$

where:

$$\langle \xi(t)\rho(q,t)\rangle = -\frac{\partial}{\partial q}\frac{g(q)}{\lambda(q)}P(q,t) + O(\lambda^{-2}) \ , \tag{35}$$

$$\langle \xi(t')\xi(s')\rho(q,t)\rangle = 2\sigma(t'-s')P(q,t) + \langle \frac{\sigma^2\rho(q,t)}{\sigma\xi(s')\sigma\xi(t')}\rangle \ . \tag{36}$$

Substituting the above two equations into Eq. 34 will lead to the Fokker-Planck equation:

$$\frac{\partial P(q,t)}{\partial t} = \frac{\partial}{\partial q}\frac{\phi'(q)}{\lambda(q)}P(q,t) + \frac{\partial}{\partial q}\frac{g(q)}{\lambda(q)}\frac{\partial}{\partial q}\frac{g(q)}{\lambda(q)}P(q,t) \tag{37}$$

$$+ \frac{\partial}{\partial q}\frac{1}{\lambda(q)^2}\frac{dg(q)}{dq}g(q)P(q,t) \ . \tag{38}$$

Since:

$$g(q)^2 = k_B T \lambda(q) \ , \tag{39}$$

Then:

$$\frac{\partial P(q,t)}{\partial t} = \frac{\partial}{\partial q}\frac{1}{\lambda(q)}\left[\phi'(q) + k_B T \frac{\partial}{\partial q}\right] P(q,t) \ . \tag{40}$$

This Fokker-Planck equation can be used to obtain the correct Boltzmann distribution and a stationary distribution under the nonstationary conditions. It can be rewritten in the following form:

$$\frac{dq}{dt} = -\frac{\phi'(q)}{\lambda(q)} - \frac{1}{\lambda^2} g'(q) g(q) + \frac{g(q)}{\lambda(q)} \xi(t) \ . \tag{41}$$

The second term shows the effect of multiplicative character of the noise in the elimination procedure. By using the simple elimination procedure, that is, setting the time derivative of the fast variables equal to zero, one gets incorrect Boltzmann distributions. Since in the iGLE equation, the random force is space dependent, we have to use this new elimination procedure.

Recall the irreversible Langevin equation (iGLE):

$$\frac{d^2 R}{dt^2} = -\int_0^t dt \tilde{g}(R(t)) \tilde{g}(R(t')) \tilde{\gamma} \frac{dR}{dt} + \tilde{g}(R(t)) \xi(t) - F(R(t)) \ . \tag{42}$$

Since

$$\tilde{\gamma}(t - t') = \tilde{\gamma}_0 e^{\frac{-(t-t')}{\tau}} \ , \tag{43}$$

in the memory-less limit,

$$\tilde{\gamma}(t - t') = 2\Gamma \delta(t - t') \ , \tag{44}$$

where

$$\Gamma = \int_0^\infty \tilde{\gamma}_0 e^{(-t/\tau)} dt = \tilde{\gamma}_0 \tau \ , \tag{45}$$

with the fluctuation-dissipation relation:

$$\langle \tilde{\xi}(t) \tilde{\xi}(t') \rangle = 2 k_B T \Gamma \delta(t - t') \ . \tag{46}$$

The iGLE becomes

$$\frac{dR}{dt} = \frac{F}{\tilde{g}(R)^2 \Gamma} - \frac{g'(R) g(R)}{(\tilde{g}(R)\Gamma)^2} + \frac{g(R)}{\Gamma \tilde{g}(R)^2} \tilde{\xi}(t) \ . \tag{47}$$

This equation has the similar structure as Eq. 41. Substitute the following relation to Eq. 47:

$$g'(R)g(R) = k_B T \Gamma \tilde{g}'(R)\tilde{g}(R) \ , \tag{48}$$

we get the new effective potential under the approximations:

$$U_{eff} = -\int_0^R \frac{F(r)dr}{\tilde{g}(r)^2\Gamma} - \frac{k_B T}{2\Gamma\tilde{g}^2(R)} \ . \tag{49}$$

Now we can plot U_{eff} as a function of polymer length to get the shape of the PMF and compare it to the simulation result. Figure 6 shows what the effective potential of mean force looks like with $A = 128, N = 102340, \zeta = 3.5, \gamma_0 = 0.15, E^{\dagger} = 5k_BT$. The barrier height becomes smaller as the polymers grow longer and eventually it becomes flat. This is why we observed that the polymers grow for a longer time. The reason that we couldn't see the minimum is because the value of $g(R(t))$ is too large. Here we show a different form of the PMF after some time scale transformation. recalling:

$$\frac{dR}{dt} = \frac{F}{\tilde{g}(R)^2\Gamma} - \frac{g'(R)g(R)}{(\tilde{g}(R)\Gamma)^2} + \frac{g(R)}{\Gamma\tilde{g}(R)^2}\tilde{\xi}(t) \ . \tag{50}$$

Multiply both side by $\tilde{g}(R)^2$,

$$\tilde{g}(R)^2\frac{dR}{dt} = \frac{F}{\Gamma} - \frac{g'(R)g(R)}{\Gamma^2} + \frac{g(R)}{\Gamma}\tilde{\xi}(t) \ , \tag{51}$$

and set $d\tau = \frac{dt}{\tilde{g}(R)^2}$,

$$\frac{dR}{d\tau} = \frac{F}{\Gamma} - \frac{k_B T \log g'(R)}{\Gamma} + \frac{g(\tilde{R})\tilde{\xi}(t)}{\Gamma} \ . \tag{52}$$

Now we get the effective potential:

$$U_{eff} = U_{old} + k_B T \log(g(R)) \ , \tag{53}$$

where $U_{old} = -\int_0^R F(r)dr$ and shown in Eq. 2.1. Figure 7 shows the potential of mean force with $\zeta = 3.5$ and $\zeta = 200$. The reason that the top figure doesn't have a minimum is because the second term of Eq. 53 is so small compared to the first term. To make the second term comparable to the first term, we have to adjust the parameter ζ to a big value. This will lead to another problem: the initial friction is so large that it will prevent polymer growth. The above simulation means that the minimum appears when the friction becomes

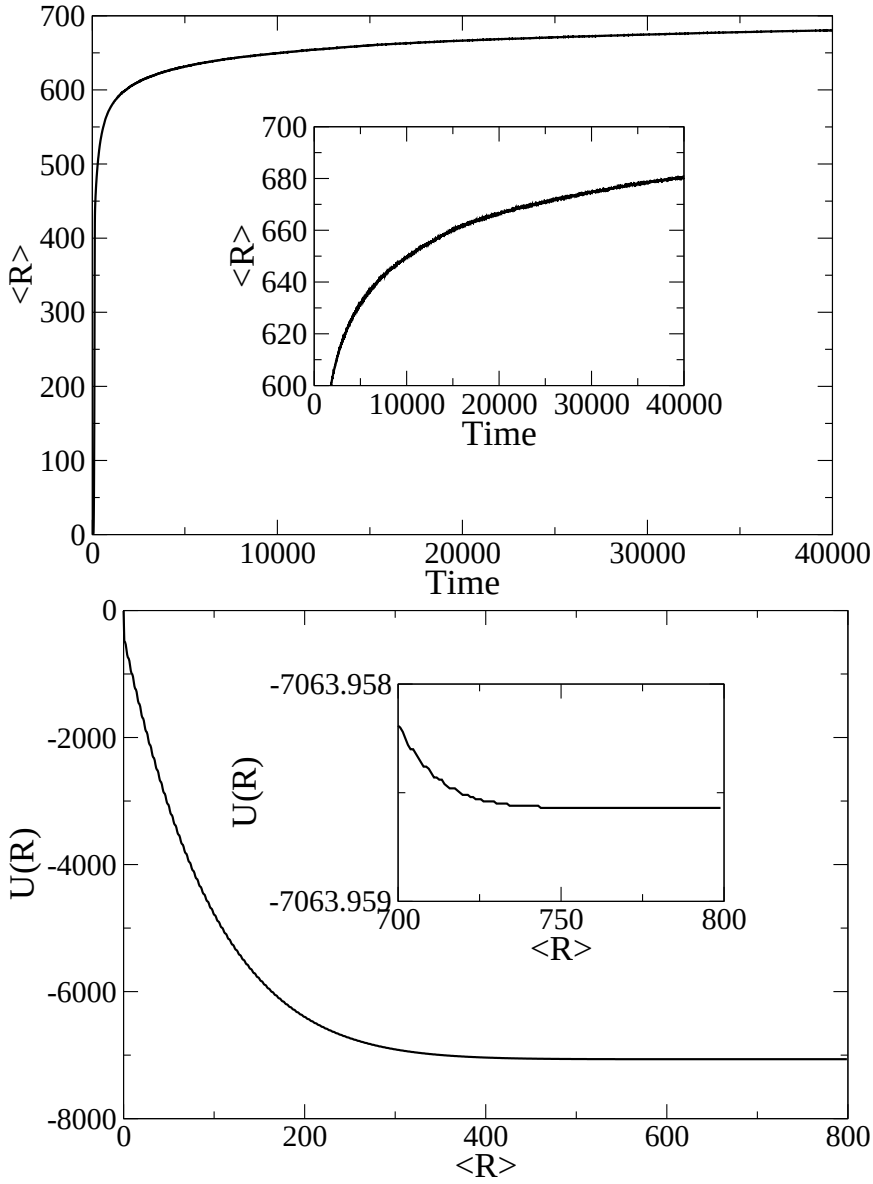

Figure 6: The bottom figure shows polymer length as a function of time with $A = 128, N = 102340, \zeta = 3.5, \gamma_0 = 0.15, E^{\dagger} = 5k_BT$ and the corresponding PMF (Eq. 49) shown in the bottom figure.

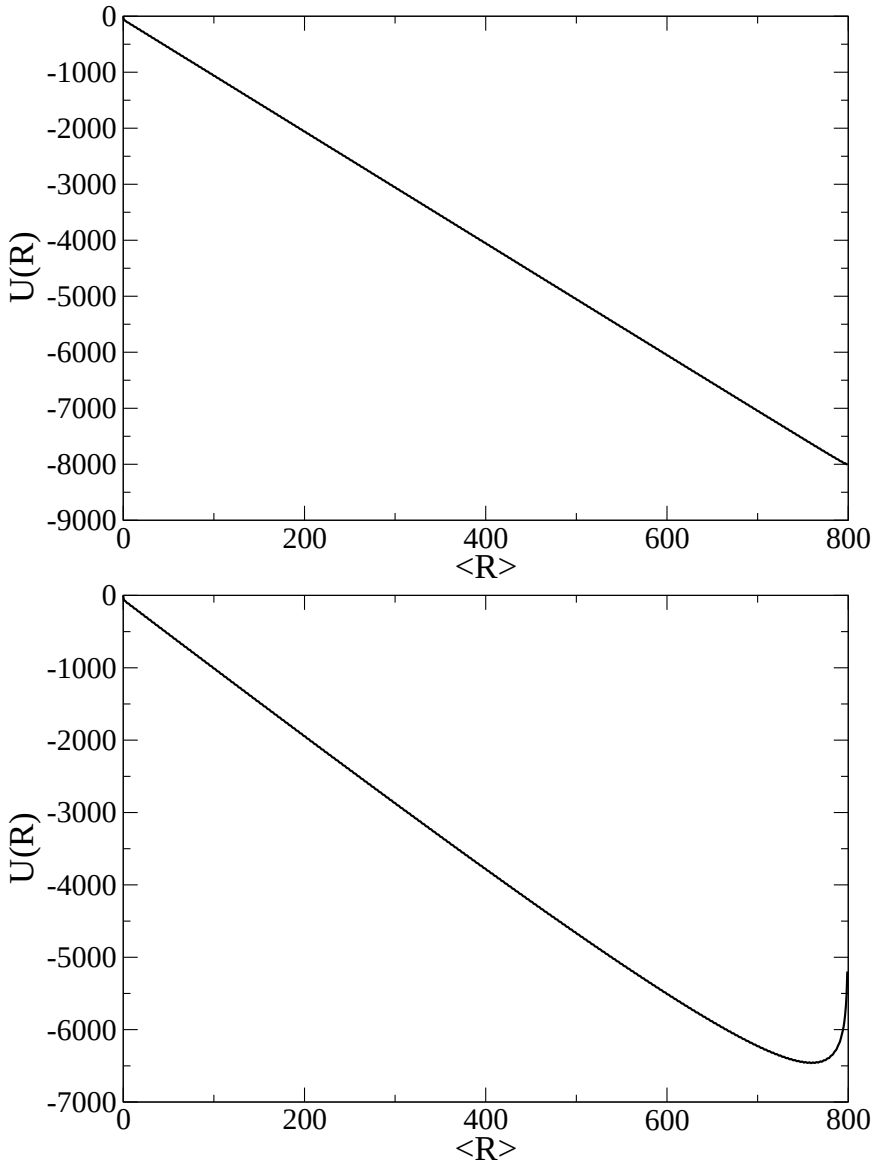

Figure 7: Potential of mean force ((Eq. 53) with $A = 128, N = 102340, \gamma_0 = 0.15, E^{\dagger} = 5k_BT$, in the top figure, $\zeta = 3.5$ and in the bottom figure $\zeta = 200$.

very large and polymerization quenches when there is a minimum. This suggests that we have to modify the PMF in order to simulate the living polymerization process. Possible answers to this question are explored in the following sections.

2.4 iGLE with Modified Friction and Potential

The motivation for suggesting a reformulating of the potential of mean force includes the following: (1) viscosity increases to a large value as the polymer grows longer.(2) the sum of the second and third term has to be comparable with the first term in magnitude in order to get the minimum. (3) the reaction rate slows down and the barrier height increases as the polymerization process proceeds. (4) the possibility to get the available monomers will become zero at a later time even though there are free monomers in the solutions. (5) the longer the polymer, the larger the steric hindrance. It is more difficult for monomers to access the active site. We propose to use the following phenomenological potential:

$$U_{new} = U_{old} + k_B T_0 A R(t) g(R(t)) - k_B T_0 A \int_0^R g(R(t)) dR \ , \tag{54}$$

where U_{old} is the merged potential shown in Eq. 2.1, $g(R(t)) = (1 - \frac{A}{N} \int dR(R/l) P(R;t))^{-\zeta}$, and $k_B T_0$ is the reference temperature with value 1 for simplicity. The corresponding force is:

$$F_{new} = F_{old} - k_B T_0 A R g'(R(t)) \ , \tag{55}$$

where $g'(R(t))$ is:

$$g'(R(t)) = \zeta \left(1 - \frac{A}{N} \int dR(R/l) P(R;t)\right)^{-\zeta - 1} \frac{A}{N} \frac{1}{A} \ . \tag{56}$$

This suggested form satisfies the five aims listed above. For small polymer lengths, the PMF is dominated by the first term shown in Eq. 54. Polymerization proceeds fast at the beginning. As the polymer grows longer, there are few monomers available in solution and reaction slows down because of the friction. The second term starts to play a role as polymer length gets larger. The barrier height increases and it becomes very difficult to have monomers attach to the polymer. Towards the end, the polymerization are quenched due to the high friction and high barrier height.

To use this model to simulate living polymerization, we have to specify the following parameters:

(1) Total number of monomers in the system.

(2) Total number of activated monomers (initiators) in the system.

(3) Solvent friction.

(4) Scaling parameter ζ.

(5) Monomer size l.

(6) The activation energy (barrier height).

(7) f_b, which specifies the relative value of forward and backward energy difference.

(8) Temperature(k_BT). Except (3) and (4), all the other values can obtained from experimental data if it is a well studied system. We will show the procedure of extracting the necessary parameters from experimental data in the following chapter.

To better understand these parameters, we want to look at the effects of solvent friction γ_0 and scaling parameter ζ on polymerization. Figure 8 shows polymer growth as a function of time with $\zeta = 0.9, 1.0, 1.1,\ A = 128, N = 102340, \gamma_0 = 10, E^\dagger = 5k_BT$. As the value of ζ increase, the average length of polymers decrease and the remaining monomers in the solutions increase. The regulation of ζ values changes the shape of the PMF, and the dynamics of the polymerization are also changed. Figure 9 shows the PMF with $\zeta = 0.9$. The minimum of the PMF is around 600 which corresponds to the black curve in Figure 8. Thus by looking at the shape of the PMF, one can learn when friction quenches polymerization.

The solvent friction is an important property. During the polymerization process, the viscosity of the solution increases. The value of γ_0 specifies the friction before polymerization. Figure 10 shows polymer growth as a function of time with $\gamma_0 = 1, 10, 100$, $A = 128, N = 102340, \zeta = 1.1$. As γ_0 increase, the dynamics of polymerization slowed down, and it took a longer time to reach equilibrium. Thus, γ_0 can be used to regulate the growth speed of the polymers and it won't affect the extent of polymerization.

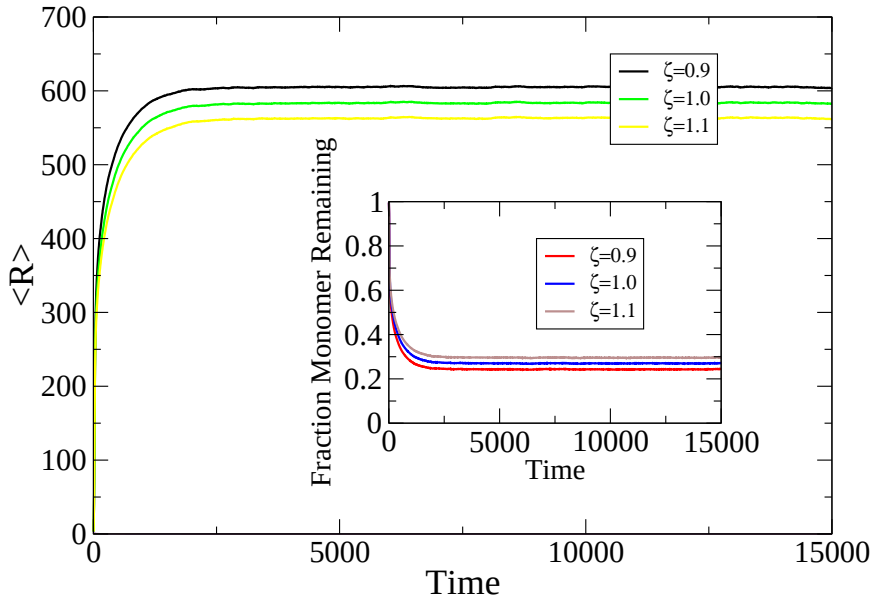

Figure 8: Time dependent polymer growth with $\zeta = 0.9, 1.0, 1.1$, $A = 128, N = 102340, \gamma_0 = 10, E^{\dagger} = 5k_BT$. The inset shows the fraction of monomer remaining as a function of time. The simulation uses the newly developed phenomenological PMF shown in Eq 54.

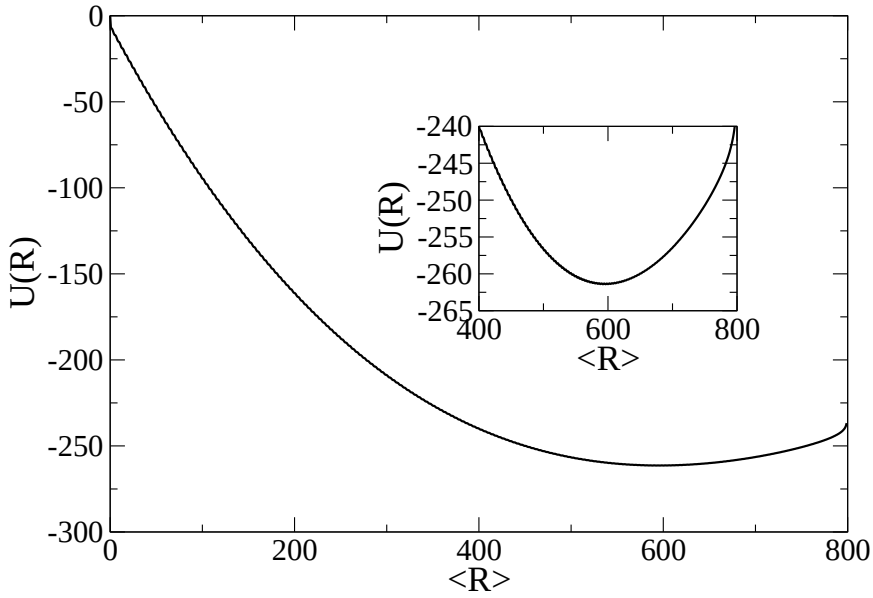

Figure 9: PMF with $\zeta = 0.9, A = 128, N = 102340, \gamma_0 = 10, E^{\dagger} = 5k_BT$. The PMF uses the phenomenological form shown in Eq 54. The inset clearly shown that there is a minimal.

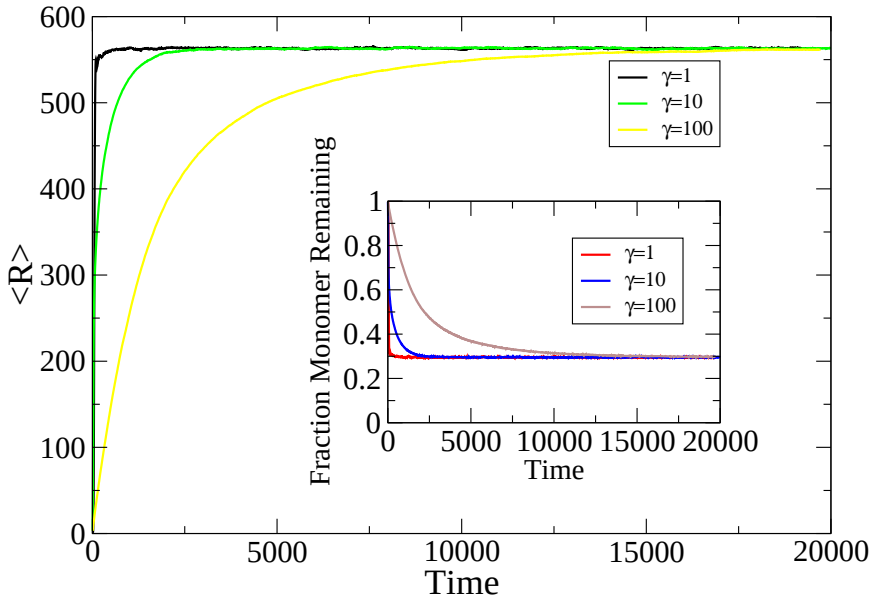

Figure 10: Time dependent polymer growth with $\gamma_0 = 1, 10, 100$, $A = 128, N = 102340, \zeta = 1.1$. The inset shows the fraction monomers remaining as a function of time. The PMF use the phenomenological form shown in Eq 54.

2.5 Discussion and Conclusions

In this chapter, some efforts have been made to describe the living polymerization process. This includes the development of $g(t)$ and the PMF within the context of the iGLE. Firstly, we studied the polymerization dynamics with the iGLE by using a modified $g(t)$ and merged harmonic PMF. By doing so, we assumed the self-similarity of the polymerization. Since the average force acting on the monomer depends on the other monomers, it is necessary to relate the number of the polymers (A), the length of the polymers and the free monomers in the model. It turns out that the friction slows down the reaction, but it doesn't quench the polymerization.

Inspired by the PMF in the high friction limit, we constructed a new phenomenological form of the PMF. This PMF is made a little bit more complicated by including two extra terms. The extra terms are necessary since the interactions between monomers changes during polymerization. Most of the parameters can be derived from experimental data. But there are two extra parameters that need to be specified. One is the solvent friction γ_0, the other is the scaling coefficient ζ. The effects of two parameters γ_0 and ζ on polymerization

have been studied. By modifying the friction kernel and PMF, we get the properties of living polymerization.

In the following chapter, we will show how to identify parameters based on the experimental data, and how to use this model to study experimental systems.

CHAPTER III

APPLICATION TO EXPERIMENTAL LIVING POLYMERIZATION AND THE VALIDATION

In the previous chapter, we have shown that the irreversible generalized Langevin equation can be used to describe the properties of living polymerization systems. In this chapter, We applied this model to simulate the dynamics of some experimental systems such as α-methylstyrene and 4-vinylbenzocyclobutene. This includes identifying the time scales, determining the parameters directly from experimental data and comparing our simulation results with the experimental data.

3.1 Experimental System one: α-methylstyrene

The first system we are interested in is the polymerization of α-methylstyrene which has been experimentally studied by Greer and coworkers [1]. Poly(α-methylstyrene) is a fully flexible linear polymer chain joined by covalent bonds. The kinetics of polymerization near the polymerization line of poly(α-methylstyrene) in the solvent tetrahydrofuran was initiated by sodium naphthalide or cesium naphthalide. In this reaction, an electron is transfered from sodium naphthalide to the α-methylstyrene to form a radical ion, which immediately dimerizes to form the propagating species. The initiation reaction is:

$$2I + 2M \underset{k_1'}{\overset{k_1}{\rightleftharpoons}} M_2^{2-} \ , \tag{57}$$

where I, M, M_2' are the initiator, monomer and activated dimer concentrations with two activated sites. The propagation and depropagation reactions are:

$$M_x^{2-} + M \underset{k_d'}{\overset{k_p}{\rightleftharpoons}} M_{x+1}^{2-} \ , \tag{58}$$

where x is the number of monomers in a polymer. Since this mechanism results in activated dimers with two active sites, the number of propagating polymers in the system is one half

the number of initiators. Table 1 shows the batch samples of living poly(α-methylstyrene) in tetrahydrofuran. Based on the experimental data, it is possible to determine the values of the parameters used in the iGLE model. To use the iGLE to describe living polymerization systems, we have to know the total number of monomers, the total number of initiators, the monomer size, the barrier height, the temperature, the solvent friction and the scaling parameter.

Table 1: Batch samples of living poly(α-methylstyrene) in tetrahydrofuran. x_m^0 is the mole fraction of initial monomer in solvent. $[M_0]$ is the concentration of initial monomer. r is the ratio of moles initiator to moles initial monomer. T_e is the equilibrium temperature for the polymerization. The data listed in the table is taken from Ref. [1]. The rate constants are obtained using the simple kinetic model of Ref. [1].

$Initiator$	x_m^0	$[M_0](mol/l)$	r	$T_e(K)$	$k_p(L/mols)/k_d(s^{-1})$
N_a	0.14680	1.7	0.0025	267	$0.20 \pm 0.01/$
	± 0.00002		± 0.0001		0.085 ± 0.005
N_a	0.145	1.7	0.0024	271	$0.18 \pm 0.01/$
	± 0.001		± 0.0001		0.12 ± 0.01

The number of monomers and initiators can be determined from the monomer concentration, the mole fraction of initial monomers and the mole ratio of initiators to initial monomers. The monomer concentration is $1.7M/l$ which corresponds to 1023400 molecules in a volume of $10^9 \dot{A^3}$. If the mole fraction of the initial monomers in solvent is 0.14680 and the mole ratio of the initiator to the initial monomers is 0.0025, then this corresponds to 2558 initiators. We have 1279 initiators in the system since each activated dimer has two active sites. The size of α-methylstyrene is about $5\dot{A}$ and the molecular weight is $118.18g/mol$. In the iGLE model, the PMF is expressed by the barrier height which is the ratio of the activation energy over thermal energy. The activation energy for this polymerization process is about $20kJ/mol$ and and the deactivation energy is $29kJ/mol$ [75]. The ratio of the barrier height over k_BT is about 9 and k_BT is in a units of kJ/mol. The reference temperature is $120K$ ($k_BT_0 = 1$). These values will be used in the following simulations.

In order to compare the simulation results with the experimental results, we have to

identify the time scale. The time scale for the iGLE is the same as the LE since the function $g(t)$ in the iGLE is dimensionless and it won't affect the time scale from the LE. The Langevin equation (LE):

$$\frac{dv}{dt} = -\frac{dU}{dx} - \gamma v + \xi(t) \; , \tag{59}$$

To make the velocity dimensionless, the following expression is used:

$$\tilde{v} = v\frac{\tau}{l} \; , \tag{60}$$

where $\tilde{v}$ is a dimensionless velocity, v is the velocity with units m/s, τ is time and l is the monomer length.

To make the potential dimensionless, the following expression is used:

$$\tilde{U} = \frac{U}{k_B T_0} \; , \tag{61}$$

where $\tilde{U}$ is dimensionless potential energy, U is the potential energy with units J and $k_B T_0$ is the reference barrier height. U is the barrier height in the model and the reference barrier height $k_B T_0 = 1$ for convenience.

Substitute Eq. 60 and Eq. 61 to Eq. 59:

$$\begin{aligned} \frac{d\tilde{v}}{d\tilde{t}}\frac{l}{\tau^2} &= -\frac{dU}{dx} - \gamma v + \zeta(t) \\ \Rightarrow \frac{d\tilde{v}}{d\tilde{t}} &= -\frac{\tau^2}{l}\frac{dU}{dx} - \frac{\tau^2}{l}\gamma v + \frac{\tau^2}{l}\zeta(t) \\ \Rightarrow \frac{d\tilde{v}}{d\tilde{t}} &= -\frac{k_B T_0 \tau^2}{l^2}\frac{d\tilde{U}}{d\tilde{x}} - \tilde{\gamma}\tilde{v} + \zeta(\tilde{t}) \; . \end{aligned} \tag{62}$$

Compare Eq. 59 and an analog of Eq. 62 in which all the variables are unitless. The following relation which is used to describe the polymerization process has to be satisfied:

$$\begin{aligned} &\frac{k_B T_0 \tau^2}{l^2} = 1 \qquad\qquad (63) \\ &\Rightarrow \tau^2 = \frac{l^2}{k_B T_0} \\ &\Rightarrow \tau^2 = \frac{5\mathring{A}^2}{1kJ/mol} \\ &\Rightarrow \tau^2 = \frac{25 * 10^{-20} m^2}{1000J/6.02 * 10^{23} molecules} \\ &\Rightarrow \tau^2 = 150 s^2 \\ &\Rightarrow \tau \approx 12s \; . \end{aligned}$$

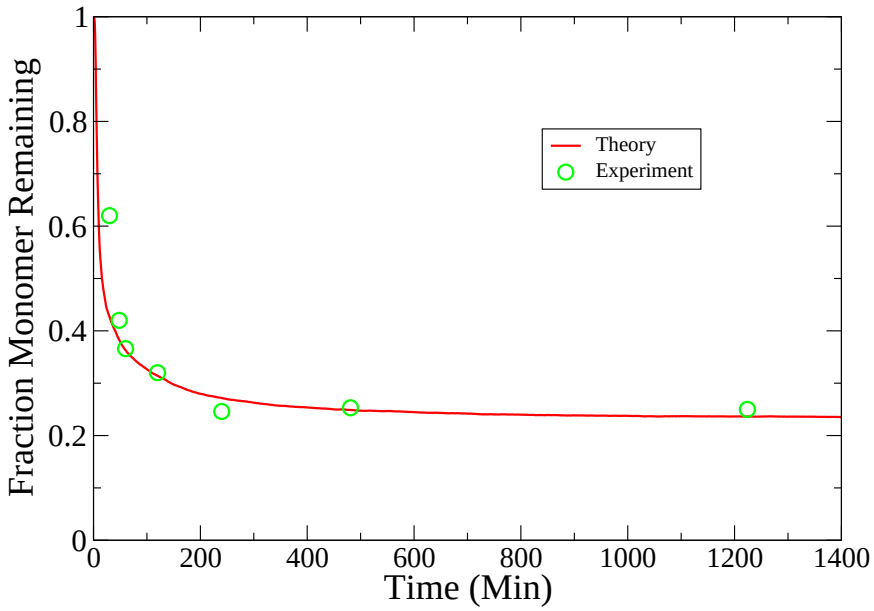

Figure 11: Experimental and theoretical fraction of monomers remaining as a function of time for poly(α-methylstyrene) in THF initiated by sodium naphthalide. The two sample batches are described in Table 1. The dots are the experimental data, and the line is the theoretical model. The simulation parameters for batch sample 1 (Dots) are: $N = 51170, A = 128, k_BT = 2.22k_BT_0, E^{\dagger} = 19.98k_BT_0, f_b = 10, \zeta = 0.95, dt = 0.004, \gamma_0 = 8$.

This dimensional analysis provides a timescale for the dimensionless iGLE in which one unit of time corresponds to 12 seconds. With this assignment, numerical simulations of the iGLE can be compared to the behavior of corresponding physical systems with specified units. In the following text, we call the first set of data ($T_e = 267$) sample 1, and the second set of data ($T_e = 271$) sample 2 as shown in Table 1. The fraction of monomer remaining as a function of time for poly(α-methylstyrene) in THF initiated by sodium naphthalide is shown in Figure 11. The dots are the experimental data (sample 1) and the line is the theoretical fit described in the text. The simulation results fit the experimental data very well with $\gamma_0 = 8$ and $\zeta = 0.95$. The equilibrium monomer concentration is reached in a relatively short amount of time and the extent of polymerization is 75%. For sample 2, first we use the same γ_0 value since both of them operate in the same solvent-tetrahydrofuran. After a temperature quench from above the polymerization temperature to below the polymerization temperature, the polymerization process was initiated and the extent of polymerization is 62% at equilibrium at a temperature of $271K$. The high

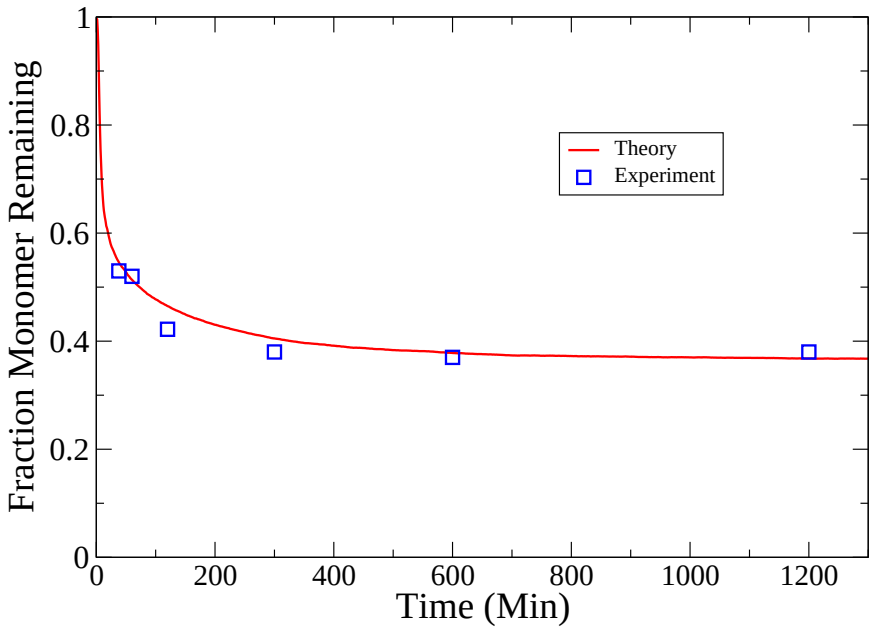

Figure 12: Experimental and theoretical fraction of monomers remaining as a function of time for poly(α-methylstyrene) in THF initiated by sodium naphthalide. The squares are experimental data and the line is our theoretical model. The simulation parameters for Batch sample 2 (Squares) are: $N = 51170, A = 123, k_BT = 2.26k_BT_0, E^{\dagger} = 19.98k_BT_0, f_b = 10, \zeta = 1.52, dt = 0.004, \gamma_0 = 8$.

equilibrium temperature makes the free energy higher since entropy and enthalpy are all negative for this reaction. We adjust the value of ζ to account for the temperature difference. The result is shown in Figure 12. The temperature change also affects the solvent friction. If there is no reaction, viscosity decreases as temperature increases. By lowering γ_0, a better fit is achieved. This is shown in Figure 13. The above simulation results suggest that the parameter ζ should be related to the temperature. Greer has studied the extent of polymerization as a function of temperature for living poly(α-methylstyrene) in THF initiated by sodium naphthalide with mole fraction of monomers $x_m^0 = 0.15378$, and the mole ratio of initiators to monomers $r = 0.0044$. Based on their data, simulations were completed. The results are shown in Table 2. Thus we obtained the relation between ζ and temperature as shown in Figure 14. As temperature increases, the value of ζ increases monotonically and the extent of polymerization increases too. As temperature decreases, the value of ζ will decrease and approach zero. At this time, the reaction goes to completion. To satisfy the above condition, the fit should be exponential instead of quadratic. The

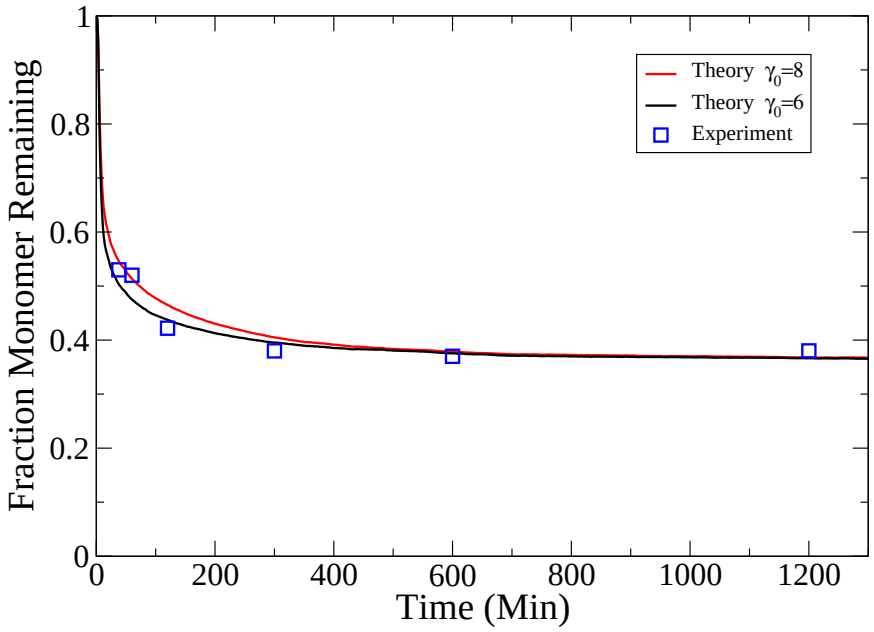

Figure 13: Experimental and theoretical fraction of monomers remaining as a function of time for poly(α-methylstyrene) in THF initiated by sodium naphthalide. The Squares are experimental data and the lines are our theoretical model with different γ_0 values.

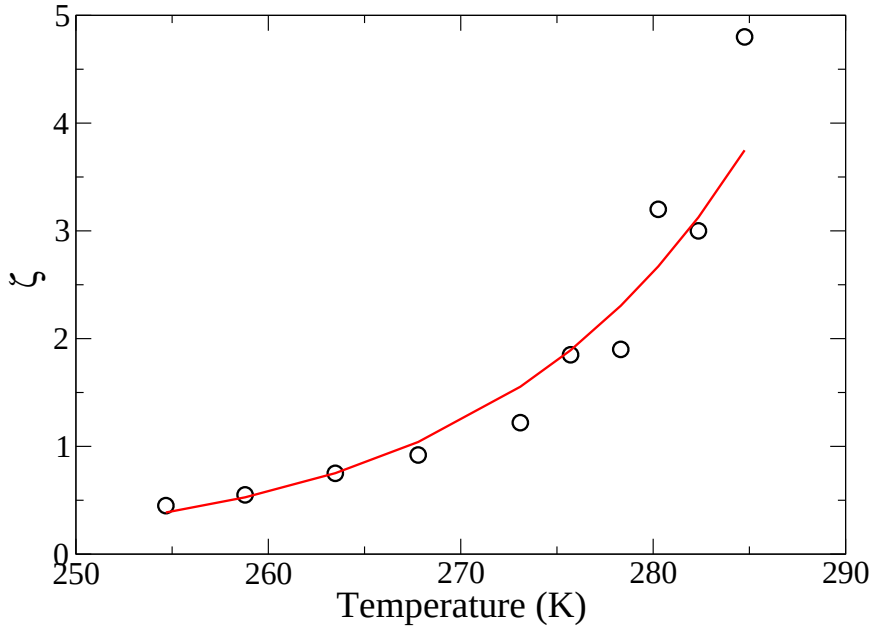

Figure 14: Extent of polymerization as a function of temperature for living poly(α-methylstyrene) in THF initiated by sodium naphthalide with $x_m^0 = 0.15378, r = 0.0044$. The solid line is the exponential fit.The corresponding simulation parameters are: $A = 204, N = 46288, f_b = 10, E^\dagger = 22.2 k_B T_0$.

Table 2: Batch samples of living poly(α-methylstyrene) in tetrahydrofuran, the table lists the data of temperature, barrier height, extent of conversion and the corresponding ζ value. The first and third columns are taken from Ref. [2].

$Temperature(K)$	$BarrierHeight(K_BT)$	$Conversion$	ζ
284.753	9.41	0.29 ± 0.02	4.8
282.350	9.487	0.41 ± 0.01	3.0
280.264	9.569	0.39 ± 0.01	3.2
278.317	9.623	0.54 ± 0.01	1.9
275.707	9.715	0.55 ± 0.01	1.85
273.095	9.808	0.668 ± 0.006	1.22
267.789	10.00	0.749 ± 0.004	0.92
263.480	10.165	0.800 ± 0.003	0.75
258.792	10.350	0.858 ± 0.003	0.55
254.677	10.520	0.894 ± 0.003	0.45

equation is: $\zeta = 1.7062e - 9e^{0.07554T}$ with a correlation coefficient of 0.9794923.

In this section, we applied the iGLE model to the poly(α-methylstyrene) system. By doing so, we gained a better understanding of the experimental system and the model itself. In the next section, we want to apply this model to a different system such as the poly(4-vinylbenzocyclobutene) to test generality.

3.2 Experimental System two: 4-vinylbenzocyclobutene

The polymerization of 4-vinylbenzocyclobutene in benzene using sec-butyllithium as the initiator at room temperature was studied recently [3]. The number of average molecular weights at different times has been measured using size exclusion chromatography (SEC). These results are shown in the Table 3. To calculate the polymer length and polymer length distribution, we have to obtain the polymer length from experimental data. The various effective lengths, i_i, listed in Table 3 have been inferred from the experimental data using the following three different procedures:

(1) Suppose the measured average molecular weight at $t = 53min$ is accurate. For living polymerization, the number average molecular weight, (M_n), is a linear function of conversion. Column 3 of Table 1 also shows the recalculated/corrected M_n in parentheses.

Table 3: polymerization of 4-vinylbenzocyclobutene in benzene using sec-butyllithium as the initiator at room temperature. ϕ is the extent of polymerization, M_n is the number average molecular weight, i_1, i_2 and i_3 are the polymer length obtained using different experimental data. The first three columns are taken from Ref. [3].

$Time(min)$	ϕ	$M_n(corrected)$	i_1	i_2	i_3
53	10%	4100	31.5	31.2	40.02
90	18%	6200(7380)	56.77	56.16	64.87
182	33%	12100(13530)	104.08	102.96	117.27
470	71%	24300(29100)	223.92	221.52	219.64

The molecular weight of the monomers is $130g/mol$, and the polymer length i_1 can be calculated using $i_1 = M_n/130$.

(2) Based on the concentration of initiators and monomers, we can calculate the ratio of monomers and initiators.($[M_0]/[I_0] = 311.68$). For simplicity, I use the integer 312, which is the polymer length when conversion is 100%. The polymer length i_2 can be calculated using conversion multiplied by maximum length.

(3) According to figure 3 in Ref. [3], the apparent rate constant is $0.00259min^{-1}$. Since $ln[M_0]/[M_t] = k_{app}t$, we can calculate the free monomer concentration $[M_t]$ at different times ($t = 53min, [M_t] = 0.21M; t = 90min, [M_t] = 0.19M; t = 182min, [M_t] = 0.15M; t = 471min, [M_t] = 0.07M$). Now we can calculate the conversion which is $1 - [M_t]/[M_0]$ $(12.827\%; 20.793\%; 37.586\%; 70.397\%)$. The polymer length i_3 is the product of the maximum length and the conversion. This procedure assume the reaction follows first-order kinetics. The length obtained is larger than that using the other two methods shown in Table 3.

In the following simulations, we use the concentration of monomers $[M]_0 = 0.24M$ and initiators $[I]_0 = 0.00077M$ to calculate the total number of the monomers and initiators. The activated monomers $A = 139$ and the total monomers $N = 43344$ if the system volume is $3.0e8\dot{A^3}$. The time scale for the polymerization of 4-vinylbenzocyclobutene can be identified if we assumes the size of 4-vinylbenzocyclobutene is $6.5\dot{A}$. Recalling the equality

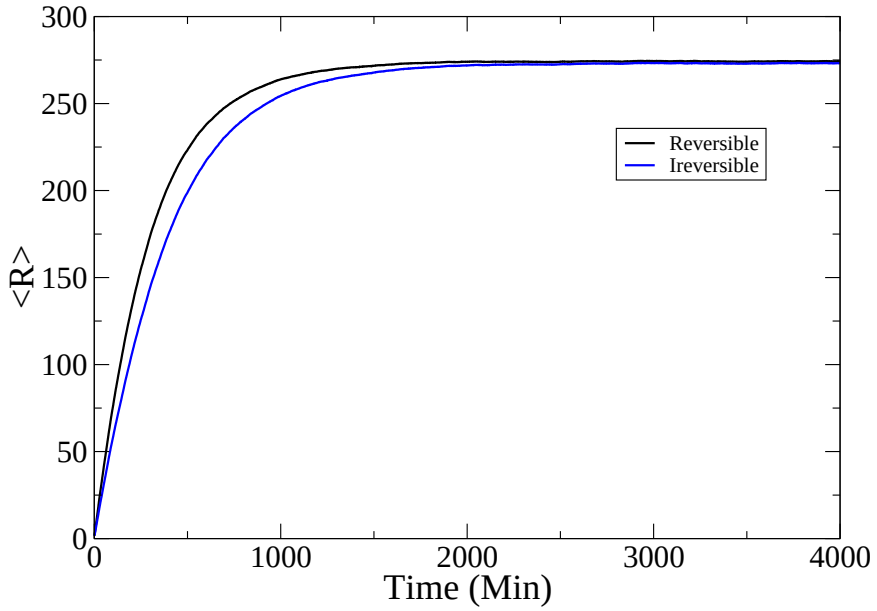

Figure 15: The average polymer length is displayed as a function of time for reversible (black) and irreversible (blue) polymerization. The simulation parameters are: $A = 139, N = 43344, \zeta = 0.5, \gamma_0 = 180$. The blue curve is obtained by turning off the back reaction.

derived in Eq. 63 based on dimensional analysis:

$$\frac{k_B T_0 \tau^2}{l^2} = 1 \tag{64}$$

$$\Rightarrow \tau^2 = \frac{l^2}{k_B T_0} \tag{65}$$

$$\Rightarrow \tau^2 = \frac{6.5\mathring{A}^2}{1kJ/mol} \tag{66}$$

$$\Rightarrow \tau^2 = \frac{42.25 * 10^{-20}\mathrm{m}^2}{1000J/6.02 * 10^{23} molecules} \tag{67}$$

$$\Rightarrow \tau^2 = 254s^2 \tag{68}$$

$$\Rightarrow \tau \approx 16s\ . \tag{69}$$

The fact that this time scale is similar to that found for α-methylstyrene is not surprising because cyclobutene won't open the ring during polymerization and the size of the two monomers are similar. Compared to poly-(α-methylstyrene), this polymerization reaction is irreversible and there are few monomers left in solution at the end. To test our model, we use the same parameter values and turn off the back reaction to simulate the irreversible reaction. As shown in Figure 15, the polymer grows faster for an irreversible reaction which

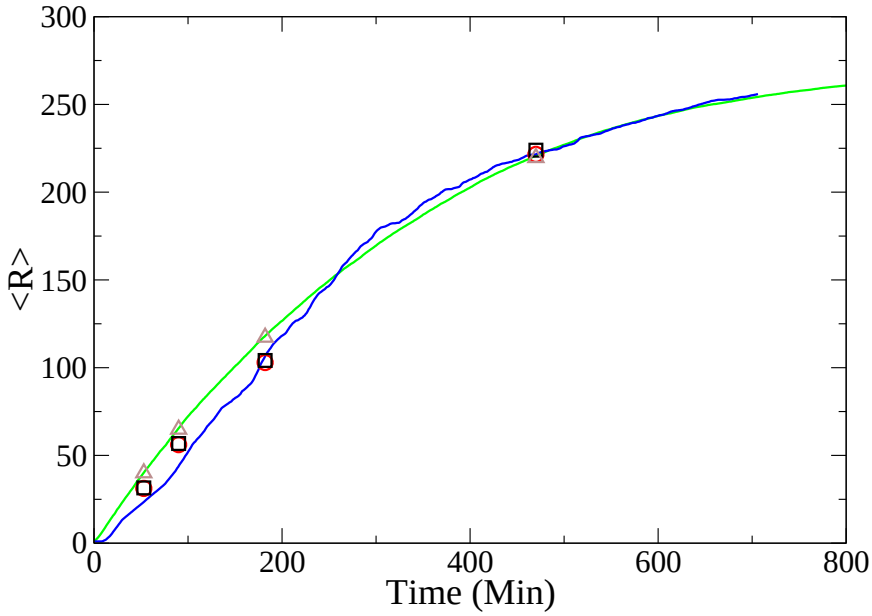

Figure 16: Theoretical and experimental polymer length as a function of time for the irreversible polymerization with different barrier height. The blue line is the simulation result using $A = 139, N = 43344,\ f_B = 30,\ \gamma_0 = 56,\ E^{\dagger} = 24.3 k_B T,\ \zeta = 0.16$, the green line is the simulation result using $A = 139, N = 43344,\ f_B = 10,\ \gamma_0 = 75,\ E^{\dagger} = 8.0 k_B T,\ \zeta = 0.5$. The dots, squares and triangles correspond to the polymer length calculated using the concentration, Mn and rate constant.

is expected.

In order to completely specify the model (whether it be solved analytically, or simulated by computation), there is one remaining unknown parameter for this system. In particular, the activation energy for the anionic polymerization of 4-vinylbenzocyclobutene is not available. Here, we use two different values for the activation energy ($20 KJ/mol$ and $63 KJ/mol$) to model the properties of this living polymerization reaction. These are the activation energy for α-methylstyrene and styrene. The reason we use these two values is because 4-vinylbenzocyclobutene and α-methylstyrene can be considered as derivatives of styrene. As before, we calculate the polymer length as a function of time with different barrier heights, as shown in Figure 16. If we use a low barrier height, a linear first-order time-conversion kinetics is seen. For barrier heights as high as $24.3 K_B T$, the polymerization rate is slow at the beginning and then speeds up showing an "S" shape behavior. This can be seen more clearly in Figure 17.

The SEC results indicate that the number average molecular weight increases with the

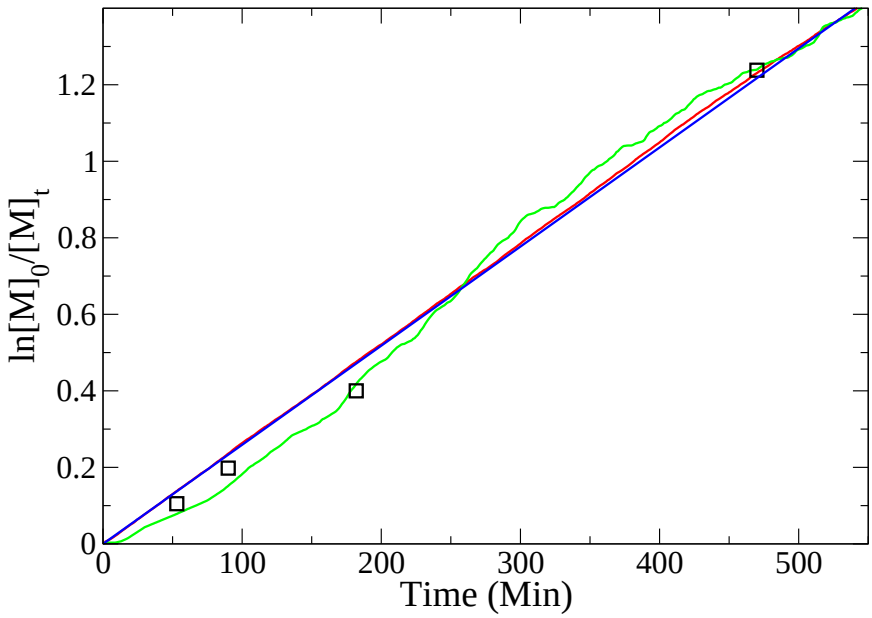

Figure 17: The kinetics of the anionic polymerization of 4-vinylbenzocyclobutene using s-BuLi as initiator in benzene at 25 degrees. The squares represent the experimental SEC results, the green line is the simulation result using $f_B = 30$, $\gamma_0 = 56$, $E^\dagger = 24.3 k_B T$, $\zeta = 0.16$, the red line is the simulation result using $f_B = 10$, $\gamma_0 = 75$, $E^\dagger = 8.0 k_B T$, $\zeta = 0.5$, and the blue line is first-order kinetics.

polymerization time. The distribution becomes narrower and narrower, which means that the polymer is approaching a uniform length. Our length distribution (figure 18) indicates this as well. It is difficult to obtain the same SEC curve because we do not know the calibration curve of the polystyrene standard under the current experimental conditions. A good way to link the experimental distribution and theory is to calculate the polydispersity index (PDI). As shown in Figure 19 and Figure 20, we obtain different PDI values with different barrier heights. By using a low barrier height, the PDI value is close to 1. This is consistent with the experimental data.

The above results show that the iGLE can be used to describe irreversible living polymerization. If the activation energy is high, it takes particles more time to cross the barriers. It is possible to get a very narrow distribution if the simulation is long enough and there is no termination and transfer reactions. This is why during living polymerization experiments, a lot of different reagents and conditions are used to get narrow distributions. In the following, we will look at a different system: anionic polymerization of styrene using

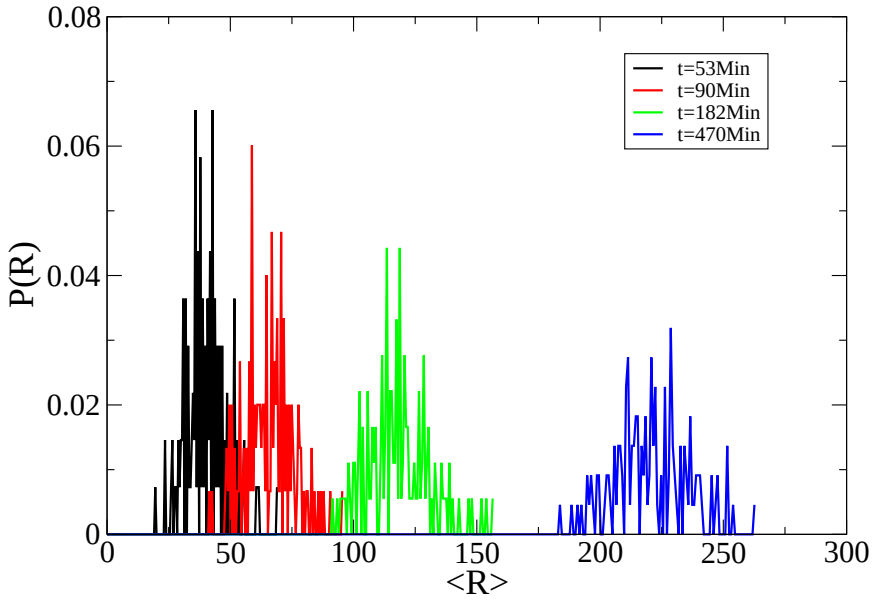

Figure 18: Polymer length distribution of poly-(4-vinylbenzocyclobutene) at different time with $A = 139, N = 43344, \zeta = 0.5, \gamma_0 = 75, f_b = 10, E^{\dagger} = 8k_BT$.

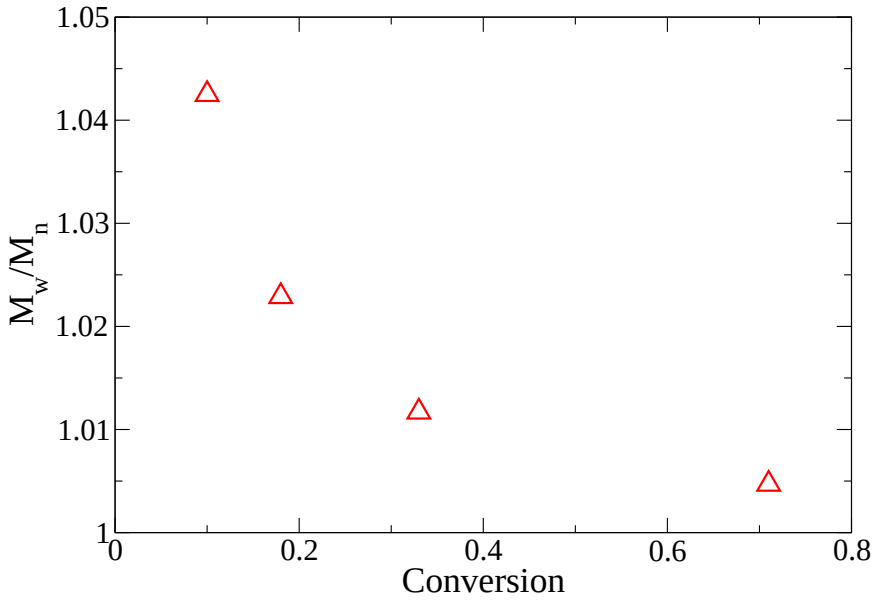

Figure 19: Polydispersity index (PDI) of poly-(4-vinylbenzocyclobutene)as a function of conversion with $E^{\dagger} = 8k_BT$. The PDI value decreases with conversion and is close to 1.

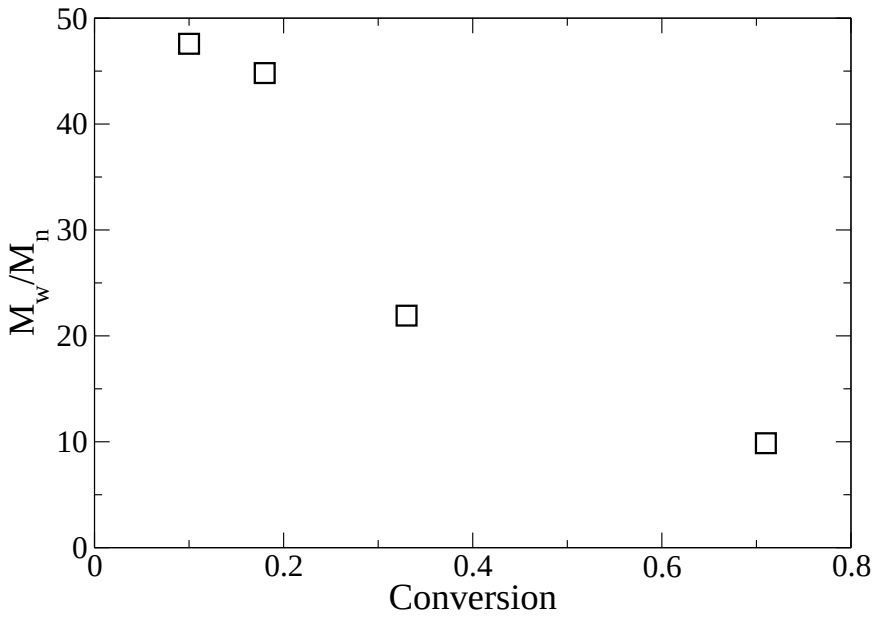

Figure 20: Polydispersity index (PDI)of poly-(4-vinylbenzocyclobutene) as a function of conversion with $E^{\dagger} = 24.3 k_B T$. The PDI value decrease with conversion and it's between 10-50.

sec-BuLi as the initiator in cyclohexane.

3.3 Experimental System three: styrene

Polymerization of styrene with initiator sec-butyllithium in cyclohexane was studied by Schubert using a commercial automated synthesizer[22]. Chang [4] studied the molecular weight distribution of this experimental system using SEC and temperature gradient interaction chromatography (TGIC) and found the TGIC method is more accurate. The polymer lengths L_{SEC} and L_{TGIC} listed in Table 4 have been inferred from experimental data. The activation energy for this reaction is $63 KJ/mol$. The total number of initiators and monomers are 289 and 174580 based on the initiator concentration ($0.00048 M$) and monomer concentration ($0.29 M$). The time scale used in this simulation is the same as α-methylstyrene since the size of styrene is almost the same as α-methylstyrene. In Figure 21, the "S" shape dynamics for polystyrene is observed too.

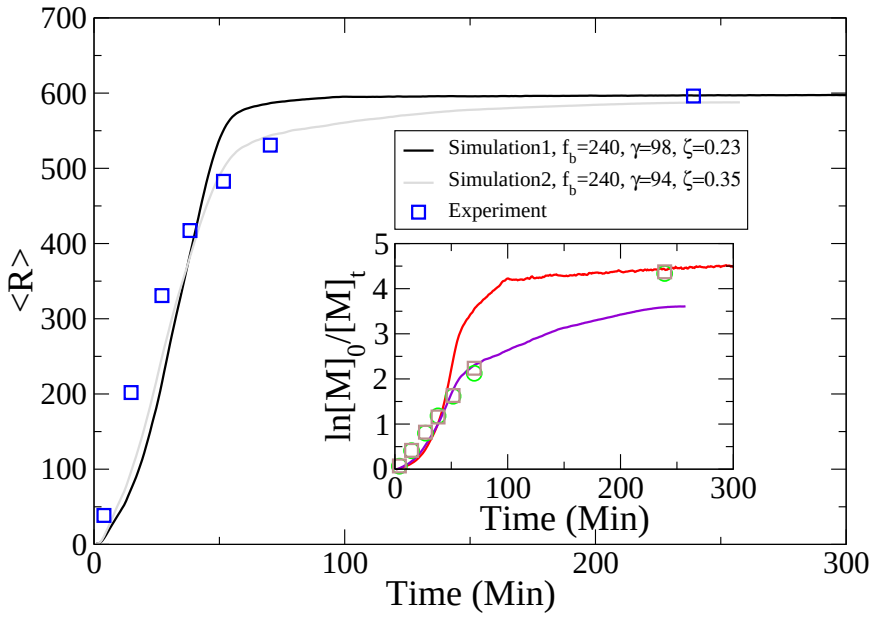

Figure 21: The polymer length as a function of time for the anionic polymerization of styrene using s-BuLi as initiator in cyclohexane at 45 degrees The simulation parameters are: $A = 289, N = 174580, E^{\dagger} = 23.77 k_B T, k_B T = 2.65 k_B T_0$. The ratio of monomers to initiators is 604. The blue square is the experimental data, gray line is for $f_b = 240, \gamma = 94, \zeta = 0.35$ and black line is for $f_b = 240, \gamma = 98, \zeta = 0.23$. The inset shows the kinetics where the circles and squares are experimental data obtained from SEC and temperature gradient interaction chromatography (TGIC).

Table 4: The molecular weight and polymer length of polystyrene. The first three columns data are taken from Ref. [4].

$Time(min)$	$M_n(SEC)$	$M_n(TGIC)$	L_{SEC}	I_{TGIC}
3.97	4300	4000	41.35	38.46
14.8	21300	21000	204.81	201.9
27.1	35000	34400	336.54	330.8
38.27	42900	43400	412.5	417.3
51.63	50400	50200	484.62	482.7
70.33	56000	55200	538.46	530.8
239.1	62000	62000	596.15	596.1

3.4 Discussion and Conclusions

In this chapter, we applied the modified iGLE model to three experimental systems such as α-methylstyrene, 4-vinylbenzocyclobutene and styrene. The dynamics of the polymerization of these three systems varies because of reagent and operation conditions. Firstly, we study the temperature effect on the polymerization of α-methylstyrene. By studying this system, we gain better understanding on the parameter ζ and γ_0 of the model. We obtained the relation between ζ and temperature, and it can be used to obtain the polymerization dynamics under different temperatures easily. To test the generality of this model, we choose an irreversible polymerization system— 4-vinylbenzocyclobutene. Since there is no activation energy data available, we use two different activation energy values to model the properties of the reaction. The polymer length distribution and PDI value have been obtained. We found that at a low barrier height, first-order kinetics was observed. Furthermore, it was found that the dynamics changes when the particles need to jump to a higher barrier. To confirm the high barrier dynamics, we apply the model to styrene and observe the similar "S" behavior dynamics.

It has been shown in this chapter that the iGLE can be used to model the dynamics of experimental living polymerization system. Using the iGLE to model polymerization provides a bridge between simple kinetics and full dynamics. It provides us additional information since structural information has been built in the model. In the next chapter,

we will use a stochastic model to describe the kinetics based on the diffusion coefficient. The first experimental system-poly(α-methylstyrene) will be used as an example.

CHAPTER IV

STOCHASTIC MODEL AND LIVING POLYMERIZATION

Living polymerization is a complex process in which the properties of the solution essentially change during the reaction, and the polymerization kinetics are strongly influenced by the characteristics of the medium. In this process the transport of monomers and their access to the reactive sites are not stationary, thus the diffusion and rate coefficients are no longer constants and depend on the state of the system. Considering that the polymerization in general has association-dissociation character, it is reasonable to treat the lengths of the polymer chains as random variables, which obey a system of coupled stochastic equations. The steady-state reaction rates for this system are derived using the theory of diffusion reactions, where integration in the coordinate phase space over the polymer configurations is performed. The rheological properties of the solution are taken into account through changing diffusion coefficients.

Diffusion-controlled phenomena such as auto-acceleration and the glass effect in conventional free-radical polymerization have been studied for a long time and proved to be very important [76, 77]. The effects of diffusion-controlled reactions on atom-transfer radical polymerization (ATRP) and reversible addition-fragmentation transfer polymerization (RAFT) demonstrate that diffusion-controlled radical termination and radical addition accelerate the polymerization rate, while diffusion-controlled propagation decreases the livingness of the polymer [78]. In this chapter, we study the diffusion effects on anionic living polymerization by including the diffusion coefficients in a stochastic model.

4.1 Chemical Stochastic Equation (CSE)

A stochastic process is the counterpart of a deterministic process. Instead of having only one possibility, it is possible to have more possibilities depending on how the process evolved with time. The Langevin equation we introduced before is a stochastic equation describing Brownian motion in a potential. In this stochastic equation, there is a deterministic term

and a stochastic term. Instead, the chemical stochastic equation can be used to describe the random chemical process by the stochastic term.. For the reaction:

$$A + B \underset{r_a}{\overset{r_d}{\rightleftharpoons}} C \ , \tag{70}$$

The number of molecules C depends on the numbers of molecules A and molecules B. In a time dt, the possibility of A colliding with B will determine how many C molecules can be formed. This is a random process and the number of reaction events during time dt can be described by the stochastic variable $\xi_{pois}(rdt)$. It obeys the Poissonian distribution and is characterized by the average number of reactions $r_a dt(r_d dt)$, and the $r_a(,r_d)$ is the association (dissociation) rate constant. This is a discrete process. The chemical stochastic equation for this reaction is:

$$dX_A = \xi_{Pois}(r_a dt) - \xi_{Pois}(r_d dt) \ . \tag{71}$$

4.2 Chemical Langevin Equation (CLE)

The relationship between stochastic and deterministic models for chemical reactions was studied by Kurtz [79]. He takes explicitly into account the volume of the reaction system. Later, Gillespie derived the chemical Langevin equation from the chemical master equation with two assumptions [80]. The assumption of Gillespie provides a new perspective on the origin and magnitude of noise in a chemical reaction system. Recently, the chemical langevin equation has been used for numerical simulations such as the analysis of cellular systems in biology [81]. Compared to chemical kinetics (deterministic), the chemical Langevin equation was used to describe the time evolution of a well-stirred chemical reactive system, taking into account stochasticity.

In the chemical stochastic equation shown in the last section, the possibility that the Poisson random variable $\xi_{pois}(rdt)$ has the integer value n is:

$$P(n; r, dt) = \frac{e^{-rdt}(rdt)^n}{n!} \ . \tag{72}$$

In the case of a large number of reaction occurrences, $rdt \gg 1$, the Poisson random variable becomes Gaussian by using Stirling's factorial approximation and the small-x approximation

for $ln(1+x)$.

$$\frac{e^{-rdt}(rdt)^n}{n!} \approx (2\pi rdt)^{-1/2} e^{\left(-\frac{(n-rdt)^2}{2rdt}\right)} , \tag{73}$$

where the normal random variable has the same mean and variance rdt as the Poisson random variable. The normal random variable can be written as the sum of the mean and the variation. Thus the CSE turns into a CLE [80]:

$$dX_A = r_a dt + \sqrt{r_a dt}\xi_1(t)\sqrt{dt} - r_d dt + \sqrt{r_d dt}\xi_2(t)\sqrt{dt} , \tag{74}$$

The rate equation is:

$$\frac{dX_A}{dt} = r_a - r_d + \sqrt{r_a}\xi_1(t) + \sqrt{r_d}\xi_2(t) , \tag{75}$$

where $\xi_i(t)$ and $\xi_i(t')$ are uncorrelated, statistically independent Gaussian noises,

$$\langle \xi_i(t)\xi_i(t') \rangle = \delta(t-t') . \tag{76}$$

4.3 Polymerization Kinetics and CSE

We apply this approach to simulate the kinetics of polymerization. For the reaction

$$P_n + M \underset{k_a}{\overset{k_d}{\rightleftharpoons}} P_{n+1} . \tag{77}$$

where P_n is a polymer with length n and M is a monomer. The rate of the polymerization is controlled partially by how fast the reactants encounter one another and partially by how fast they react once they meet. From the theory of diffusion-controlled reactions, the rate constants are:

$$k_a = \frac{K_a}{1-\kappa_a \tilde{g}(0)}; k_d = \frac{K_d}{1-\kappa_a \tilde{g}(0)} , \tag{78}$$

where κ_a and κ_d are the intrinsic association and dissociation rates. The function $\tilde{g}(s)$ is the Laplace transform of the partial probability $g(t)$ of finding two particles in contact at time t if initially they were in contact.

Given the two propagators for two reactive sites –Green functions $G_m(r_1, r; t)$ and $G_p(r_1, r; t)$–are known, $g(t)$ is expressed as :

$$g(t) = \int G_m(r_1, 0; t) G_p(r_1, 0; t) dr_1 . \tag{79}$$

Since $g(t \rightharpoonup \infty) = \lim_{n\to 0} s\tilde{g}(s)$,then $\tilde{g}(0)$ is defined by the behavior of the probability $g(t)$ at infinitely large times. The Green function for the monomers is:

$$G_m(r,0,t) = \frac{1}{4\pi Dt} e^{-\frac{r^2}{4Dt}} \ . \tag{80}$$

The Green function for the polymers is:

$$G_p(r,0,t) = \frac{1}{2\pi\phi_n(t)} e^{-\frac{r^2}{2\phi_n(t)}} \ . \tag{81}$$

At $t \to \infty$, the mean square displacement for the polymer is:

$$\begin{aligned} \phi_n(t) = & \quad 2D_n t + \frac{4nb^2}{3\pi^2} \sum_{p=1}^{\infty} \frac{1}{p^2} \\ = & \quad 2D_n t + \frac{4nb^2}{3\pi^2} \frac{1}{6} \pi^2 \\ = & \quad 2D_n t + \frac{2nb^2}{9} \ . \end{aligned} \tag{82}$$

The mean displacement for the monomers is: $\phi_m(t) = 2D_m t$. Now we integrate:

$$\begin{aligned} g(t) = & \quad (\frac{3}{2\pi})^{3/2} [3\phi_m(t) + 3\phi_n(t)]^{-3/2} \\ = & \quad (\frac{3}{2\pi})^{3/2} [6D_m t + 6D_n t + \frac{2}{3} Nb^2]^{-3/2} \\ = & \quad \left(\frac{3}{12\pi(D_m + D_n)} \right)^{(3/2)} \frac{1}{(1+a)^{3/2}} \ , \end{aligned} \tag{83}$$

where $a = \frac{Nb^2}{9(D_m + D_n)}$.

$$\tilde{g}(s) \overset{s \ll 1}{\approx} \frac{1}{[4\pi(D_m + D_n)]^{(3/2)}} \frac{2}{\sqrt{a}} [1 - \sqrt{\pi a s}] \ , \tag{84}$$

where $D_n = D_0/n$ is the diffusion coefficient of the whole polymer and b is the bond length.

$$\tilde{g}(0) = \frac{1}{4\pi \sqrt{\frac{\pi n}{9}} (D_m + D_n) b} \ . \tag{85}$$

The diffusion coefficient for the monomer D_m is scaled as the polymer is growing:

$$D_m = D_\infty + \frac{D_0 - D_\infty}{1 + (n/n_0)^2} \ , \tag{86}$$

where n_0 is the length of polymer when entangling begins.

4.4 Model Validation

To study the diffusion effect, we apply this model to the polymerization of α-methylstyrene. The experimental data (monomer concentration, mole fraction of monomers, ratio of the mole initiators to moles of initial monomer) is shown in Table 1. Based on these data, we determine the parameters. In this model, we assume the polymer grows from one active end. Figure 22 shows the fraction of monomers remaining as a function of time for poly(α-methylstyrene) in THF initiated by sodium naphthalide. If we use a relatively small diffusion coefficient in the simulation, the numerical results deviate significantly from the experimental data. The model fits the experimental data very well if we use a very large diffusion coefficient. This indicates that this is a kinetically controlled reaction and there is little diffusion effect in this system. In this limit, the model is consistent with the general kinetic model. But it is more general compared to the kinetic model since it includes the diffusion coefficients in the model. It would be very interesting to explore the region where the kinetics and diffusion compete with each other. This region is usually called the glass-transition region.

4.5 Discussion and Conclusions

By using experimental data and the rate constant obtained from the kinetic model, this model can be used to provide more information on diffusion during polymerization. If we assume there is diffusion effect in the polymerization process, that is, we can set the diffusion coefficient to a value that is the same order as the intrinsic rate constant, but keep the overall reaction rate the same. By doing this, we found that the polymerization slow down dramatically, although it will reach equilibrium after a long time. But the dynamics is different compared to the experimental data. If we decrease the diffusion coefficients, the simulation results will approach the experimental result. This indicates that the polymerization process is a kinetically controlled process.

The iGLE we introduced in the previous chapters was a bridge between the kinetic model and molecular dynamics. It is computationally efficient and provides the necessary information for the polymerization process. Since the structure information has been built in

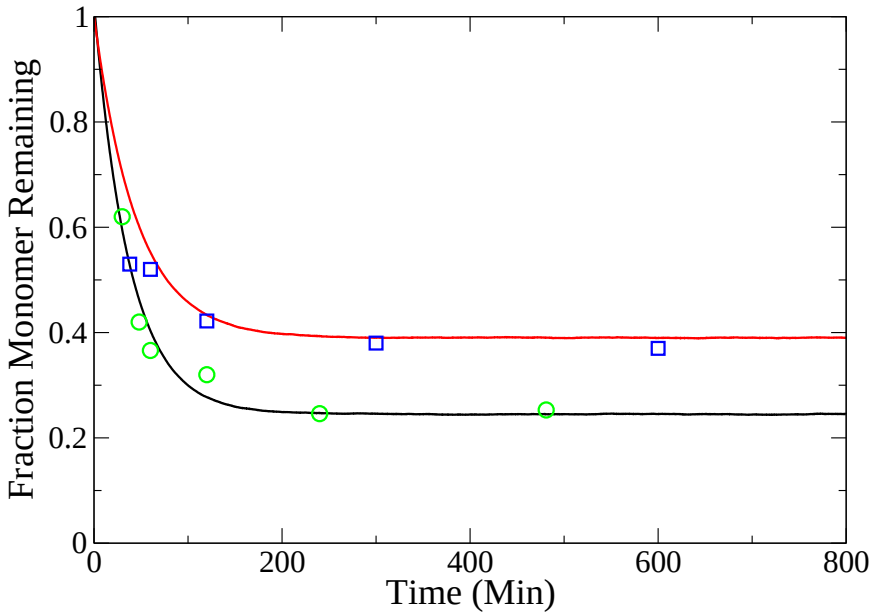

Figure 22: Fraction of monomers remaining as a function of time for poly(α-methylstyrene) in THF initiated by sodium naphthalide. Dots and squares are experimental data and the lines correspond to the model. The parameter for sample 1 is: $nam = 1279, ntm = 1023400, \kappa_a a = 333 A^3 s^{-1}, \kappa_d = 0.085 s^{-1}, D = D_\infty = 1.0e8 \dot{A}^2 s^{-1}, V = 1.0e9 \dot{A}^3$. The parameter for sample 2 is: $nam = 1228, ntm = 1023400, \kappa_a a = 300 A^3 s^{-1}, \kappa_d = 0.12 s^{-1}, D = D_\infty = 1.0e8 \dot{A}^2 s^{-1}, V = 1.0e9 \dot{A}^3$. where nam is the number of the activated monomer, ntm is the total number of monomers in the system and V is the system volume.

the model, we can know more about the viscosity and the interaction between the monomers and polymers by obtaining the dynamics of the polymerization. This information can't be obtained from the simple stochastic equation. By including the diffusion coefficients in the stochastic model, we can obtain the diffusion effect in the process, and this information can't obtained through the iGLE. These two methods are complementary and it can help to better understand polymerization dynamics.

CHAPTER V

DO THE DYNAMICS CHANGE IF THE FRICTION IS ASYMMETRIC?

In the previous chapter, the iGLE model has been used to study the dynamics of polymerization. It has been found that the friction kernel and PMF play an important role in obtaining the time-dependent properties. In this chapter, we want to understand the effect of the friction kernel on equilibrium properties. Specifically, we want to investigate whether or not the equilibrium position of the double-well particles is affected by the asymmetry in the nonstationary friction.

In former work [82], it has been shown that the average position of a stochastic particle in a double well is different for two different environments. If the environment is stationary, the average position is zero no matter where you put the particles. If the environment is nonstationary, the average position is shifted to the left well. This has been explained by the asymmetry in the friction. Recently we found that asymmetry in the equilibrium value of $\langle R \rangle$ decreases (and eventually goes away)as dt is lowered. This is shown in Fig. 23. Even when equipartition is followed fairly well, a large time step may significantly affect the results. A time step that works at low friction ($low\langle R \rangle$) may be too large at higher friction ($large\langle R \rangle$). The specified parameters for the iGLE simulations with the function $g(t) = R(t)^{\zeta}$ are: $N = 100, \gamma_0 = 8000, \zeta = 1$. To make this more clear, we try to use an analytical derivation to prove it.

5.1 iGLE Projection of the Mechanical System

Compared to the GLE, $iGLE$ includes a switching function $g(t)$ to characterize the nonstationary (irreversible) change in the solvent response. The time-dependent iGLE Hamiltonian is [58]:

$$H_{iGLE} = \frac{1}{2}p_q^2 + \{V_{(q)} + \delta V_1(q,t) + \delta V_2[q(\cdot),t]\} - g(t)[\sum_{i=1}^{n} c_i x_i]q + \sum_{i=1}^{n}[\frac{1}{2}p_i^2 + \frac{1}{2}\omega_i^2 x_i^2] \ , \quad (87)$$

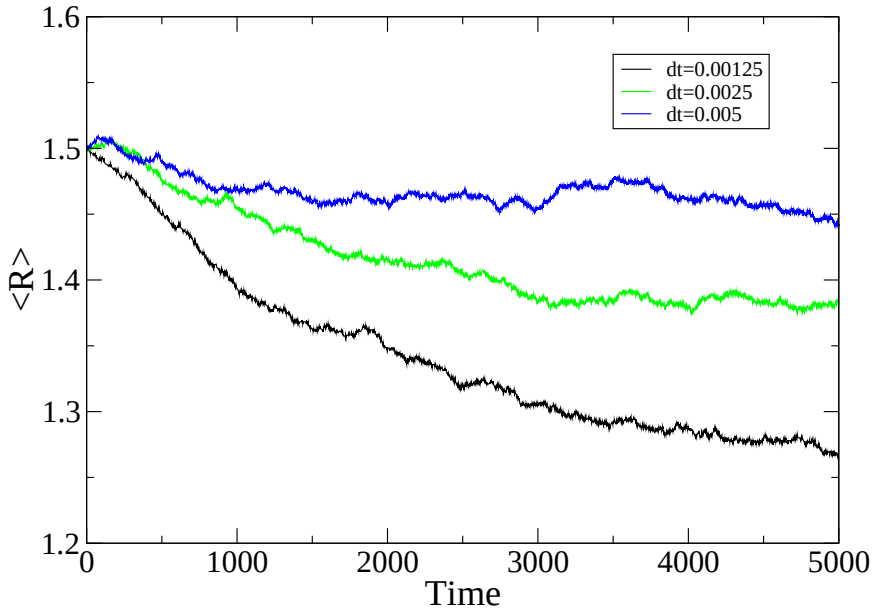

Figure 23: The average polymer length is displayed as function of time for the double well potential with time step 0.1125, 0.0025, and 0.005. For simplicity, the parameters are in dimensionless units. The minima of the double well are set at $R = 1$ and $R = 2$, and the barrier height is 2 at $R = 1.5$.

where (q, p_q) and (x_i, p_i) are the system coordinates and the ith bath mode, respectively. The parameter c_i is the coupling strength between the system and the ith bath mode with frequency ω_i. V_q is the potential of mean force (PMF),

$$V^{tot}(q, x; t) = \{V_{(q)} + \delta V_1(q, t) + \delta V_2[q(\cdot), t]\} - g(t)[\sum_{i=1}^{n} c_i x_i]q + \sum_{i=1}^{n} [\frac{1}{2}\omega_i^2 x_i^2] \,, \tag{88}$$

where

$$\delta V_1(q, t) = \frac{1}{2} g(t)^2 \sum_{i=1}^{n} \frac{c_i^2}{\omega_i^2} q^2 \,, \tag{89}$$

$$\delta V_2[q(\cdot), t] = \frac{1}{2} \int_0^t dt' a(t, t')[q(t') - q(t)]^2 - \frac{1}{2}[\int_0^t dt' a(t, t') q(t')^2] \,, \tag{90}$$

where

$$a(t, t') = g(t)\dot{g}(t')\gamma_0(t - t') \,. \tag{91}$$

Hamilton's equation of motion can be obtained from the above Hamiltonian equation:

$$\dot{q} = \frac{\partial H_{iGLE}}{\partial p_q} = p_q \,, \tag{92}$$

$$\dot{p_q} = -\frac{\partial H_{iGLE}}{\partial q} = -\frac{\partial V_{(q)}}{\partial q} - \frac{\partial(\delta V_1(q, t))}{\partial q} - \frac{\partial \delta V_2[q(\cdot), t]}{\partial q_{(t)}} + g(t)[\sum_{i=1}^{n} c_i x_i] \,. \tag{93}$$

$$\dot{q}_i = \frac{\partial H_{iGLE}}{\partial p_i} = p_i \ , \tag{94}$$

$$\dot{p}_i = -\frac{\partial H_{iGLE}}{\partial x_i} = g(t)c_i q - \omega_i^2 x_i^2 \ . \tag{95}$$

The second-order differential equation can be obtained by combining Eq. 94 and Eq. 95. We obtain $x_i(t)$ after Laplace transform:

$$\begin{aligned} x_i(t) &= (x_i(0) - \frac{c_i}{\omega_i^2} g(0)q(0)) \cos(\omega_i t) + \frac{\dot{x}_i(0)}{\omega_i} \sin(\omega_i t) \\ &+ \frac{c_i}{\omega_i^2} g(t)q(t) - \frac{c_i}{\omega_i^2} \int_0^t dt' \cos[\omega_i(t-t')] \frac{d}{dt'}[g(t')q(t')] \ . \end{aligned} \tag{96}$$

We obtain another second-order differential equation by combining Eq. 92 and Eq. 93. Inserting $x_i(t)$ into this equation leads to:

$$\begin{aligned} \dot{p_q} &= \dot{\dot{q}} = -\frac{\partial V_(q)}{\partial q} - g(t) \int_0^t dt' [\sum_{i=1}^{n} \cos[\omega_i(t-t')]] g(t') q(\dot{t'}) \\ &+ g(t)[\sum_{i=1}^{n} c_i (x_i(0) - \frac{c_i}{\omega_i^2} g(0)q(0)) \cos(\omega_i t) + \frac{\dot{x}_i(0)}{\omega_i} \sin(\omega_i t)] \\ &- \frac{\partial(\delta V_1(q,t))}{\partial q} + g(t)^2 \sum_{i=1}^{N} \frac{c_i^2}{\omega_i^2} q_{(t)} \\ &- \frac{\partial \delta V_2[q(\cdot),t]}{\partial q(t)} - g(t) \int_0^t dt' [\cos[\omega_i(t-t')]] \dot{g}(t') q(t') \ . \end{aligned} \tag{97}$$

From Eq. 89 and Eq. 90,we obtain:

$$\frac{\partial(\delta V_1(q,t))}{\partial q} = g(t)^2 \sum_{i=1}^{N} \frac{c_i^2}{\omega_i^2} q_{(t)} \ , \tag{98}$$

$$\frac{\partial \delta V_2[q(\cdot),t]}{\partial q(t)} = -\int_0^t dt' a(t,t') \left[q(t') + q(t)[\frac{\partial q(t')}{\partial q(t)} - 1] \right] \ . \tag{99}$$

Eq. 99 is complicated and we would like to study it in the following two limits:

- For a strongly correlated case (short time): $\frac{\partial q(t')}{\partial q(t)} \approx 1$.
- For a weakly correlated case (long time): $a(t,t') \propto e^{\frac{-(t-t')}{\tau}} \approx 0$.

Thus Eq. 99 can be approximated by:

$$\frac{\partial \delta V_2[q(\cdot),t]}{\partial q(t)} \approx -\int_0^t dt' a(t,t') q(t') \ . \tag{100}$$

Substituting Eq. 98 and Eq. 100 into Eq. 97, we obtain:

$$\dot{v} = -\frac{\partial V(q)}{\partial(q)} - \int_0^t dt' \gamma(t,t') v(t') + \xi(t) \ , \tag{101}$$

where

$$\xi(t) = g(t) \left[\sum_{i=1}^{n} c_i (x_i(0) - \frac{c_i}{\omega_i^2} g(0) q(0)) \cos(\omega_i t) + \frac{\dot{x}_i(0)}{\omega_i} \sin(\omega_i t) \right] \ , \tag{102}$$

$$\begin{aligned} \gamma(t,t') &= g(t) \int_0^t dt' \left[\sum_{i=1}^{n} \cos[\omega_i (t-t')] \right] g(t') & (103) \\ &= g(t) \gamma_0 (t-t') g(t') \ . & (104) \end{aligned}$$

It has been proved that the random force $\xi(t)$ satisfies the nonstationary fluctuation-dissipation relation (FDR), so Eq. 101 is the iGLE.

5.2 iGLE Projection of the Mechanical System for $g(t)$ is Time-dependent

As shown in Eq. 104, the function $g(t)$ appears in the friction kernel of the iGLE. What we want to know is the effect of the friction kernel on the equilibrium position of particles, that is, how the position $\langle R \rangle$ is affected by $g(t)$. In this section, we will investigate how the equilibrium position is affected by the friction if $g(t)$ is time-dependent. We will start with a simple case, and then move to a more complicated case.

5.2.1 Ansatz: $\delta V_2[q(\cdot), t]$ can be ignored.

From Eq. 88, we obtain:

$$\frac{\partial V^{tot}(q,x;t)}{\partial q} = \frac{\partial V(q)}{\partial q} + \frac{\partial(\delta V_1(q,t))}{\partial q} - g(t)[\sum_{i=1}^{n} c_i x_i] \ . \tag{105}$$

Suppose the double well has minima at $q = 1$ and $q = q^{\dagger}$. At this two points, $\frac{\partial V(q)}{\partial q} = 0$. Although not obvious, these points are also part of the solution for the full-dimensional system. We now show this by construction. The minima for the full-dimensional system must satisfy:

$$\frac{\partial V^{tot}(q,x;t)}{\partial q} = 0 \ , \tag{106}$$

$$\frac{\partial V^{tot}(q,x;t)}{\partial x_i} = 0 \ . \tag{107}$$

By solving Eq. 106, we obtain:

$$x_i = g(t)\frac{c_i}{\omega_i^2}q \ . \tag{108}$$

If $q = 1$, then $x_i = g(t)\frac{c_i}{\omega_i^2}$;

If $q = q^\dagger$, then

$$x_i^\dagger = g(t)\frac{c_i}{\omega_i^2}q^\dagger \ . \tag{109}$$

Insert the corresponding x_i into the following equation,

$$\frac{\partial V^{tot}(q,x;t)}{\partial x_i} = \omega_i^2 x_i - g(t)c_i q \ . \tag{110}$$

We find at these two points, Eq. 110 equals zero. That is, these two set of solutions satisfy Eq. 106 and Eq. 107. The minima don't change if $g(t)$ is time-dependent and $\delta V_2[q(\cdot),t]$ is ignored.

5.2.2 Ansatz: $\delta V_2[q(\cdot),t]$ can't be ignored.

From Eq. 88, we obtain:

$$\frac{\partial V^{tot}(q,x;t)}{\partial q} = \frac{\partial V(q)}{\partial q} + \frac{\partial(\delta V_1(q,t))}{\partial q} + \frac{\partial \delta V_2[q(\cdot),t]}{\partial q(t)} - g(t)[\sum_{i=1}^{n} c_i x_i] \ . \tag{111}$$

Suppose the double well has minima at $q = 1$ and $q = q^\dagger$. An explicit form of the potential for the double well is:

$$V(q) = A(q-1)^2(q-q^\dagger)^2 \ , \tag{112}$$

where A is a real number. At these two points, $\frac{\partial V(q)}{\partial q} = 0$. As before, we attempt to find a solution for the many-dimensional potential assuming that the minima remains at the value for the one-dimensional potential, namely $q = 1$ and $q = q^\dagger$.

By setting $\frac{\partial V^{tot}(q,x;t)}{\partial q} = 0$, we obtain

$$x_i = g(t)\frac{c_i}{\omega_i^2}q - \frac{1}{g(t)}\int_0^t dt' a(t,t')q(t') \ . \tag{113}$$

We get two different values for x_i after inserting $q = 1$ and $q = q^\dagger$ into above equation. By inserting the corresponding q and x_i value into the following equation,

$$\frac{\partial V^{tot}(q,x;t)}{\partial x_i} = \omega_i^2 x_i - g(t)c_i q \ , \tag{114}$$

we find $\frac{\partial V^{tot}(q,x;t)}{\partial x_i} \neq 0$. Hence the solutions require $q \neq 1$ and $q \neq q^\dagger$. This suggest that the minima changed if we consider the term $\delta V_2[q(\cdot),t]$. Assume one of the minima moved from $q=1$ to $q=q_{m1}$, and another minima moved from $q=q^\dagger$ to $q=q_{m2}$, then

$$\frac{\partial V(q)}{\partial q} = 2A(q-1)(q-q^\dagger)^2 + 2A(q-1)^2(q-q^\dagger) \ . \tag{115}$$

At $q=q_{m1}$, $x_{im1} = \frac{g(t)C_i q_{m1}}{\omega_i^2}$.

Inserting x_{im1} into Eq. 109, we obtain:

$$\begin{aligned} &2A(q_{m1}-1)(q_{m1}-q^\dagger)^2 + 2A(q_{m1}-1)^2(q_{m1}-q^\dagger) \quad + \quad g(t)^2 \sum_{i=1}^{N} \frac{c_i^2}{\omega_i^2} q(t) \\ &- \int_0^t dt' a(t,t') q(t') - g(t)^2 \sum_{i=1}^{N} \frac{c_i^2}{\omega_i^2} q(t) = 0 \ . \end{aligned} \tag{116}$$

where

5.2.2.1 For ohmic friction: $\gamma_0(t-t') \approx \gamma_0(0)\delta(t-t')$.

$$\int_0^t dt' a(t,t') q(t') = \gamma_0(0) g(t) \dot{g}(t) q(t) \ , \tag{117}$$

5.2.2.2 Perturbative treatment of exponential friction. First we consider: $\gamma_0(t-t') \approx \exp\frac{(-(t-t'))}{\tau}$, then we suppose the friction is ohmic friction.

$$\begin{aligned} \int_0^t dt' a(t,t') q(t') &= g(t) \int_0^t dt' \dot{g}(t') \gamma_0(t-t') q(t') \\ &= g(t) \left[\int_0^t dt' [\frac{d}{dt'} g(t')] \gamma_0(t-t') q(t') \right] \\ &= g(t) \left[g(t') \gamma_0(t-t') q(t') \mid_0^t - \int_0^t dt' g(t') \frac{d}{dt'} [\gamma_0(t-t') q(t')] \right] \\ &= g(t) \left[g(t) \gamma_0(0) q(t) - g(0) \gamma_0(t) q(0) \right] \\ &- g(t) \left[\int_0^t dt' g(t') \left[\gamma_0(t-t') \dot{q}(t') + \frac{1}{\tau} \gamma_0(t-t') q(t') \right] \right] \\ &= \gamma_0(0) g(t)^2 q(t) - g(0) \gamma_0(t) q(0) \\ &- g(t) \int_0^t dt' g(t') \gamma_0(t-t') [\dot{q}(t') + \frac{1}{\tau} q(t')] \ . \end{aligned} \tag{118}$$

For $t \gg 0$, $g(0)\gamma_0(t) \approx 0$. If the friction has no memory, then $\gamma_0(t-t') \approx \gamma_0(0)\delta(t-t')$. Taking the thermodynamic equilibrium velocity $\langle \sqrt{v(t)^2} \rangle = \sqrt{K_b T}$, Eq. 118 can be

simplified to:

$$\int_0^t dt' a(t,t') q(t') = \gamma_0 g(t)^2 q(t) - g(t) \int_0^t dt' g(t') \gamma_0(0) \delta(t-t') [\dot{q}(t') - \frac{1}{\tau} q(t')] \quad (119)$$

$$\approx (1 - \frac{1}{\tau}) \gamma_0 g(t)^2 q(t) - \gamma_0 g(t)^2 \sqrt{K_b T} \, . \quad (120)$$

Inserting Eq. 120 into Eq. 116, we obtain:

$$2A(q_{m1}-1)(q_{m1}-q^\dagger)^2 + 2A(q_{m1}-1)^2(q_{m1}-q^\dagger) - (1-\frac{1}{\tau})\gamma_0 g(t)^2 q(t) + \gamma_0 g(t)^2 \sqrt{K_b T} = 0 \, . \quad (121)$$

Suppose we use the following form of $g(t)$ [83]:

$$g^2(t) = g^2(-\infty) + \frac{1}{2}\left[g^2(\infty) - g^2(-\infty)\right] \left(1 + \frac{\exp(\frac{t}{\tau_g}) - 1}{\exp(\frac{t}{\tau_g}) + 1}\right) \, . \quad (122)$$

We use the same parameters as in the Ref. [83]: $\gamma_0(0) = 1.0$, $g^2(\infty) = 10.0$, $g^2(-\infty) = 0.0$, $K_b T = 2.0$. If the barrier height is 2 for the double well, then $A = 32$. The equation can be simplified:

$$64(q_{m1}-1)(q_{m1}-2)^2 + 64(q_{m1}-1)^2(q_{m1}-2) - \left[(1-\frac{1}{\tau})q - \sqrt{2}\right] * 5.0 \left[1 + \frac{\exp(\frac{t}{\tau_g}) - 1}{\exp(\frac{t}{\tau_g}) + 1}\right] = 0 \, . \quad (123)$$

By solving this equation, we obtain the value q_{m1}. Similarly, we get the value of q_{m2}. The minima changed with time as shown in the following:

If $\tau_g = 0.2$, $\tau = 0.5$

For $t = -1$,	$q_1 = 0.9975.$	$q_2 = 1.5061$	$q_3 = 1.9964$
For $t = -0.5$,	$q_1 = 0.9738.$	$q_2 = 1.5723$	$q_3 = 1.9539$
For t goes to ∞ ,	$q_1 = 0.796.$	$q_2 = 1.85 + 0.447i$	$q_3 = 1.85 - 0.447i$

It is clear that $q_{m1} \neq 1 or q^\dagger$. This means that the minima do change to new positions at some time, and it also changes the equilibrium position of the double well.

5.3 iGLE Projection of the Mechanical System for $g(t)$ is Space-dependent

In this section, we assume $g(t)$ is space dependent and use the same Hamiltonian shown in section I. If $g(t)$ is a function of the position (g(t)=g(q;t)), (that is, friction is space

dependent), the minima for the full-dimensional system must satisfy:

$$\frac{\partial V^{tot}(q,x;t)}{\partial x_i} = \omega_i^2 x_i - c_i q g(q;t) = 0 \ , \tag{124}$$

$$\frac{\partial V^{tot}(q,x;t)}{\partial q} = \frac{\partial V(q)}{\partial q} + \frac{\partial(\delta V_1(q,t))}{\partial q} + \frac{\partial \delta V_2[q(\cdot),t]}{\partial q(t)} - \left[g(q;t) + q\frac{\partial g(q;t)}{\partial q(t)}\right]\left[\sum_{i=1}^{n} c_i x_i\right] = 0 \ , \tag{125}$$

where

$$\frac{\partial(\delta V_1(q,t))}{\partial q} = \sum_{i=1}^{N} \frac{c_i^2}{\omega_i^2}\left[g(q;t)^2 q(t) + g(q;t)q(t)^2\frac{\partial g(q;t)}{\partial q}\right] , \tag{126}$$

$$\begin{aligned}\frac{\partial \delta V_2[q(\cdot),t]}{\partial q(t)} &= \int_0^t dt' \gamma_0(t-t')\left[-q(t') + q(t) - q(t)\frac{\partial q(t')}{\partial q}\right]\left[g(q;t)\dot{g}(q;t')\right] \\ &+ \frac{1}{2}\int_0^t dt' \gamma_0(t-t')\left[-2q(t')q(t) + q(t)^2\right] \\ &\left[\dot{g}(q;t')\frac{\partial g(q;t)}{\partial q} + g(q;t)\frac{\partial g(q;t')}{\partial q}\right] \ .\end{aligned} \tag{127}$$

We consider the following cases:

(1)$\delta V_2[q(\cdot),t]$ can be ignored

(2)$\delta V_2[q(\cdot),t]$ can't be ignored

5.3.1 Ansatz: $\delta V_2[q(\cdot),t]$ can be ignored.

The double well has two minima at $q = 1$ and $q = q^\dagger$. At these two points, $\frac{\partial V(q)}{\partial q} = 0$. By setting the following equation equal to zero, $\frac{\partial V^{tot}(q,x;t)}{\partial q} = 0$, we obtain:

$$x_i = \sum_{i=1}^{N} \frac{c_i}{\omega_i^2} g(q;t) q_t \ . \tag{128}$$

inserting x_i into the following equation,

$$\frac{\partial V^{tot}(q,x;t)}{\partial x_i} = \omega_i^2 x_i - c_i q g(q;t) \ , \tag{129}$$

and we find $\frac{\partial V^{tot}(q,x;t)}{\partial x_i} = 0$. So if g(t) is space-dependent and ignoring $\delta V_2[q(\cdot),t]$, the positions of the minima don't change.

5.3.2 Ansatz: $\delta V_2[q(\cdot),t]$ can't be ignored.

If $g(q;t) = q(t)$, then we get the following relations:

$$g(q;t') = q(t') \ , \tag{130}$$

$$\dot{g}(q;t') = \frac{\partial q(t')}{\partial t'} \ , \tag{131}$$

$$\dot{g}(q;t) = \frac{\partial q(t)}{\partial t} \ , \tag{132}$$

$$\frac{\partial g(q;t)}{\partial q} = 1 \ , \tag{133}$$

$$\frac{\partial \dot{g}(q;t')}{\partial q} = \frac{\partial^2 q(t')}{\partial q \partial t'} \ . \tag{134}$$

By inserting these relations into Eq. 126 and Eq. 127, we obtain:

$$\frac{\partial(\delta V_1(q,t))}{\partial q} = 2q(t)^3 \sum_{i=1}^{N} \frac{c_i^2}{\omega_i^2} \ , \tag{135}$$

$$\begin{aligned} \frac{\partial \delta V_2[q(\cdot),t]}{\partial q(t)} &= \int_0^t dt' \gamma_0(t-t') \left[-2q(t')q(t) + \frac{3}{2}q(t)^2 \right] \frac{\partial q(t')}{\partial t'} \\ &+ \int_0^t dt' \gamma_0(t-t') \left[-q(t)^2 - q(t)^2 q(t') + \frac{1}{2}q(t)^3 \right] \frac{\partial^2 q(t')}{\partial q(t) \partial t'} \ . \end{aligned} \tag{136}$$

Let's look at Eq. 136,

- For a strongly correlated case (short time): $\frac{\partial^2 q(t')}{\partial q(t) \partial t'} = 0$.
- For a weakly correlated case (long time): $a(t,t') \propto e^{\frac{-(t-t')}{\tau}} \approx 0$.

To get the analytic solution, we have to remove the integral in Eq. 136 by using different approximations.

5.3.2.1 For ohmic friction

As before, we suppose there is no memory and use the thermodynamic velocity. Eq. 136 can be simplified:

$$\frac{\partial \delta V_2[q(\cdot),t]}{\partial q(t)} = -\frac{1}{2}\gamma_0(0) q(t)^2 v(t) \ , \tag{137}$$

and we obtain:

$$2A(q_m-1)(q_m-q^\dagger)^2 + 2A(q_m-1)^2(q_m-q\dagger) + 2q_m^3 \sum_{i=1}^{N} \frac{c_i^2}{\omega_i^2} - \frac{1}{2}\gamma_0 q(t)^2 v(t) - 2q_m^3 \sum_{i=1}^{N} \frac{c_i^2}{\omega_i^2} = 0 \ , \tag{138}$$

By setting $q^\dagger = 2$, $A = 32$, and changing the value of $\gamma_0(0)$, we obtain the following different solutions:

For $\gamma_0(0) = 0.5$,	$q_1 = 1.0057.$	$q_2 = 1.4758$	$q_3 = 2.021$
For $\gamma_0(0) = 1$,	$q_1 = 1.0117.$	$q_2 = 1.452935$	$q_3 = 2.0409$
For $\gamma_0(0) = 6$,	$q_1 = 1.1360.$	$q_2 = 1.20425$	$q_3 = 2.1928$
For $\gamma_0(0) = 8000$,	$q_1 = 0.09 - 0.27i.$	$q_2 = 0.09 + 0.27i$	$q_3 = 35.57$

So if g(t) is space-dependent and $\delta V_2[q(\cdot), t]$ is included in the PMF, the minima move right, and the maxima move left.

5.3.2.2 perturbative treatment of the exponential friction

Eq. 136 can be simplified:

$$\begin{aligned}
\frac{\partial \delta V_2[q(\cdot),t]}{\partial q(t)} &= \int_0^t dt' \gamma_0(t-t') \left[-2q(t')q(t) + \frac{3}{2}q(t)^2 \right] \frac{\partial q(t')}{\partial t'} \\
&= -\int_0^t dt' \frac{d}{dt'}[\gamma_0(t-t')] \left[-2q(t')q(t) + \frac{3}{2}q(t)^2 \right] q(t') \\
&\quad -\int_0^t dt' [\gamma_0(t-t')] \left[-2q(t)\frac{\partial q(t')}{\partial t'} \right] q(t') \\
&\quad -\gamma_0(t-t') \left[-2q(t')q(t) + \frac{3}{2}q(t)^2 \right] q(t') \mid_0^t \\
&= -\int_0^t \frac{1}{\tau}[\gamma_0(t-t')] \left[-2q(t')q(t) + \frac{3}{2}q(t)^2 \right] q(t') \\
&\quad +2\int_0^t dt' q(t)\dot{q}(t')q(t')\gamma_0(t-t') - \frac{1}{2}\gamma_0(0)q(t)^3 \, . \qquad (139)
\end{aligned}$$

(1) Applying the ohmic friction, the above equation can be simplified as the following:

$$\frac{\partial \delta V_2[q(\cdot),t]}{\partial q(t)} = -\frac{1}{2}(1-\frac{1}{\tau})\gamma_0(0)q(t)^3 - \gamma_0[-2q(t)^2 v(t)] \, , \qquad (140)$$

so we obtain:

$$\begin{aligned}
& 2A(q_m-1)(q_m-q^\dagger)^2 + 2A(q_m-1)^2(q_m-q\dagger) + 2q_m^3 \sum_{i=1}^N \frac{c_i^2}{\omega_i^2} \\
- \quad & \frac{1}{2}(1-\frac{1}{\tau})\gamma_0 q(t)^3 - \gamma_0[-2q(t)^2 v(t)] - 2q_m^3 \sum_{i=1}^N \frac{c_i^2}{\omega_i^2} = 0 \, , \qquad (141)
\end{aligned}$$

By setting $q^\dagger = 2$, $A = 32$, $\tau = 0.714$, and changing the value of γ_0, we obtain the following different solutions:

For $\gamma_0 = 1000$,	$q_1 = -6.4395.$	$q_2 = -0.6864$	$q_3 = 0.2646$
For $\gamma_0 = 1$,	$q_1 = 0.9611.$	$q_2 = 1.755 - 0.19i$	$q_3 = 1.755 + 0.19i$
For $\gamma_0 = 0.1$,	$q_1 = 0.9953.$	$q_2 = 1.523$	$q_3 = 1.979$

(2) If we continue the calculation of Eq. 139, we obtain:

$$\begin{aligned}\frac{\partial \delta V_2[q(\cdot),t]}{\partial q(t)} &= -\int_0^t dt' \frac{1}{\tau}[\gamma_0(t-t')]\left[-2q(t')q(t)+\frac{3}{2}q(t)^2\right]q(t') \\ &\quad +2q(t)[-\dot{q}(t')\gamma_0(t-t')q(t') - \frac{1}{\tau}\gamma_0(t-t')q(t')^2 + q(t')^2\gamma_0(t-t')\ |_0^t] \\ &\quad -\frac{1}{2}\gamma_0(t-t')q(t)^3\ . \end{aligned} \tag{142}$$

Now we apply the ohmic friction, and Eq. 139 can be simplified :

$$\frac{\partial \delta V_2[q(\cdot),t]}{\partial q(t)} = \frac{3}{2}(1-\frac{1}{\tau})\gamma_0(0)q(t)^3 - 2\gamma_0(0)q(t)^2 v(t)\ , \tag{143}$$

and we obtain:

$$\begin{aligned}&2A(q_m-1)(q_m-q^\dagger)^2 + 2A(q_m-1)^2(q_m-q^\dagger) + 2q_m^3\sum_{i=1}^N \frac{c_i^2}{\omega_i^2} \\ &+\frac{3}{2}(1-\frac{1}{\tau})\gamma_0 q(t)^3 - 2\gamma_0 q(t)^2 v(t) - 2q_m^3\sum_{i=1}^N \frac{c_i^2}{\omega_i^2} = 0\ , \end{aligned} \tag{144}$$

By setting $q^\dagger = 2$, $A = 32$, $\tau = 0.714$, and changing the value of γ_0, we obtain the following different solutions:

For $\gamma_0 = 1000$,	$q_1 = -7.45.$	$q_2 = 0.125 - 0.31i$	$q_3 = 0.125 + 0.31i$
For $\gamma_0 = 1$,	$q_1 = 1.084.$	$q_2 = 1.2704$	$q_3 = 2.189$
For $\gamma_0 = 0.1$,	$q_1 = 1.0055.$	$q_2 = 1.4769$	$q_3 = 2.024$

(3) The second term of Eq. 139 can be simplified:

$$\begin{aligned}&\int_0^t dt' q(t)\dot{q}(t')q(t')\gamma_0(t-t') \\ &= q(t)\left[-\int_0^t \frac{d}{dt'}[q(t')\gamma_0(t-t')]q(t') + q(t')^2\gamma_0(t-t')\ |_0^t\right] \\ &= q(t)\left[-\frac{1}{\tau}\int_0^t [q(t')^2\gamma_0(t-t')]dt' \int_0^t \gamma_0(t-t')\dot{q}(t')dt' + q(t)^2\gamma_0(0)\right]\ . \end{aligned} \tag{145}$$

then we obtain:

$$\int_0^t dt' q(t)\dot{q}(t')q(t')\gamma_0(t-t') = -\frac{q(t)}{2\tau}\int_0^t \gamma_0(t-t')q(t')^2 dt' + \frac{1}{2}q(t)^2\gamma_0(0) \ . \tag{146}$$

Now applying the ohmic friction:

$$\frac{\partial \delta V_2[q(\cdot),t]}{\partial q(t)} = \frac{1}{2}(1-\frac{1}{\tau})\gamma_0(0)q(t)^3 \ , \tag{147}$$

we obtain:

$$\begin{aligned} & 2A(q_m-1)(q_m-q^\dagger)^2 + 2A(q_m-1)^2(q_m-q^\dagger) + 2q_m^3\sum_{i=1}^N \frac{c_i^2}{\omega_i^2} \\ + \quad & \frac{1}{2}(1-\frac{1}{\tau})\gamma_0 q(t)^3 - 2q_m^3\sum_{i=1}^N \frac{c_i^2}{\omega_i^2} = 0 \ . \end{aligned} \tag{148}$$

By setting $q^\dagger = 2$, $A = 32$, $\tau = 0.714$, and changing the value of γ_0, we obtain the following different solutions:

For $\gamma_0 = 1000$,	$q_1 = -9.272.$	$q_2 = 0.65 - 0.38i$	$q_3 = 0.65 + 0.38i$
For $\gamma_0 = 1$,	$q_1 = 1.003.$	$q_2 = 1.4797$	$q_3 = 2.024$
For $\gamma_0 = 0.1$,	$q_1 = 1.0003.$	$q_2 = 1.4979$	$q_3 = 2.002$

5.4 Discussion and Conclusions

The above analysis shows that the minima changes if $g(t)$ is space dependent and $\delta V_2[q(\cdot),t]$ is included in the Hamiltonian. Applying the same approximations during different steps give the different results. The double well starts to stretch and become asymmetric under different frictions.

If we ignore $\delta V_2[q(\cdot),t]$, the average position of double well particles is zero when $g(t)$ is time dependent/space dependent. If we include $\delta V_2[q(\cdot),t]$, the average position of double well particles is not zero, but it is hard to tell the exact position of particles. They may shift to the left well, or to the right well. And the shape of the double well is modified as the friction changes. Further analysis/simulations need to be done to better answer this question.

CHAPTER VI

CONCLUSION

The reaction dynamics of living polymerization has been studied by two different methods. The first method is a general study of the dynamics of a living polymer system in a non-equilibrium environment using the irreversible generalized Langevin equation (iGLE) to describe the microscopic changes in the polymer length. The nonstationary changes in the solvent due to the changing composition of the dense and reacting polymers has been introduced through modifications of the friction and potential of mean force in the iGLE. The second method focuses, instead, on the distributions of the polymers (and polymer lengths), and introduces a nonstationary diffusion reaction theory to describe the polymerization process.

6.1 The iGLE

The irreversible generalized Langevin equation can be used to model polymer systems where the environment is changed over time by the polymerization itself. For thermosetting polymerization, the polymerization is quenched by the diffusion-limited mechanism. For living polymerization systems, the process is more interesting since the active end is "alive" the entire time if there is no termination. This leads to dynamic chain lengths. As the polymer length becomes longer, the interaction between the reaction coordinate and bath will increase. This was incorporated into the function $g(t)$ included in the friction kernel, where $g(t)$ is a function of the average polymer length. The friction slows down the polymerization process, but will the equilibrium properties change if the friction is asymmetric? We found that the double well stretches with the friction and the minima of the double well also changes. However it is hard to say which direction the particles would prefer. Developing a different algorithm/analytic method may be a solution to better understand this problem.

The current study focused on the thermodynamics and kinetic properties of living polymerization. That is, one has to include the mechanism of living polymerization: the polymerization quenching due to the completion of monomers. To this aim, instead of using a merged harmonic potential, a new potential was proposed to account for the dynamic change due to the number of the monomers in solution, the chemical equilibrium and steric effect. Although it is a phenomenological model, it can be used to model the living polymerization process and give the correct dynamics. We also spend some effort on getting the analytical form of potential of mean of force. In this derivation, we use the Boltzmann distribution and stationary phase approximations. It turns out this analysis doesn't help much. The PMF we obtained is similar to the merged harmonic potential because of the decrease of the monomer concentration. Better approximation need to developed in the future. This suggest that polymerization is a nonequilibrium process and we must use a different PMF. This is why we developed and used a phenomenological PMF in the iGLE.

In addition to obtaining the equilibrium properties using this model, time-dependent properties such as polymer length, polymer length distribution and polydispersity index have also been obtained. We applied the model to the α-polystyrene system and the results agree with the experimental results very well. To test the generality of the model, we chose 4-vinylbenzocyclobutene and styrene. These two systems are irreversible processes and polystyrene has a very high activation energy. Instead of observing linear kinetics, we got an "S" shape behavior. The polymerization rate slows down at the beginning and then increases. At later time, it slows down again because of entanglement. In the 4-vinylbenzocyclobutene system, the experimental data shows the same trend, but not for the styrene system. The calculated PDI result with low barrier height is consistent with the experimental data for 4-vinylbenzocyclobutene system. This model works when the barrier height is about 10 times the thermal energy. If the barrier height is about 20 times the thermal energy, there is less of a possibility for the particles to cross the barrier in a short time. We have to incorporate new mechanisms in the model in the future.

6.2 The Stochastic Model

The stochastic model was used to study the diffusion effect in living polymerization systems. We apply this model to the α-methylstyrene system and found that it is a kinetically controlled process. It would be interesting to find a system in which the kinetics and diffusion compete in some region.

Suggestions for future work include the incorporation of the polymer relaxation time and also the development of an irreversible generalization of the chemical Langevin equation so as to include memory effects. The success of this work will help obtain the time-dependent rate constant and take into account the environment responses, thus we can better describe the dynamics of polymerization.

6.3 Connections between Models and Experiments

In the current study, we have compared the results with several experimental systems and validated the models that have been developed to describe living polymerization processes. In the iGLE, we use α-methylstyrene as a paradigmatic example and infer the parameter values from experimental data. We put those values back into our model, adjust other parameters and obtain the consistency between the simulation results and experimental results. We gain better understanding of our parameters based on the experimental data. For example, we get the relation of parameter ζ as a function of temperature as shown in Figure 14. If an experimentalist wants to know the kinetics of polymerization under different temperatures, we can simply adjust the value of ζ and run the simulation. They don't need to worry about the termination and transfer reactions that may happen during the process. We can also study the effect of initiator/monomer concentration on polymerization, but unfortunately, there is not enough experimental data available.

We also use α-methylstyrene as an example so as to study the diffusion effect on polymerization. Combining experimental data and simple kinetic results, we obtain diffusion coefficients and understand how much diffusion affects in a particular polymerization process. Usually, we would think that diffusion effects play a big role when the polymers grow longer, but this is not always true, especially for anionic polymerization processes.

Our models have successfully described several experimental systems and can be extended to other living polymerization systems. By introducing a series of electron-withdrawing groups into the frame work of α-methylstyrene and styrene, the reactivity of these monomers is changed. Assuming that we have all the necessary data, we can extract the parameter values from experimental data and obtain the dynamics of these living polymerization systems by modifying solvent friction γ_0 and scaling coefficient ζ. It is also possible to study the temperature effect on anionic polymerization of monomers containing functional groups, such as 4-vinylbenzocyclobutene, 4-cyano-α-methylstyrene and 4-cyano-styrene. By comparing all these simulation results, it is possible to help determine the best reaction conditions.

In either cases, experimentalists and theorists need to work together since both complement each other. Experimental data can be used to test the theoretical models, and theorist can run simulations with different conditions to help understand the properties of different polymer systems.

APPENDIX A

POISSON DISTRIBUTION

For the reaction:

$$M + I \rightarrow MI \ , \tag{149a}$$

$$M_{i+1}I + M \rightleftharpoons M_{i+1}I \ , \tag{149b}$$

where MI is the activated monomer, the rate constant for initiation and propagation is k_i and k_p respectively, the concentration of the initiator is $[I]_0$, and the concentration of monomer at time t is $[M]_t$. If the initiation rate is much faster than the propagation rate, then the concentration of the activated monomers is the same as the concentration of the initiators. Assuming no termination and transfer reactions, then:

$$-\frac{d[M]_t}{dt} = k_p[M]_t[I]_0 \ . \tag{150}$$

The solution for the above equation is

$$[M]_t = [M]_0 e^{-k_p[I]_0 t} \ . \tag{151}$$

During the reaction, the dynamic chain length can be defined as: $r = \frac{[M]_0 - [M]_t}{I_0}$. If the conversion reaches 100%, the chain length reaches the maximum chain length, which is the ratio of the monomers to initiators.

$$\frac{dr}{dt} = -\frac{1}{[I]_0}\frac{d[M]_t}{dt} = k_p[M]_t \ . \tag{152}$$

To get the Poisson distributions, we start with:

$$-\frac{d[MI]}{dt} = k_p[MI][M]_t = -\frac{d[MI]}{dr}\frac{dr}{dt} = -\frac{d[MI]}{dr}k_p[M]_t \ , \tag{153}$$

then we can obtain:

$$-\frac{d[MI]}{dr} = [MI] \ . \tag{154}$$

The solution for the above equation is:

$$[MI] = [MI]_0 e^{-r} = [I]_0 e^{-r} \ , \tag{155}$$

The rate equation for $[M_2I]$ is:

$$\frac{d[M_2I]}{dt} = k_p[MI][M]_t - k_p[M_2][M]_t \ . \tag{156}$$

After substitution and integration,

$$[M_2I] = r[I]_0 e^{-r} \ . \tag{157}$$

Using the same procedure, we obtain:

$$[M_3I] = \frac{1}{2} r^2 [I]_0 e^{-r} \ . \tag{158}$$

So the general formula for n-mers:

$$[M_iI] = \frac{1}{(i-1)!} r^{i-1} [I]_0 e^{-r} \ , \tag{159}$$

and the mol fraction of the i-mers in the polymer $x_(i)$ is:

$$x_i = \frac{1}{(i-1)!} r^{i-1} e^{-r} \ . \tag{160}$$

This is exactly the form of Poisson distribution.

APPENDIX B

POTENTIAL OF MEAN FORCE

B.1 Polymer Model—The Effected Potential for the Nearest-neighbor Monomers

We consider a coarse-grained bead-spring model for the polymer chain in which the bonded interaction is described by the harmonic potential,

$$V_{osc}(r) = \frac{k}{2}(r - r_0)^2 \, . \tag{161}$$

In addition, we consider a LJ nonbonding potential between the free monomer and the last bound monomer,

$$V_{lj}(r) = 4\varepsilon[(\frac{\delta}{r})^{12} - (\frac{\delta}{r})^6] \, , \tag{162}$$

where $\delta = \frac{l_0}{2^{\frac{1}{6}}}$, $\varepsilon = \frac{kl_0^2}{72}$, l_0 is bond length. This parameter choice guarantees the same equilibrium distance between the centers of the monomers and the same oscillation frequency at the minima for both potentials.

Since each monomer is treated as a hard sphere with a diameter $L < l_0$, a reflecting wall condition should be added to the potentials. But in the framework of the stiff chain approximation used here, it doesn't cause problem because of the strict confinement of monomers which fluctuate around their equilibrium in very narrow limits. In this case, for simplicity, we use a harmonic potential instead of the finitely extensible nonlinear elastic (FENE) potential and they should give the same results.

The association between the polymer system and the iGLE include the construction of the PMF and modifying friction kernel. Here we are interested in the exact form of PMF instead of the phenomenological form. We are interested in a partition function for the following group of $n + 2$ monomers: the $(n + 1)$ polymers and a free monomer which is the closest to the last bound monomer. The nearest distributions have been used in different field of statistical mechanics. In this model, we neglect any interaction between free monomers and a chain, and amongst free monomers themselves. We also ignore the

excluded volume effect. The concentration of the free monomers is $C(m) = \frac{m}{V}$, where m is the number of the free monomers.

To make the reaction proceed, that is, only the closest free monomer can attach to the polymer, we need to modify the LJ interaction.

B.1.1 Dense Solution Limit: Uniformly Distributed Monomers

The probability to find the first nearest-neighbor monomer to the polymer between r and $r + dr$ is denoted by $dP(1, r)$. This probability must be equal to the probability that no monomers exist interior to r (denoted by $dp_{no}(r; r_i)$) times the probability that a monomer does exist between r and $r + dr$ (denoted by $dp_{yes}(r; r)$), where $L < r_i < r$ and L is the size of the monomer [84].

In dense solution, $dp_{yes}(r; r) = 4\pi r^2 C(m)dr$, so $dp_{no}(r; r_i) = 1 - dp_{yes}(r; r)$. The probability to find the first closest particle at r with dr is:

$$dP(1, r) = \prod_{i=1}^{\infty} dp_{no}(r; r_i) dp_{yes}(r; r) \; . \tag{163}$$

Thus:

$$\begin{aligned}
\ln dP(1, r) &= \ln[dp_{no}(r; r_1)] + \ln[dp_{no}(r; r_2)] + \cdots \ln[dp_{no}(r; r_\infty)] + \ln[dp_{yes}(r; r)] \\
&= \ln[1 - 4\pi C(m) r_1^2 dr] + \ln[1 - 4\pi C(m) r_2^2 dr] + \cdots \\
&+ \ln[1 - 4\pi C(m) r_\infty^2 dr] + \ln[4\pi C(m) r^2 dr] \\
&= -4\pi C(m) r_1^2 dr - 4\pi C(m) r_2^2 dr \cdots - 4\pi C(m) r_\infty^2 dr + \ln[4\pi C(m) r^2 dr] \\
&= -4\pi C(m) \int_L^r r^2 dr + \ln[4\pi C(m) r^2 dr] \\
&= -\frac{4\pi}{3} C(m)(r^3 - L^3) + \ln[4\pi C(m) r^2 dr] \; ,
\end{aligned} \tag{164}$$

and we obtain:

$$\begin{aligned}
dP(1, r) &= e^{-\frac{4\pi}{3} C(m)(r^3 - L^3)} 4\pi C(m) r^2 dr \\
&= e^{-\frac{4\pi}{3} C(m)(r^3 - L^3)} C(m) dV \; .
\end{aligned} \tag{165}$$

By including the closest particle, the new modified LJ potential for a dense solution becomes:

$$dV e^{-\beta V_{eff}(r,m)} = e^{-\beta V_{lj}} dP(1, r) = e^{-\beta V_{lj}} e^{-\frac{4\pi}{3} C(m)(r^3 - L^3)} C(m) dV \; , \tag{166}$$

and this implies:

$$\beta V_{eff}(r,m) = \beta V_{lj}(r) + 4\pi C(m)\int_L^r x^2 dx - \ln C(m)\ . \tag{167}$$

B.1.2 Dilute Solution Limit: Boltzmann Distributed Monomers

In dilute solution, $dp_{yes}(r;r) = 4\pi r^2 C(m) e^{-\beta V_{lj}} dr$, and $dp_{no}(r;r_i) = 1 - dp_{yes}(r;r)$. The probability to find the first closest particle at r with dr is:

$$dP(1,r) = \prod_{i=1}^{\infty} dp_{no}(r;r_i) dp_{yes}(r;r)\ . \tag{168}$$

Thus,

$$\begin{aligned}
\ln dP(1,r) &= \ln[dp_{no}(r;r_1)] + \ln[dp_{no}(r;r_2)] + \cdots \ln[dp_{no}(r;r_\infty)] + \ln[dp_{yes}(r;r)] \\
&= \ln[1 - 4\pi C(m) e^{-\beta V_{lj}} r_1^2 dr] + \ln[1 - 4\pi C(m) e^{-\beta V_{lj}} r_2^2 dr] + \cdots \\
&+ \ln[1 - 4\pi C(m) e^{-\beta V_{lj}} r_\infty^2 dr] + \ln[4\pi C(m) e^{-\beta V_{lj}} r^2 dr] \\
&= -4\pi C(m) e^{-\beta V_{lj}} r_1^2 dr - 4\pi C(m) e^{-\beta V_{lj}} r_2^2 dr \cdots - 4\pi C(m) e^{-\beta V_{lj}} r_\infty^2 dr \\
&+ \ln[4\pi C(m) e^{-\beta V_{lj}} r^2 dr] \\
&= -4\pi C(m)\int_L^r e^{-\beta V_{lj}} r^2 dr + \ln[4\pi C(m) e^{-\beta V_{lj}} r^2 dr]\ ,
\end{aligned} \tag{169}$$

and we obtain:

$$\begin{aligned}
dP(1,r) &= e^{-4\pi C(m)\int_L^r e^{-\beta V_{lj}} r^2 dr} 4\pi C(m) r^2 e^{-\beta V_{lj}} dr \\
&= e^{-4\pi C(m)\int_L^r e^{-\beta V_{lj}} r^2 dr} e^{-\beta V_{lj}} C(m) dV\ .
\end{aligned} \tag{170}$$

By including this nearest distribution,the modified LJ for dilute solution:

$$\beta V_{eff}(r,m) = 2\beta V_{lj}(r) + 4\pi C(m)\int_L^r e^{-\beta V_{lj}(x)} x^2 dx - \ln C(m)\ . \tag{171}$$

B.2 Polymer Model—the Partition Function for n Connected Harmonic Springs

Suppose $\vec{r_1}$, $\vec{r_2}\cdots$ are vectors that point to each monomer from the first monomer. Here we use the stiff chain approximation.

For $n = 2$, $Q_3 = e^{-\beta V_3}$, where n is the bond number. We calculate the partition function using actual (true) potentials:

$$\begin{aligned} e^{-\beta V_3} &= \int_L^\infty d\vec{r}_1 \int_L^\infty d\vec{r}_2 e^{-\frac{u(\vec{r_1})+u(\vec{r_2}-\vec{r_1})}{k_B T}} \delta(|\vec{r_1}| + |\vec{r_2} - \vec{r_1}| - R_c) \\ &= \int_L^\infty d\vec{r}_1 e^{-\frac{u(\vec{r1})}{k_B T}} \int_L^\infty d\vec{r} e^{-\frac{u(\vec{r})}{k_B T}} \delta[|\vec{r}| - (Rc - |\vec{r_1}|)] \\ &= 4\pi \int_L^\infty d\vec{r}_1 e^{-\frac{u(\vec{r_1})+u(R_c-\vec{r_1})}{k_B T}} (R_c - r_1)^2 \\ &= 4\pi \int_L^\infty d\vec{r}_1 (R_c - r_1)^2 e^{-\frac{k}{2k_B T}[(r_1-l_0)^2+(R_c-r_1-l_0)^2]} \ . \end{aligned} \tag{172}$$

The exponent can now be rearranged by completing the squares and regathering the terms so that terms not involving the integrating variable, $\vec{r}_1$, can be factored out:

$$\begin{aligned} e^{-\beta V_3} &= 4\pi \int_L^\infty d\vec{r}_1 (R_c - r_1)^2 e^{-\frac{2k}{2k_B T}[(r_1-\frac{R_c}{2})^2+(l_0-\frac{R_c}{2})^2]} d\vec{r}_1 \\ &= 4\pi (R_c - \frac{Rc}{2})^2 e^{-\frac{2k}{2k_B T}(l_0-\frac{R_c}{2})^2} \int_L^\infty d\vec{r}_1 e^{-\frac{2k}{2k_B T}(r_1-\frac{R_c}{2})^2} \\ &= 4\pi \frac{Rc^2}{4} e^{-\frac{2k}{2k_B T}(l_0-\frac{R_c}{2})^2} \pi Rc^2 \sqrt{\frac{\pi k_B T}{k}} \\ &= \pi^2 R_c^4 e^{-\frac{2k}{2k_B T}(l_0-\frac{R_c}{2})^2} \sqrt{\frac{\pi k_B T}{k}} \\ &= \pi^2 R_c^4 e^{-\frac{k}{4k_B T}(R_c-2l_0)^2} \sqrt{\frac{\pi k_B T}{k}} \\ &= (4\pi)^2 l_0^4 e^{-\frac{k}{4k_B T}(R_c-2l_0)^2} \sqrt{\frac{\pi k_B T}{k}} \ , \end{aligned} \tag{173}$$

For $n = 3$, $Q_4 = e^{-\beta V_4}$, where n is bond number, we use an effective potential in the derivation. This means that we apply the results shown in Eq. 173 to the following calculation

which simplifies the procedure.

$$
\begin{aligned}
e^{-\beta V_4} &= \Upsilon_4 \int_L^\infty d\vec{r}_3 \int_{2L}^\infty d\vec{R}_c e^{-\frac{k}{4k_BT}(R_c-2l_0)^2} e^{-\frac{k}{2k_BT}(r_3-l_0)^2} \delta(|\vec{R}_c| + |\vec{r_3}| - R_{new}) \\
&= \Upsilon_4 \int_{-\infty}^\infty d\vec{R}_c e^{-\frac{k}{4k_BT}(R_c-2l_0)^2} \int_{-\infty}^\infty d\vec{r}_3 4\pi r_3^2 e^{-\frac{k}{2k_BT}(r_3-l_0)^2} \delta(r_3 - (R_{new} - R_c) \\
&= \Upsilon_4 4\pi \int_{-\infty}^\infty d\vec{R}_c (R_{new} - R_c)^2 e^{-\frac{k}{4k_BT}(R_c-2l_0)^2} e^{-\frac{k}{2k_BT}(R_{new}-R_c-l_0)^2} \\
&= \Upsilon_4 4\pi \int_{-\infty}^\infty d\vec{R}_c (R_{new} - R_c)^2 e^{-\frac{3k}{2k_BT}[(l_0-\frac{R_{new}}{3})^2 + \frac{1}{2}(R_c - \frac{2}{3}R_{new})^2]} \\
&= \Upsilon_4 4\pi e^{-\frac{3k}{2k_BT}(l_0-\frac{R_{new}}{3})^2} \int_{-\infty}^\infty d\vec{R}_c (R_{new} - R_c)^2 e^{-\frac{3k}{4k_BT}(R_c-\frac{2}{3}R_{new})^2} \\
&= \Upsilon_4 4\pi e^{-\frac{3k}{2k_BT}(l_0-\frac{R_{new}}{3})^2} (R_{new} - \frac{2}{3}R_{new})^2 \sqrt{\frac{4\pi k_B T}{3k}} \\
&= \Upsilon_4 4\pi \frac{2}{\sqrt{3}} \sqrt{\frac{\pi k_B T}{k}} e^{-\frac{3k}{2k_BT}(l_0-\frac{R_{new}}{3})^2} \\
&= (4\pi)^3 l_0^6 \frac{2}{\sqrt{3}} \frac{\pi k_B T}{k} e^{-\frac{k}{6k_BT}(R_{new}-3l_0)^2} \ , \qquad (174)
\end{aligned}
$$

where some factors have been collected into the single term,

$$\Upsilon_4 \equiv (4\pi)^3 l_0^6 \frac{2}{\sqrt{3}} \frac{\pi k_B T}{k} \ . \qquad (175)$$

If we use the true potentials, instead, then we can obtain the same result as in Eq. 174 if $kl_0^2 \gg k_b T$.

A similar derivation, now follows for the calculation of the effective potential for $n = 4$:

$$
\begin{aligned}
e^{-\beta V_5} &= \chi_4 \int_L^\infty d\vec{r}_4 \int_{2L}^\infty d\vec{R}_c e^{-\frac{k}{6k_BT}(R_c-3l_0)^2} e^{-\frac{k}{2k_BT}(r_4-l_0)^2} \delta(|\vec{R}_c| + |\vec{r_4}| - R_{new}) \\
&= \chi_4 \int_{-\infty}^\infty d\vec{R}_c e^{-\frac{k}{4k_BT}(R_c-3l_0)^2} \\
&\quad \int_{-\infty}^\infty d\vec{r}_4 4\pi r_4^2 e^{-\frac{k}{2k_BT}(r_4-l_0)^2} \delta\left((r_4 - (R_{new} - R_c)\right) \\
&= \chi_4 \int_{-\infty}^\infty d\vec{R}_c (R_{new} - R_c)^2 e^{-\frac{k}{6k_BT}(R_c-3l_0)^2} e^{-\frac{k}{2k_BT}(R_{new}-R_c-l_0)^2} \\
&= \chi_4 \int_{-\infty}^\infty d\vec{R}_c (R_{new} - R_c)^2 e^{-\frac{4k}{2k_BT}[(l_0-\frac{R_{new}}{4})^2 + \frac{1}{3}(R_c - \frac{3}{4}R_{new})^2]} \\
&= \chi_4 4\pi e^{-\frac{4k}{2k_BT}(l_0-\frac{R_{new}}{4})^2} \int_{-\infty}^\infty d\vec{R}_c (R_{new} - R_c)^2 e^{-\frac{4k}{6k_BT}(R_c-\frac{3}{4}R_{new})^2} \\
&= \chi_4 4\pi e^{-\frac{4k}{2k_BT}(l_0-\frac{R_{new}}{4})^2} (R_{new} - \frac{3}{4}R_{new})^2 \int_{-\infty}^\infty d\vec{R}_c e^{-\frac{4k}{6k_BT}(R_c-\frac{3}{4}R_{new})^2} \\
&= \chi_4 4\pi l_0^2 e^{-\frac{k}{8k_BT}(R_{new}-4l_0)^2} \sqrt{\frac{6\pi k_B T}{4k}} \\
&= (4\pi)^4 l_0^8 \sqrt{2} (\frac{\pi k_B T}{k})^{\frac{3}{2}} e^{-\frac{k}{8k_BT}(R_{new}-4l_0)^2} \ , \qquad (176)
\end{aligned}
$$

where some factors have been collected into the single term,

$$\chi_4 \equiv (4\pi)^3 l_0^6 \frac{2}{\sqrt{3}} \frac{\pi k_B T}{k} \ . \tag{177}$$

Now we can summarize and get the reversible work for polymer with n bond near $R_c = nl_0$, assuming a weak dependence on terms that are constant:

$$Q_n^b(R_c) = (4\pi)^n \sqrt{\frac{2^{n-1}}{n}} (\frac{\pi k_B T}{k})^{\frac{n-1}{2}} l_0^{2n} e^{-\frac{k}{2nk_BT}(R_c - nl_0)^2} \ . \tag{178}$$

We could get a more general form if we use R_c instead of nl_0:

$$Q_n^b(R_c) = (4\pi R_c^2)^n (\frac{2\pi k_B T}{k})^{\frac{n-1}{2}} \frac{1}{n^{2n+\frac{1}{2}}} e^{-\frac{k}{2nk_BT}(R_c - nl_0)^2} \ . \tag{179}$$

Since a monomer can't attach to a polymer from any direction, we include this steric effect by adding $\frac{\Omega}{4\pi}$, which means the available solid angle to reaction:

$$Q_n^b(R_c) = (4\pi \frac{\Omega}{4\pi} R_c^2)^n (\frac{2\pi k_B T}{k})^{\frac{n-1}{2}} \frac{1}{n^{2n+\frac{1}{2}}} e^{-\frac{k}{2nk_BT}(R_c - nl_0)^2} \ . \tag{180}$$

Also, we need to normalize this function:

$$Q_n^b(R_c) = (\Omega R_c^2)^n (\frac{2\pi k_B T}{k})^{\frac{n-1}{2}} \frac{1}{n^{2n+\frac{1}{2}}} \frac{1}{V^n} e^{-\frac{k}{2nk_BT}(R_c - nl_0)^2} \ . \tag{181}$$

B.3 Polymer Model—Monomer Attach to Polymer

If one monomer interact with this polymer, we need to add an effected LJ potential to the harmonic spring.

$$\begin{aligned}
& Q_{n+1}^e(R_{new}) \\
= \ & (\Omega)^n R_c^{2n} (\frac{2\pi k_B T}{k})^{\frac{n-1}{2}} \frac{1}{n^{2n+\frac{1}{2}}} \frac{1}{V^{n+1}} \int_{-\infty}^{\infty} \\
& \int_L^{\infty} e^{-\frac{k}{2nk_BT}(R_c - nl_0)^2} e^{-\beta V_{eff}} \delta(R_c + r - R_{new}) dr dR_c \\
= \ & (\Omega)^n R_c^{2n} (\frac{2\pi k_B T}{k})^{\frac{n-1}{2}} \frac{1}{n^{2n+\frac{1}{2}}} \frac{1}{V^{n+1}} \int_L^{\infty} \int_{-\infty}^{\infty} e^{-\frac{k}{2nk_BT}(R_c - nl_0)^2} \delta[R_c - (R_{new} - r)] dR_c \\
& e^{-\beta V_{eff}} 4\pi r^2 (\frac{\Omega}{4\pi}) dr \\
= \ & (\Omega)^{n+1} (\frac{2\pi k_B T}{k})^{\frac{n-1}{2}} \frac{1}{n^{2n+\frac{1}{2}}} \frac{1}{V^{n+1}} \int_L^{\infty} (R_{new} - r)^{2n} r^2 e^{-\frac{k}{2nk_BT}(R_{new} - r - nl_0)^2 - \beta V_{eff}} dr \\
= \ & A \int_L^{\infty} e^{-\beta U(r, Rc)} dr \ ,
\end{aligned} \tag{182}$$

where A is the constant and we define:

$$U(r, R_{new}) = \frac{k}{2n}(R_{new} - r - nl_0)^2 + V_{eff} - \beta^{-1}(\ln r^2 + \ln(R_{new} - r)^{2n}) \ , \tag{183}$$

and

$$U''(r, R_{new}) = \frac{k}{n} + V''_{eff}(r, m) + 2\beta^{-1}(\frac{1}{r^2} + \frac{n}{(R_{new} - r)^2}) \ . \tag{184}$$

The stationary phase method is an approach for solving integrals analytically by evaluating the integrands in regions where they contribute the most. Now we can use the stationary phase approximation to get the partition function for small and large R_{new}.

$$Q^e_{n+1}(R_{new}) = C \times e^{-\beta U(r1min(R_{new}), R_{new})} \sqrt{\frac{2\pi}{U''(r1min(R_{new}), R_{new})}} \ , \tag{185}$$

$$Q^e_{n+1}(R_{new}) = C \times e^{-\beta U(r2min(R_{new}), R_{new})} \sqrt{\frac{2\pi}{U''(r2min(R_{new}), R_{new})}} \ . \tag{186}$$

where $C = (\Omega)^{n+1}(\frac{2\pi k_B T}{k})^{\frac{n-1}{2}} \frac{1}{n^{2n+\frac{1}{2}}} \frac{1}{V^{n+1}}$, r1min, r2min are the minimum position for the whole potential.

The overall partition function is the following:

$$\begin{aligned} Q(R_{new}) &= \sum_{n=2}^{n} [Q^e_{n+1}(R_{new}) + Q^b_n(R_{new})] \\ &= Be^{-\beta U_{PMF}(R_{new})} \ . \end{aligned} \tag{187}$$

Using this method, it is possible to find the potential of mean force (PMF).

REFERENCES

[1] Zhuang, J., Sarkar Das, S., Nowakowski, M. D., and Greer, S. C., Living poly(α-methylstyrene) near the polymerization Line. 6. Chemical kinetics, *Physica A*, vol. 244, pp. 522–535, 1997.

[2] Sarkar Das, S., Ploplis Andrews, A., and Greer, S. C., Living poly(*alpha* - methylstyrene) near the polymerization line: IV. Extent of polymerization as a function of temperature, *J. Chem. Phys.*, vol. 102, pp. 2951–2959, 1995.

[3] Sakellariou, G., Baskaran, D., Hadjichristidis, N., and Mays, J. W., Well-defined poly(4-vinylbenzocyclobutene): Synthesis by living anionic polymerization and characterization, *Macromolecules*, vol. 39, pp. 3525–3530, 2006.

[4] Lee, W., Lee, H., Cha, J., Chang, T., J.Hanley, K., and P.Lodge, T., Molecular weight distribution of polystyrene made by anionic polymerizaton, *Macromolecules*, vol. 33, pp. 5111–5115, 2000.

[5] Szwarc, M., Living polymers, *Nature*, vol. 178, pp. 1168–1169, 1956.

[6] Szwarc, M., Levy, M., and Milkovich, R., Polymerization initiated by electron transfer to monomer: A new method of formation of block polymers, *J. Am. Chem. Soc.*, vol. 78, pp. 2656–2657, 1956.

[7] Webster, O. W., Living polymerization methods, *Science*, vol. 251, pp. 887–893, 1991.

[8] O'Shaughnessy, B. and Vavylonis, D., Dynamics of living polymers, *Eur. Phys. J.*, vol. 12, pp. 481–496, 2003.

[9] O'Shaughnessy, B. and Vavylonis, D., The ultrasensitivity of living polymers, *Phys. Rev. Lett.*, vol. 90, p. 118301, 2003.

[10] Hadjichristidis, N., Latrou, H., Pitsikalis, M., and Mays, J., Macromolecular architectures by living and controlled/living polymerizations, *Prog. Poly. Sci.*, vol. 31, pp. 1068–1132, 2006.

[11] Yagci, Y. and Tasdelen, M. A., Mechanistic transformations involving living and controlled/living polymerization methods, *Prog. Poly. Sci.*, vol. 31, pp. 1133–1170, 2006.

[12] Brown, W. B. and Szwarc, M., Molecular weight distribution of living polymers, *Trans. Faraday Soc.*, vol. 54, pp. 416–419, 1958.

[13] Miyake, A. and Stockmayer, W. H., Theoretical reaction kinetics of reversible living polymerization, *Die Makromolekulare Chemie*, vol. 88, pp. 90–116, 1965.

[14] Milchev, A. and Rouault, Y., A Monte Carlo study of thermodynamic relaxation in living polymers, *J. Phys. II*, vol. 5, pp. 343–347, 1995.

[15] Sarkar Das, S., Zhuang, J., Ploplis Andrews, A., Greer, S. C., Guttman, C., and Blair, W., Living poly(α-methylstyrene) near the polymerization line. VII. Molecular weight distribution in a good solvent, *J. Chem. Phys.*, vol. 111, pp. 9406–9417, 1999.

[16] Dudowicz, J., Freed, K. F., and Douglas, J., Lattice model of living polymerization. I. Basic thermodynamic properties, *J. Chem. Phys.*, vol. 111, pp. 7116–7130, 1999.

[17] Turner, M. S. and Cates, M. E., The relaxation spectrum of polymer length distribution, *Journal De Physique*, vol. 51, pp. 307–316, 1990.

[18] Ishizone, T., Okazawa, Y., Ohnuma, K., Hirao, A., and Nakahama, S., Anionic polymerization of monomers containing functional groups. 8. Anionic living polymerization of 4-cyano-α-methylstyrene, *Macromolecules*, vol. 30, pp. 757–763, 1997.

[19] Hirao, A., Loykulnant, S., and Ishizone, T., Recent advance in living anionic polymerization of functionalized styrene derivatives, *Prog. Poly. Sci.*, vol. 27, pp. 1399–1471, 2002.

[20] Dreyfuss, M. P. and Dreyfuss, P., p-Chlorophenyldiazonium Hexafluorophosphate as a catalyst in the polymerization of tetrahydrofuran and other cyclic ethers, *J. Poly. Science: Part A-1*, vol. 4, pp. 2179–2200, 1966.

[21] Roucher, T. G. and Wetton, R. E., Synthesis of narrow distribution polytetrahydrofuran, *Polymer*, vol. 17, pp. 205–211, 1976.

[22] Guerrero-Sanchez, C., Abeln, C., and Schubert, U. S., Automated parallel anionic polymerizations:enhancing the possibilities of a widely used technique in polymer synthesis, *J. Polym. Sci. A Polym. Chem.*, vol. 43, pp. 4151–4160, 2005.

[23] Bird, R. B., Armstrong, R. C., and Hassager, O., *Dynamics of polymeric liquids, Vol 1, Fluid mechanics*. NY: Wiley-Interscience, 1987.

[24] Kramers, H. A., Brownian motion in a field of force and the diffusional model of chemical reactions, *Physica (Utrecht)*, vol. 7, pp. 284–304, 1940.

[25] Einstein, A., On the movement of small particles suspended in stationary liquids required by the molecular-kinetic theory of heat, *Ann. Phys.*, vol. 17, p. 549, 1905. "On the theory of Brownian motion," *ibid.* **19**, 371 (1906).

[26] Brown, R., A brief account of microscopical observations made in the months of June, July, and August, 1827, on the particles contained in the pollen of plants; and on the general existence of active molecules in organic and inorganic bodies, *Philos. Mag.*, vol. 4, p. 161, 1828. *ibid.* **6**, 161 (1829).

[27] Brown, R., A brief account of microscopical observations made in the months of June, July, and August, 1827, on the particles contained in the pollen of plants; and on the general existence of active molecules in organic and inorganic bodies, *Philos. Mag.*, vol. 4, p. 161, 1828. "Additional Remarks on Active Molecules," *ibid.* **6**, 161 (1829).

[28] Langevin, P., Sur la théorie du mouvement Brownien, *Comptes Rednus de l'Acacemie de Sciences (Paris)*, vol. 146, p. 530, 1908.

[29] van Kampen, N. G., *Stochastic processes in physics and chemistry*. New York: North-Holland, 1981.

[30] Pollak, E., Grabert, H., and Hänggi, P., Theory of activated rate processes for arbitrary frequency dependent friction: Solution of the turnover problem, *J. Chem. Phys.*, vol. 91, pp. 4073–4087, 1989.

[31] Hänggi, P., Talkner, P., and Borkovec, M., Reaction-rate theory: Fifty years after Kramers, *Rev. Mod. Phys.*, vol. 62, pp. 251–341, 1990. and references therein.

[32] Mel'nikov, V. I. and Meshkov, S. V., Theory of activated rate processes: Exact solution of the Kramers Problem, *J. Chem. Phys.*, vol. 85, pp. 1018–1027, 1986.

[33] Pollak, E., Theory of activated rate processes: A new derivation of Kramers' expression, *J. Chem. Phys.*, vol. 85, pp. 865–867, 1986.

[34] Lindenberg, K. and Cortés, E., Thermal relaxation of systems with quadratic heat bath coupling, *Physica A*, vol. 126A, p. 489, 1984.

[35] Carmeli, B. and Nitzan, A., Theory of activated rate processes: Position dependent friction, *Chem. Phys. Lett.*, vol. 102, pp. 517–522, 1983.

[36] Haynes, G. R., Voth, G. A., and Pollak, E., A theory for the thermally activated rate constant in systems with spatially dependent friction, *Chem. Phys. Lett.*, vol. 207, pp. 309–316, 1993.

[37] Haynes, G. R., Voth, G. A., and Pollak, E., A theory for the activated barrier crossing rate constant in systems influenced by space and time dependent friction, *J. Chem. Phys.*, vol. 101, pp. 7811–7822, 1994.

[38] Greer, S. C., Physical chemistry of equilibrium polymerization, *J. Phys. Chem.*, vol. 102, pp. 5413–5422, 1998.

[39] Tobolsky, A. V. and Eisenberg, A., Transition phenomena in equilibrium polymerization, *J. Colloid Sci.*, vol. 17, p. 49, 1962.

[40] Oosawa, F., *Thermodynamics of polymerization of protein*. NY: Academic Press, 1975.

[41] Oosawa, F., Asakura, K., Hotta, K., Imai, N., and Ooi, T., G-F transition of actin as a fibrous condensation, *J. Polym. Sci*, vol. 37, pp. 323–336, 1959.

[42] Oosawa, F. and Kasai, M., Theory of linear and helical aggregations of macromolecules, *J. Mol. biol*, vol. 4, p. 10, 1962.

[43] Ivin, K. J., Thermodynamics of addition polymerization processes, in *Reactivity, Mechanism, and structure in polymer chemistry* (Jenkins, A. D. and Ledwith, A., eds.), p. 514, NY: John Wiley, 1974.

[44] Semenchenko, V. and Soldatova, E., Thermodynamics of polymers. 5. phase transiton in liquid sulfur, *Coll. J.-USSR*, vol. 28, p. 589, 1966.

[45] Wheeler, J. C. and Pfeuty, P., The $n \to 0$ vector model and equilibrium polymerization, *Phys. Rev. A*, vol. 24, pp. 1050–62, 1981.

[46] Flory, P. J., Thermodynamics of high polymer solutions, *J. Chem. Phys.*, vol. 10, pp. 51–61, 1942.

[47] Meyer, K. H., The compound entropies of systems with long-chain compounds and their statistical explanation, *Z. Phys. Chem. Abt. B*, vol. 44, pp. 383–391, 1939.

[48] Huggins, M. L., Some properties of solutions of long-chain compounds, *J. Phys. Chem.*, vol. 46, pp. 151–158, 1942.

[49] Flory, P. J., Statistical thermodynamics of semi-flexible chain molecules, *Proc. R. Soc. London (A)*, vol. 234, pp. 60–73, 1956.

[50] Flory, P. J., Phase equilibria in solutions of rod-like particles, *Proc. R. Soc. London (A)*, vol. 234, pp. 73–89, 1956.

[51] DiMarzio, E. A. and Gibbs, J. H., Chain stiffness and the lattice theory of polymer phases, *J. Chem. Phys.*, vol. 28, pp. 807–813, 1958.

[52] Gibbs, J. H. and DiMarzio, E. A., Nature of the glass transition and the glassy state, *J. Chem. Phys.*, vol. 28, pp. 373–383, 1958.

[53] de Gennes, P. G., Exponents for the excluded volume problem as derived by the Wilson method, *Phys. Lett.*, vol. 38A, p. 339, 1972.

[54] des Cloiseaux, J., The Lagrangian theory of polymer solutions at intermediate concentrations, *J. Phys. (Paris)*, vol. 36, p. 281, 1975.

[55] Daoud, M., Cotton, J. P., Farnoux, B., Jannik, G., Sarma, G., Benoit, H., Duplessix, R., Picot, C., and de Gennes, P. G., Solutions of flexible polymer neutron experiments and interpretation, *Macromolecules*, vol. 8, pp. 804–819, 1975.

[56] Huopaniemi, I., Luo, K., Ala-Nissila, T., and Ying, S.-C., Langevin dynamics simulations of polymer translocation through nanopores, *J. Chem. Phys.*, vol. 125, p. 124901, 2006.

[57] Munk, T., Hallatschek, O., Wiggins, C. H., and Frey, E., Dynamics of semi-flexible polymers in a flow field, *Phys. Rev. E*, vol. 74, p. 041911, 2006.

[58] Hernandez, R., The projection of a mechanical system onto the irreversible generalized Langevin equation (iGLE), *J. Chem. Phys.*, vol. 111, pp. 7701–7704, 1999.

[59] Frenkel, D. and Smit, B., *Understanding molecular Simulation: From algorithms to application*. NY: Academic Press, 1996.

[60] Groot, R., *Novel methods in soft matter simulations*. Lecture notes in Physics, Berlin: Springer Verlag, 2004.

[61] Hoogerbrugge, P. J. and Koelman, J. M. V. A., Simulating microscopic hydrodynamic phenomena with dissipative particle dynamics, *Europhys. Lett.*, vol. 19, pp. 155–160, 1992.

[62] Koelman, J. M. V. A. and Hoogerbrugge, P. J., Dynamic simulation of hard sphere suspensions under steady shear, *Europhys. Lett.*, vol. 21, pp. 363–368, 1993.

[63] Zheng, K. M., Greer, S. C., Corrales, L. R., and Ruiz-Garcia, J., Living poly(α-methylstyrene) near the polymerization line: II. Phase diagram in methylcyclohexane, *J. Chem. Phys.*, vol. 98, pp. 9873–9880, 1993.

[64] Zwanzig, R., Memory effects in irreversible thermodynamics, *Phys. Rev.*, vol. 124, p. 983, 1961.

[65] Kubo, R., The fluctuation-dissipation theorem, *Rep. Prog. Phys.*, vol. 29, pp. 255–284, 1966.

[66] Mori, H., Transport, collective motion, and Brownian motion, *Prog. Theor. Phys.*, vol. 33, pp. 423–455, 1965.

[67] Nitzan, A., Activated rate processes in condensed phases: The Kramers theory revisited, *Adv. Chem. Phys.*, vol. 70, pp. 489–555, 1988.

[68] Hynes, J. T., The theory of reactions in solution, in *Theory of Chemical Reaction Dynamics* (Baer, M., ed.), vol. 4, pp. 171–234, Boca Raton, FL: CRC, 1985.

[69] Hynes, J. T., Chemical reaction dynamics in solution, *Annu. Rev. Phys. Chem.*, vol. 36, pp. 573–597, 1985.

[70] Vogt, M. and Hernandez, R., An idealized model for nonequilibrium dynamics in molecular systems, *J. Chem. Phys.*, vol. 123, p. 144109, 2005.

[71] Hernandez, R. and Somer, F. L., Stochastic dynamics in irreversible nonequilibrium environments. 2. A model for thermosetting polymerization, *J. Phys. Chem. B*, vol. 103, pp. 1070–1077, 1999.

[72] Kirkwood, J. G., Statistical Mechanics of Fluid Mixtures, *J. Chem. Phys.*, vol. 3, pp. 300–313, 1935.

[73] Straub, J. E., Borkovec, M., and Berne, B. J., Non-Markovian activated rate processes: Comparison of current theories with numerical simulation data, *J. Chem. Phys.*, vol. 84, pp. 1788–1794, 1986.

[74] Sancho, J. M., San Miguel, M., and Durr, D., Adiabatic elimination for systems of Brownian particles with nonconstant damping coefficients, *J. Stat. Phys.*, vol. 28, pp. 291–305, 1982.

[75] Kalnin'sh, K. K., Polymerization/Depolymerization mechanism for "living" sodium poly-α-Methylstyryl and sodium polystyryl, *Russian Journal of Applied Chemistry*, vol. 74, pp. 1913–1919, 2001.

[76] Shipp, D. A. and Matyjaszewski, K., Kinetic analysis of controlled/living radical polymerizations by simulations. 1. The importance of diffusion-controlled reactions, *Macromolecules*, vol. 32, p. 2948, 1999.

[77] Shipp, D. A. and Matyjaszewski, K., Kinetic analysis of controlled/living radical polymerizations by simulations. 2. Apparent external orders of reactions in atom transfer radical polymerization, *Macromolecules*, vol. 33, p. 1553, 2000.

[78] Delgadillo-Velazquez, O., Vivaldo-Lima, E., Quintero-Ortega, I. A., and Zhu, S., Effects of diffusion-controlled reactions on atom-transfer radical polymerization, *AIChE J.*, vol. 48, pp. 2597–2608, 2002.

[79] Kurtz, T. G., The relationship between stochastic and deterministic models for chemical reactions, *J. Chem. Phys.*, vol. 57, pp. 2976–278, 1972.

[80] Gillespie, D. T., The chemical Langevin equation, *J. Chem. Phys.*, vol. 113, pp. 297–306, 2000.

[81] Goutsias, J., A hidden Markov model for transcriptional regulation in single cells, *IEEE/ACM Trans. Comput. Biol. bioinf.*, vol. 3, pp. 57–71, 2006.

[82] Hernandez, R. and Somer, F. L., Nonstationary stochastic dynamics & applications to chemical physics, in *Theoretical Methods in Condensed Phase Chemistry* (Schwartz, S. D., ed.), pp. 91–116, The Netherlands: Kluwer Academic, 2000.

[83] Hernandez, R. and Somer, F. L., Stochastic dynamics in irreversible nonequilibrium environments. 1. The fluctuation-dissipation relation, *J. Phys. Chem. B*, vol. 103, pp. 1064–1069, 1999.

[84] Bhattacharjee, B., nth-nearest-neighbor distribution functions of an interacting fluid from the pair correlation function: A hierarchical approach, *Phys. Rev. E*, vol. 67, p. 041208, 2003.